UCLouvain

AGRO LOUVAIN

Faculté des bioingénieurs

Soil tillage detection performances using Sentinel time series and Copernicus product in Wallonia

Author	Majedeh Baladi
Supervisor	Pierre Defourny
Co-supervisor	Tom Kenda
Readers	Charles Bielders
	Jean Bouchat

Academic year 2024-2025

Final dissertation presented for the award of a master's degree in [120] Agriculture and Bio-industries, Professional focus: Geo-Information Science and Earth Observation for Environmental Modelling and Management [SAIV2MS/GM]

ACKNOWLEDGEMENTS

First and foremost, I would like to express my gratitude to my supervisor, Professor Pierre Defourny, for his invaluable guidance, constructive feedback, and unwavering support throughout the course of this study. His expertise and insightful advice have been instrumental in shaping both the direction and quality of this research.

I am also sincerely thankful to my second supervisor, Tom Kenda, for his constant availability, thoughtful suggestions, and patient encouragement. His readiness to assist and his practical support have made a significant difference in overcoming many of the challenges I encountered during this journey.

A heartfelt thanks goes to my family, whose love and emotional support have been a source of strength and motivation. Although we were separated by distance, their encouragement was always present and deeply felt. Their belief in me has played an essential role in helping me reach this important milestone.

I am also grateful to my friends for their encouragement, companionship, and for providing moments of relief and joy during this demanding period.

Lastly, I would like to acknowledge the use of OpenAI's ChatGPT, which I used as a tool to refine and clarify parts of my writing and brainstorming assistant throughout the research and thesis writing process.

TABLE OF CONTENT

LIST OF FIGURES

LIST OF TABLES

List of Abbreviations & Acronyms

BPM	Best Management Practices
BSB	Bare Soil Before
CCD	Coherence Change Detection
CP	Cropping Patterns
DOY	Day of Year
DpRVI	Dual-polarization Radar Vegetation Index
ESA	European Space Agency
GSD	Ground Sampling Distance
HR	High Resolution
HRL	High Resolution Layer
IEEE	Institute of Electrical and Electronics Engineers
IGARSS	International Geoscience and Remote Sensing Symposium
IW	Interferometric Wide Swath
L7	Landsat-7
L8	Landsat-8
L9	Landsat-9
LPIS	Land Parcel Identification System
MMU	Minimum Mapping Unit
MR	Medium Resolution
NBR2	Normalized Burn Ratio
NDVI	Normalized Difference Vegetation Index
OA	Overall Accuracy
PA	Producer Accuracy
RCM	Canada’s RADARSAT Constellation Mission
S1	Sentinel-1
S2	Sentinel-2
SAR	Synthetic Aperture Radar
SLC	Single Look Complex
SVM	Support Vector Machine
UA	User Accuracy
VH	Vertical send and Horizontal receive polarization
VV	Vertical send and Vertical receive polarization

INTRODUCTION

Ensuring food security is fundamental to human development and survival. However, growing global populations combined with escalating climate change impacts have intensified the pressures on agricultural systems, posing significant challenges to maintaining food security (Hou et al., 2021; Tian et al., 2021, Wang et al., 2025).

The environmental toll of conventional agricultural practices has become increasingly untenable. Intensive farming systems—marked by frequent tillage and the extensive use of synthetic fertilizers and pesticides—have contributed significantly to soil degradation, water contamination, and the decline of biodiversity. In response to these adverse impacts, there is growing global interest in regenerative agriculture systems. These approaches offer both economic and ecological benefits, making them attractive to farmers, policymakers, and environmental stakeholders alike. Economically, conservation practices can reduce production costs through lower fuel and labour requirements, enhance yield stability by increasing plant-available water, and ultimately improve profit margins. Ecologically, such systems promote higher soil organic carbon content, greater biological activity, improved soil structure and porosity, enhanced agroecological diversity, and reductions in both soil erosion and greenhouse gas emissions (Derpsch et al., 2010).

Consequently, monitoring conventional agriculture methods across large agricultural landscapes is crucial for understanding land management trends and promoting sustainable practices. Yet, such monitoring remains challenging, particularly when relying on traditional field surveys, which are time-consuming, spatially limited, and often lack temporal precision.

Satellite-based remote sensing provides a promising alternative, offering repeatable, scalable, and timely observations of land surface conditions. Yet, detecting tillage events from space remains difficult due to the subtle and short-lived nature of surface changes, the influence of precipitation, vegetation cover, and soil moisture (Satalino et al., 2018; Robertson et al., 2023).

Therefore, this study aims to contribute to the growing field of remote sensing for agricultural monitoring by evaluating and enhancing radar-based algorithms for tillage detection by building upon prior work.

CHAPTER ONE

LITERATURE REVIEW

This chapter presents an overview of the state of the art on the thesis topic, covering soil management practices and tillage detection algorithms.

1.1. Regenerative and Conventional Agriculture

Regenerative agriculture is an approach to farming that aims to keep ecosystems healthy and resilient, with a strong emphasis on improving soil health. It focuses on crop and livestock production methods that, by working with natural processes, enhance both the quality of farm products and the resources they depend on, such as soil, water, and biodiversity (O'Donoghue et al., 2022). Key practices of regenerative agriculture include keeping the soil covered, minimizing soil disturbance, maintaining live roots in the ground year-round, encouraging diverse plant and animal life, integrating livestock, and cutting back or eliminating synthetic chemicals like fertilizers and pesticides (Ahmed et al., 2021; Sharma et al., 2024).

Regenerative and conservation agriculture approach includes three key pillars:

• minimal soil disturbance through no-till practices: under minimal soil disturbance, two practices—reduced tillage and minimum tillage—are included, both of which are highly beneficial for maintaining proper soil health. With minimal soil disturbance (i.e., no inversion tillage), arthropod habitats are less disrupted, creating micro-environments that support their growth, development, and survival (Nunes et al., 2020; and Jacobsen et al., 2022; as cited in Jasrotia et al., 2023).

• maintaining a permanent soil cover: the main practices under this principle include organic amendments, mulching, and cover crops. Permanent soil cover is crucial for protecting the soil from the adverse effects of changing weather, such as heavy rainfall and direct sunlight. It also modifies the soil microclimate, providing shelter for both micro and macro-organisms, which in turn enhances soil biodiversity (Ghosh et al., 2010; and Bhan and Behera, 2014 as cited in Jasrotia et al., 2023).

• species diversification (implementing crop rotations): intercropping and mixed cropping are the primary practices under this principle. Diversifying crop rotation involves a system that includes three or more different crops. In addition to providing a varied "diet" for soil microorganisms, crop rotations offer different types of habitats for both flora and fauna. Enhanced soil health may help reduce the incidence of insect pests, weeds, and diseases through improved biological control (Dumanski et al., 2006; Kassam et al., 2009; and Wang et al., 2021 as cited in Jasrotia et al., 2023).

Cover crops play a vital role in enhancing the accumulation of organic matter on the surface soil horizon. This effect is further amplified when combined with no-tillage. Higher levels of carbon and nitrogen have been reported under no-tillage and conservation tillage systems compared to conventional ploughing since covering the field can enhance soil biodiversity, boosts soil biological activity, and promotes carbon sequestration (Hobbs et al., 2008).

Conventional agriculture, on the other hand, refers to a farming approach characterized by intensive practices aimed at maximizing yields and economic efficiency. Central to this approach is a strong reliance on synthetic inputs, including chemical fertilizers and pesticides, coupled with intensive tillage and limited crop rotation. These strategies are predominantly yield-driven, often disregarding the substantial production costs associated with machinery, labour, fuel, and tillage equipment. The environmental repercussions of such practices are considerable. Conventional systems contribute to both physical and biological soil degradation, evidenced by significant losses in soil organic carbon and declines in soil biodiversity. This deterioration undermines overall soil health. Furthermore, the continual stress placed on the soil ecosystem diminishes its resilience, weakening its capacity to withstand climatic extremes such as droughts and increasingly frequent and severe rainfall events. These climate-related disruptions, in turn, threaten the long-term sustainability of crop productivity (Al-Kaisi and Lal, 2021; as cited in Sumberg and Giller, 2022).

1.2. Soil Management Practices

Tillage practice is manipulating the soil mechanically in order to increase the crop production. This will significantly affect the characteristics of soil such as temperature, water content, infiltration, and evapotranspiration processes (Busari et al., 2015). Tillage practices have increased agricultural productivity but if done continuously, can have disruptive effects on soil structure, organic matter loss, and soil erosion acceleration (Lal, 1993; Hassan et al., 2022).

Tillage practices are usually classified into either “conventional” or “conservation” tillage based on crop residues management and tillage depth.

1.2.1. Conventional Tillage

Conventional tillage involves high degree of soil disturbance by mixing soil surface layers. These practices change soil structure and environment and leave less than 30% of crop residues on the soil surface (FAO, 2001). Conventional tillage is a series of operations which are typically categorised as either "primary" or "secondary" tillage. The main objective of primary tillage is to control weeds and bury crop residues, while secondary tillage aims to prepare a firm seedbed that promotes good germination (FAO, 2001). Conventional tillage involves deep ploughing and disc harrowing (Gupta Choudhury et al., 2014) and can reach depths of up to 50 cm (FAO, 2001).

Conventional tillage initially enhances soil chemical and physical properties, such as drainage and bulk density. It mechanically controls weeds, diseases, and pests by incorporating crop residues into the soil. Additionally, deep ploughing helps disrupt compacted shallow layers, promoting root penetration and growth. However, over time, it leads to soil degradation. The repeated practice of ploughing at the same depth results in a compacted subsurface layer that obstructs soil pores and hinders drainage. Furthermore, frequent tillage accelerates soil moisture loss and has a major impact on soil microorganisms, disrupting biological activity and biodiversity due to excessive disturbance and the removal of surface residues. It also hastens the decomposition of organic matter. Ultimately, conventional tillage depletes and damages natural resources (FAO, 2001; FAO, n.d.; Busari et al., 2015). Figures 1.1 to 1.5 illustrate conventional tillage practices and the machinery used to implement them.

Figure 1.1: Deep tillage. Adapted from Shutterstock (2024), https://www.shutterstock.com/.

Figure 1.2: Disc plough. Adapted from JCBL (2024), https://tinyurl.com/bdd6yfj5.

Figure 1.3: Disc ploughing. Adapted from QUIVOGNE (n.d.), https://tinyurl.com/nhhev2sy.

Figure 1.4: Moldboard plough. Adapted from JCBL (2024), https://tinyurl.com/bdd6yfj5.

Figure 1.5: Moldboard ploughing. Adapted from Riechmann Bros (n.d.), https://tinyurl.com/4zfnty49.

1.2.2. Conservation Tillage

Conservation tillage is an important part of regenerative agriculture. These practices leave at least 30% of crop residues on the soil surface to protect the soil from direct impact of sunlight and raindrops (FAO, 2001). Depending on factors such as climate, soil properties, and crop characteristics, conservation tillage can vary from reduced or no-till methods to more intensive tillage practice (mulch tillage, ridge tillage, contour tillage) (Okorie and Niraj, 2022; Busari et al., 2015). Figures 1.6 and 1.7 illustrate conservation tillage practices.

Figure 1.6: Strip till, Adapted from KUHN (n.d.), https://tinyurl.com/nhhwakza.

Figure 1.7: Ridge tillage, Adapted from Kristensen et al., 2006.

The shift from conventional tillage practices to conservation tillage practices, if done in alignment with conservative agriculture principles, can improve soil structure and soil organic carbon, minimize soil erosion risks, decrease fluctuations in soil temperature, and improve soil quality (Busari et al., 2015). Hence, the monitoring and mapping of conventional tillage practices are essential, as they enable the assessment of progress toward sustainable agricultural practices.

1.3. Basic Principles of SAR Remote Sensing

One of the main advantages of using remote sensing to monitor agricultural practices is its ability to continuously and consistently observe changes over time and space (Thenkabail, 2010). The most common method of environmental monitoring using satellite remote sensing is the use of optical imagery. However, clouds and cloud shadows are a drawback of optical sensors, resulting in missing data and gaps in optical imagery. In contrast, microwave radiation has wavelengths above the size of cloud particles, allowing it to pass through clouds unaltered. One sensor that takes advantage of active microwave radiation is synthetic aperture radar (SAR) (Van Tricht et al., 2018; Joshi et al., 2016).

SAR sensors have shown high potential in detecting bare soil surface characteristics because of how they impact the radar signals. Soil moisture and soil roughness are two soil characteristics that affect many processes on soil surface such as infiltration and decomposition of particles. Soil moisture affects the signal based on the soil dielectric properties, while soil roughness influences how the radar waves are reflected and as a result, the intensity of the reflected signal (Baghdadi et al., 2012).

To effectively analyse the interactions between radar signals and soil surface characteristics, it is essential to understand key SAR variables that describe these interactions. Two important variables are the backscatter coefficient and the coherence, which provide valuable insights into the physical properties and temporal changes of the soil surface. These variables are derived from SAR observations, in which sensors emit microwaves and record the amplitude and phase of the signals backscattered from the ground surface.

1.3.1. Coherence

Coherence measures the spatial alignment of phase and amplitude information between two complex SAR signals acquired over the same area at different times, with values ranging from 0 to 1. It reflects how well the signals match within a specified window area. If the observed ground surface changes between these periods, the distance from the satellite shifts, causing variations in phase and amplitude. Coherence is therefore sensitive to surface changes, detecting shifts below the microwave wavelength and making it useful for monitoring changes in the Earth's surface (McNairn et al., 2024; Cho et al., 2023).

To calculate coherence, SAR images from two periods with identical observation conditions are aligned, and a complex correlation is performed. For two consecutive SAR images, S1 and S2, coherence is calculated using the following equation (Voormansik et al., 2020):

$$\gamma = \frac{|\langle s_1 s_2^* \rangle|}{\sqrt{\langle s_1 s_1^* \rangle \langle s_2 s_2^* \rangle}}, \quad 0 \leq \gamma \leq 1$$

Here, * represents the complex conjugate, and ⟨ ⟩ denotes the averaging process.

1.3.2. Backscatter Coefficient

The backscatter coefficient represents the ratio of the power of a scattered wave received at the radar's location from a unit ground area to the power of a uniformly scattered wave when microwaves hit the same area. This coefficient indicates the strength of the signal received. Because the received wave's power changes with observation conditions—such as the distance between the satellite and Earth's surface, wavelength, and incidence angle—the signal can be converted to a backscatter coefficient. This standardization allows for comparison between images taken under different observation conditions. The backscatter coefficient is calculated using the following equation (Cho et al., 2023):

$$\sigma^0 = 10.\log_{10}(DN^2)$$

In this context, σ^0 represents the backscatter coefficient in decibels, and DN is the Digital Number (amplitude value of the pixel in the Sentinel-1 (S1) GRD image).

To further understand the variation in backscattered signals, it is important to distinguish between surface and volume scattering, two key mechanisms that influence how radar waves interact with the ground. Volume scattering involves multiple interactions within a medium, such as a forest canopy or layers of soil or snow, where radar waves are scattered by particles located at different heights or depths. In contrast, surface scattering involves single or multiple interactions at the surface, where radar waves are directly reflected or scattered by the ground or surface features, affecting the return signal (Joerg et al., 2017; Syahali & Ewe, 2016).

These scattering mechanisms directly affect the radar backscattering signal, which is highly sensitive to surface roughness. When the surface is smooth, only specular reflection occurs and no signal reaches the antenna, therefore, it would appear dark, whereas in rougher surfaces, the ratio of specular reflection decreases and the wave is diffused in all directions, which making it appear brighter. Additionally, the radar signal is influenced by radar parameters such as incident angle, wavelength, and polarization (Sabery et al., 2021; Baghdadi et al., 2012; Srivastava et al., 2006). Figure 1.8 shows backscattering signals based on the surface roughness.

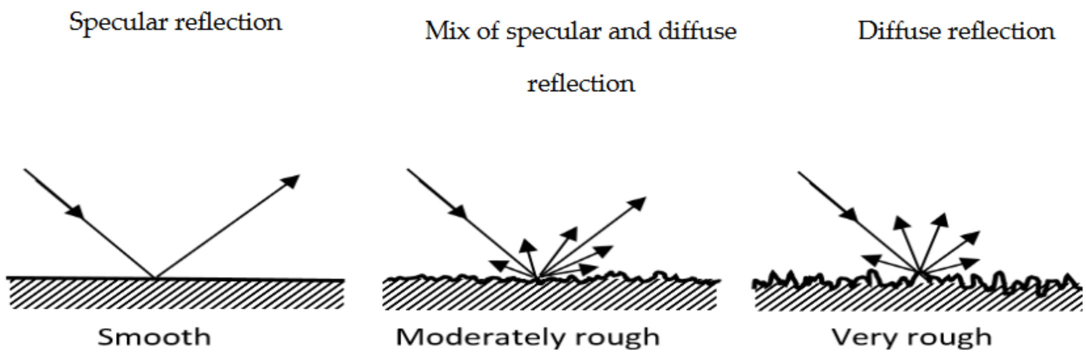

Figure 1.8: radar reflection from smooth and rough surfaces, showing specular and diffuse reflections (Sabery et al., 2021)

The surface roughness magnitude is a function of frequency and incident angle, meaning that the classification of the surface into smooth and rough can change with the SAR sensor parameters. According to Fraunhofer criterion, the surface appears smooth if its rms height (h) follows the equation below where θ is the incidence angle (Srivastava et al., 2006):

$$h < \frac{\lambda}{32\cos(\theta)}$$

The unit of h is length, depending on the units used for the wavelength, it could be metres, nanometres, etc. Cut-off values of rms height for a surface to be detected as smooth at 45° incidence angle is given in Table 1.1.

Table 1.1: rms height for a surface to be detected as smooth at 45° incidence angle at C, L and P-bands (Srivastava et al., 2006).

Wavelength (λ)	Smoothness criterion (h <)
5.6 cm	0.25
23.5 cm	1.04
85 cm	3.76

Radar Parameters Influencing Backscattering Signals

As mentioned earlier, radar signals are influenced by factors such as frequency, which determines how well the signal can penetrate different surfaces. Lower frequencies, such as those in the L-band, can penetrate the canopy and interact with both the stem and the underlying soil, even reaching deeper layers. On the other hand, C-band frequencies tend to be reflected more by the canopy itself or the topsoil in case of bare surface, while shorter wavelengths, such as those in the Xband, interact mainly with the top of the canopy (Sivasankar et al., 2018, Balenzano et al., 2011). The microwave frequency bands utilised in remote sensing applications, along with their respective frequencies and wavelengths, are enumerated in Table 1.2.

Table 1.2: SAR frequency bands used in remote sensing and their associated frequency and wavelength range (Sivasankar et al., 2018).

Band	Frequency (GHz)	Wavelength (cm)
P	0.23 - 1	3 - 130
L	1 - 2	15 - 30
S	2 - 4	7.5 - 15
C	4 - 8	3.75 - 7.5
X	8 - 12.5	2.4 - 3.75

Incident angle also plays a significant role in how radar signals interact with agricultural targets. At lower incidence angles, the radar signal can pass through vegetation and interact with the soil beneath. However, at higher incidence angles, the signal is more affected by the crops and vegetation on the surface (Sivasankar et al., 2018; Srivastava et al., 2006). For rough surfaces, the strength of the SAR backscatter signal remains relatively consistent between low and high incidence angles. In contrast, for smooth surfaces, the backscatter signal at higher incidence angles is significantly weaker than at lower incidence angles. This results in a larger difference in backscatter values (σ_{low}^{0} - σ_{high}^{0}) for smooth fields, while rough fields exhibit a smaller difference. The angular response of multi-incidence angle SAR data can be used to distinguish tilled field from others. However, the time difference between the acquisition of low and high incidence angle SAR data can limit the effectiveness of this matter, especially when there is a significant time gap between passes (Srivastava et al., 2006).

The final radar parameter to be considered is that of polarization, which plays a crucial role in determining how the radar signal interacts with different surfaces. Polarization refers to the orientation of the plane in which an electromagnetic wave oscillates. In radar systems, signals can be transmitted and received in different polarizations by controlling the polarization settings in both the transmission and reception paths. For example, a signal transmitted in vertical polarization and received in horizontal polarization is denoted as VH. Similarly, a horizontally transmitted and horizontally received signal is denoted as VV, and other combinations follow the same convention (NASA, n.d.). By manipulating the signal's polarization, either in horizontal or vertical, it is possible to enhance the radar's sensitivity to specific targets, such as soil or vegetation (Sivasankar et al., 2018). The dual-polarization of X and C-band backscattering coefficients has been employed to discern variations in soil roughness attributable to different tillage practices (Zhang, 2024). Figure 1.9 presents the different polarization combinations commonly used by SAR sensors.

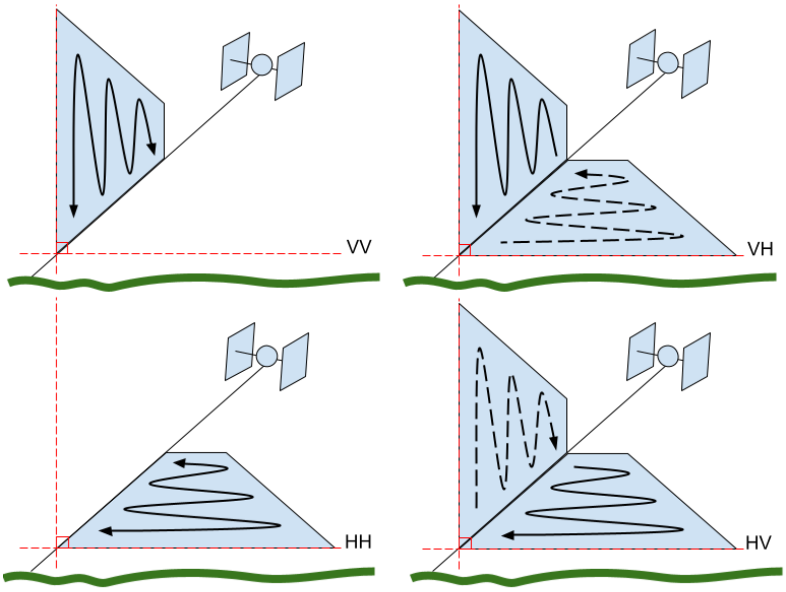

Figure 1.9: SAR signals transmitted and received either vertically (V) or horizontally (H) - transmit listed first, receive second, Adapted from ASF (n.d.), https://tinyurl.com/yhyujt4a.

1.4. Accuracy Metrics for Detections

Overall Accuracy (OA) is the most widely reported metric and is calculated as the ratio of correctly classified instances (TP and TN) to the total number of cases (TP + TN + FP + FN), as shown below (Harikrishnan,2019):

$$Overall\ Accuracy = \frac{TP + TN}{TP + TN + FP + FN}$$

Despite its popularity, OA can be misleading, particularly in cases where class distributions are imbalanced. It treats all types of classification errors equally and does not distinguish between false positives and false negatives.

To gain a more nuanced understanding of model performance, additional metrics such as precision and recall are often used. Precision reflects the proportion of correctly predicted positive cases relative to all predicted positives, while recall, also known as sensitivity, indicates the proportion of actual positives correctly identified (Harikrishnan,2019).

$$Precision = \frac{TP}{TP + FP}$$

$$Recall = \frac{TP}{TP + FN}$$

The F1-score offers a balanced metric by taking the harmonic mean of precision and recall, making it especially useful when evaluating models under class imbalance.

$$F1 - score = 2 \times \frac{Precision \ \times Recall}{Precision + Recall}$$

1.5. Tillage Detection Methods

This section provides an overview of various methods developed for the detection of tillage practices. For each case, key aspects including the study area, methodology, results, and accuracy are presented. A concise summary of this review is provided in Table 1.3.

1.5.1. KappaZeta

KappaZeta is a company based in Estonia, specializing in AI-driven satellite data analytics with expertise in radar remote sensing. They have developed an AI-based tillage detection algorithm that utilizes satellite remote sensing data from the Baltic Sea region. The study encompasses Sweden, Denmark, Finland, Estonia, Latvia, Poland, Northern Germany, and Lithuania. This algorithm is designed to classify tillage practices to support sustainable agricultural management, relying on a combination of multi-sensor satellite data and ground truth information. The research is funded by the European Space Agency and is being developed over the period 2024–2026. Although no scientific publications on the algorithm are available yet, the following information was obtained from the company's website and a webinar held in August 2024.

a. Study Area

The ground truth data, crucial for model training and validation, were sourced from farmers and agricultural agencies, totalling 8,766 data points. These data were collected from Finland (2020–2021), Estonia (2018–2022), Denmark (2022), Sweden (2021–2022), and Lithuania (2022). Data from Poland and Northern Germany were included, but the exact years of collection are not given. However, the dataset was still insufficient for robust model training. Therefore, they supplemented the model with high-resolution imagery from Google Earth and orthophotos.

b. Methodology

The tillage detection algorithm integrates spectral indices derived from multi-sensor satellite time series. S1 (backscatter and coherence), S2, and Landsat-8 and Landsat 9 data are being used. The workflow begins with preprocessing satellite imagery and generating time-series coherence data. The input data are classified into three tillage categories based on crop residue cover after harvest:

- Conventional tillage: Leaves <15% crop residue.
- Conservation tillage: Leaves 15–30% crop residue.
- Zero tillage: Retains > 30% crop residue.

Moreover, 6 days and 12 days coherence intervals were evaluated for detecting tillage events. The dataset of 6-day coherence model was divided into Nordic countries (Sweden, Denmark, Finland) and Baltic Sea countries (Estonia, Latvia, Poland, Northern Germany, and Lithuania) to improve regional performance. Twelve-day coherence model was applied uniformly across all countries, benefiting from a larger ground truth dataset and providing enhanced detection accuracy. Additionally, the conservation tillage algorithm focuses only on crop types that are common in Europe—maize, wheat, oat, barley, and rapeseed—to simplify classification and enhance performance.

c. Result

The algorithm classifies tillage practices by detecting changes in crop residue cover using time-series data. While conventional tillage was detected with high accuracy, conservation tillage presented challenges due to the variability in crop residue influenced by environmental conditions, particularly rainfall. For example, wet residues were often misclassified as absent due to limited training data covering such scenarios.

d. Validation and Performance

The model's performance was evaluated using F1-scores for both conventional and conservation tillage detection. The F1-score evaluates a model's accuracy, which has imbalanced datasets, by using the confusion matrix to calculate precision (User Accuracy – UA) and recall (Producer Accuracy – PA) and combines these metrics to measure how effectively the model makes correct predictions across the entire dataset. For conventional tillage, the 6-day coherence model achieved an F1-score of 89.2% in the Nordic region, while the Baltic Sea countries performed better with an F1-score of 94.9%. The 12-day coherence model, benefiting from a larger training dataset, further improved performance with an F1-score of 95.4%. Conservation tillage detection was more challenging due to the variability in crop residue. The 6-day coherence model yielded an F1-score of 86.3%, whereas the 12-day coherence model achieved a slightly lower score of 83.4%.

Two key limitations adversely affected the model's overall performance. First, variability in crop residue frequently led to misclassifications. Second, a regional bias—caused by sparse ground truth data in Northern Germany and Poland—compromised the model's accuracy in these areas.

1.5.2. Satalino et al.

A notable algorithm is proposed by Satalino et al. in 2018 and further developed in 2024, which employs S1 and S2 data to identify tillage practices, using bare or sparsely vegetated crop fields. This approach is grounded in the integration of SAR and optical data, providing a framework for detecting tillage-induced changes in the landscape. This algorithm encompasses Italy and Spain data. The following information is based on the conference paper published in IEEE International Geoscience and Remote Sensing Symposium (IGARSS) in 2018 and later in 2024.

Satalino et al., 2018

a. Study area

The primary test site was the Apulian Tavoliere plain in southern Italy – a semi-arid, extensive cereal-growing area, where intensive tillage is common. Ground truth data was collected in 2015.

b. Methodology

The approach leverages both radar and optical satellite data. SAR images are processed into time-series of co-registered backscatter (VH and VV polarizations) at approximately 100m resolution. S2 multi-spectral imagery is used to derive the Normalized Difference Vegetation Index (NDVI), which identifies bare or sparsely vegetated fields. Fields with NDVI below a set threshold were considered sufficiently bare for tillage detection.

The algorithm implements a multi-temporal, multi-scale change detection on the S1 SAR data. In particular, VH is analysed because of its high sensitivity to surface roughness changes caused by tillage. The method examines changes in VH over time at two spatial scales – the field resolution (~0.1 km – HR) and a broader medium resolution (~5 km – MR). If a significant change in VH occurs on an individual field but no corresponding change is observed over the surrounding 5 km region, it is flagged as a likely tillage event. This two-scale comparison helps decouple local tillage effects from broad-scale disturbances such as rainfall-driven soil moisture changes. In essence, a large VH signal change confined to a single parcel is attributed to a tillage-induced roughness change, whereas widespread VH changes across many fields at once are assumed to be environmental in origin. The classification approach is threshold-based.

c. Results

Detected tillage events appeared as distinct anomalies in the SAR time-series, aligning with known field disturbances. In particular, intense ploughing—characterized by deep soil inversion—resulted in a notable increase in VH backscatter, consistent with the expected rise in surface roughness. Temporally, the method effectively captured the timing of tillage operations throughout the year, successfully identifying events such as post-harvest ploughing and distinguishing them from periods with no soil disturbance.

d. Validation and Performance

First results on data acquired in 2017 indicate that the methodology can identify the tilled/no-tilled classes with an overall accuracy of 83%.

Satalino et al., 2024

a. Study Area

The algorithm leverages a diverse dataset derived from three distinct geographical regions: the Apulian Tavoliere and Jolanda di Savoia in Italy, and Castile and León in Spain. Ground truth data was collected for the Italian sites over the years 2020, 2021, and 2022, while for the Spanish site, data was gathered from 2018 to 2021. This dataset includes detailed annotations of tillage events, including geographic coordinates, the date of the activity (with associated uncertainty), and the type of tillage practice (rolling or ploughing). Notably, the algorithm does not account for harrowing due to its intermediate effects on soil roughness, which are less distinct compared to rolling and ploughing.

b. Methodology

The algorithm's core methodology is based on time-series analysis of both S1 and S2 data. The heart of the change detection approach lies in the use of the S1 cross-polarized backscatter ratio $\tau 21$ (calculated as the ratio of VH backscatter on two subsequent dates) and the co-polarized interferometric (InSAR) coherence ($\rho 21$). These two features exhibit complementary sensitivities to changes in surface roughness. For instance, rolling generally decreases $\tau 21$, indicating a negative change, while ploughing increases $\tau 21$, suggesting a positive change. In contrast, the coherence value $\rho 21$ consistently decreases following tillage practices, irrespective of the type.

S1 provides data at a 40-meter resolution with acquisitions every 6 days, although in 2022 the frequency decreased to every 12 days due to the unavailability of S1B. S2 data, with a higher temporal resolution (5-day acquisitions, except when cloud cover is present), is used to compute the NDVI. To ensure that the two datasets are comparable, the NDVI was resampled to a 40-meter resolution and co-registered with the corresponding SAR observation stacks.

To detect changes at different spatial scales, the algorithm distinguishes between local or high (~0.1 km) Resolution (HR) and medium (~5.0 km) Resolution (MR) changes, the same as the initial algorithm developed in 2018. Tillage events are typically associated with local-scale roughness changes. The algorithm then uses Boolean logic to combine the results of change detection at the HR and MR. The OR operator maximizes the detection of tilled areas by capturing more events, while the AND operator reduces the number of detected events but provides higher confidence, making it suitable for identifying robust tillage changes.

c. Result

Events detected at the MR or both at HR and MR are masked out, while the remaining events are classified as tillage changes. The classification uses a majority rule within the boundaries of agricultural parcels to determine the tillage class. If more than 50% of the pixels in a parcel are detected as tilled, it is classified as tilled (rolling or ploughing); otherwise, it is classified as non-tilled (NT). Additionally, parcels where more than 40% of the pixels are masked at the MR are labelled as non-classified (NC). This approach is applied only to parcels larger than 1 hectare.

d. Validation and Performance

The performance of the algorithm was evaluated using a multi-year ground truth dataset across the three study sites. The OA of the model is 81%. OA evaluates the performance of classification models by measuring the proportion of correctly classified cases out of the total cases. PA for individual tillage classes exceeded 76%, with the rolling class achieving the highest PA of 87%. UA was similarly high, with the NT class yielding the best UA at 88%. However, 27.8% of the events were classified as NC, and 2.7% were masked due to vegetation. For comparison, the algorithm was also tested using the AND operator and by relying solely on incoherent data (i.e., only $\tau 21$). These alternative configurations yielded lower OAs of 76% and 77%, respectively, underscoring the superior performance of the OR operator.

1.5.3. Chome et al.

Chome et al have developed a tillage detection model leveraging unmatched polarimetric and temporal resolutions of S1 SAR C-band data. It aims to identify and classify agricultural practices at the parcel level, such as tillage and cover crop management, while evaluating the influence of observation geometry (ascending vs. descending orbits) on classification accuracy. Using backscatter variations linked to surface roughness and soil moisture, the model was validated against a reference dataset comprising in-situ observations and farmers' declarations, offering insights into field use and tillage practices in southern Belgium's croplands. This study was presented at the Living Planet Symposium held in Prague in 2016.

a. Study Area

The research was conducted in a 14,000 km² agricultural region in southern Belgium (Walloon region), characterized by diverse crops, including winter wheat, barley, beetroot, potato, maize, rapeseed, and legumes. Field data were collected for 535 parcels, with 107 parcels fully described through farmer interviews and the remaining 428 observed in the field.

The dataset included parcel polygons, dates of specific practices (e.g., tillage, ploughing), and field conditions.

b. Methodology

Satellite data were acquired using S1A C-band dual-polarization (VV and VH) sensors. The study utilized 17 descending orbit images (orbit 110) and 16 ascending orbit images (orbit 161), spanning July 4, 2015 to February 17, 2016. Precipitation data from 29 meteorological stations were integrated to mask pixels affected by rainfall exceeding 1 mm within three hours of image acquisition.

The training dataset (286 fields) was refined by removing outliers, defined as fields with backscatter deviations exceeding three root mean square errors. The remaining 142 fields formed the validation dataset. S1 SAR data of the dataset underwent a three-step preprocessing chain using SNAP's S1 toolbox. This included applying precise orbits, calibrating backscatter values, removing thermal noise, debursting, multilooking, and terrain correction using Shuttle Radar Topographic Mission 1-second DEM.

Changes in backscatter coefficients (σ_{VV} and σ_{VH}) were analysed to detect modifications in surface roughness, soil moisture, and crop canopy volume during tillage and cover crop management. Backscatter variations were key indicators:

- Increased backscatter, particularly in VV polarization, signalled tillage due to enhanced surface roughness.
- very limited increase in VV backscatter indicated no-till practices.
- Decreased VH backscatter and backscatter ratios were associated with long cover crops not subjected to tillage until late winter.

c. Result

Field use was classified into four categories: short cover crops, long cover crops, winter wheat, and grasslands. Winter crops like rapeseed were excluded due to their limited presence. The classification employed a Support Vector Machine (SVM) approach using backscatter values (σ_{VV}, σ_{VH}, and their ratios) from both ascending and descending orbits.

Short cover crops, tilled at both installation and destruction stages, exhibited stable backscatter ratios. Long cover crops, tilled later, showed stable VV and decreasing VH backscatter. Winter wheat displayed stable but noisy backscatter patterns, while grasslands consistently had lower backscatter values.

d. Model Validation and Performance

The model's OA ranged from 78% to 80%, varying by field use. Excluding outlier fields improved OA significantly to 87%. The results highlighted better performance for descending orbits (78%) compared to ascending orbits (58%), potentially due to the influence of morning dew on surface humidity, amplifying backscatter differences.

However, challenges arose in classifying winter wheat fields, as their backscatter behaviour is intermediate between that of short and long cover crops, making them more difficult to categorize accurately. Another limitation of the current model is its inability to fully account for the variability in soil conditions, farming calendars, and tillage practices across different regions. Additionally, the influence of acquisition timing and observation geometry on classification accuracy remains uncertain.

1.5.4. Zhou et al.

Zhou et al. developed a classification model to predict conservation agriculture practices in the Walloon region of Belgium by integrating field data, remote sensing techniques, and machine learning methods. A key feature of this model is its ability to differentiate between inversion and non-inversion tillage practices. The algorithm was developed as part of a PhD thesis at Université catholique de Louvain, which was successfully defended in 2024.

a. Study Area

The study was conducted in the Walloon region of Belgium, covering a total area of 16,901 km². Management practices for 247 fields under conservation agriculture were collected for the years 2020–2021 through semi-structured interviews with 221 farmers. The database included details on tillage type(non-inversion/inversion) and depth, direct seeding, livestock presence, and other management aspects. To enhance data diversity, a snowballing method was used to identify additional farmers.

b. Methodology

SAR data from Sentinel-1 was used for tillage detection, while precipitation data and spectral indices—specifically NDVI and the Normalized Burn Ratio 2 (NBR2)—were employed to assess soil cover extent and differentiate between bare soil and cover crops. Phenological information, dominant crop types, and vegetation index thresholds facilitated the identification of cover crops. NDVI and NBR2 values were analysed during the intervals between annual cropping cycles (referred to as "inter" periods), which were classified into three categories: cover crop, bare soil, and fallow. To mitigate moisture-related effects on NBR2, data points associated with precipitation exceeding 2.5 mm were excluded. Growing seasons were delineated based on NDVI thresholds, and the temporal overlap between annual crops and cover crops was used to quantify the presence and duration of cover cropping.

c. Result

Conservation and conventional agricultural practices were classified using a random forest algorithm, with key indicators derived from a combination of time-series spectral and meteorological data. Tillage practices were evaluated based on the length of intervals between annual crops. Short intervals—defined as periods of less than 30 days—were excluded, as satellite imagery lacked the temporal resolution to reliably detect tillage activities during such brief windows. For longer intervals (greater than 30 days), two modelling approaches were applied. In the absence of cover crops, tillage was classified using a model (Model I) based on the mean and minimum values of NBR2, NDVI, and radar backscatter (VV and VH). When cover crops were present, a second model (Model II) was employed, which incorporated not only the spectral indices but also the proportion of cover crop and bare soil durations to improve classification accuracy.

d. Model Validation and Performance

The models were validated using 10-fold cross-validation, and their performance was further evaluated through an external accuracy matrix provided by Soil Capital. For the classification of cover crops and soil cover, the model achieved an overall accuracy of 86% when compared to observed data from Soil Capital. In the classification of non-inversion and inversion tillage practices, the model reached an accuracy of 66% based on 10-fold cross-validation using interview datasets. This accuracy improved to 76% when externally validated against Soil Capital data.

A key challenge encountered in this study was the detection of short-term tillage activities. Due to the rapid completion of soil preparation, such events often fall outside the temporal resolution of satellite imagery, making them difficult to capture. This limitation highlights the broader difficulty of accurately classifying tillage practices that occur within short temporal windows.

1.5.5. Robertson et al.

Robertson et al. developed an algorithm using coherence to detect post-harvest tillage activities. The following information is based on the paper published in Heliyon in 2023.

a. Study area

The study was conducted in the Medway region of southern Ontario, Canada, located north of London. This predominantly agricultural area is primarily devoted to the cultivation of corn, soybean, and wheat. Ground truth data were collected from 101 agricultural parcels, with field surveys conducted approximately on a weekly basis. These surveys recorded key management activities in details, including harvesting, tillage, cover crop seeding, chemical termination, and instances of no change.

b. Methodology

The study leveraged C-band SAR data from both the European S1 and Canada's RADARSAT Constellation Mission (RCM) to monitor field activities during autumn. A time series of SAR images was acquired over the study area, and sixteen coherence change detection (CCD) image pairs were generated, each representing coherence between two acquisitions separated by a short interval. The core principle is that if a field's surface remains unchanged between dates, SAR phase coherence remains high; in contrast, management events such as harvesting or ploughing disturb the soil or crop structure, leading to a drop in coherence. The method also accounts for background coherence, which should remain high during localized field changes—otherwise, a drop in coherence may be attributed to broader factors like precipitation.

SAR data processing was carried out using ESA's SNAP software to compute coherence for each image pair. Coherence values were extracted at the field level and compared to observed field activities. Additionally, RCM's polarimetric capabilities were used to calculate the Volume/Surface scattering ratio (V/S) for each field. The V/S ratio offered complementary insight into scattering mechanism changes, supporting interpretation of whether a coherence drop resulted from vegetation removal or soil disturbance.

c. Results

Coherence metrics provided valuable insight into the nature of agricultural activities. Specifically, coherence values enabled the differentiation between field operations such as tillage and harvest and further allowed distinctions among harvest events based on crop type. Fields that underwent a change between SAR acquisitions exhibited a marked drop in coherence—often falling below 0.20—while fields that remained unchanged retained substantially higher coherence values. Importantly, the integration of S1 and RCM data significantly improved the temporal resolution of activity detection. This multi-sensor CCD approach enabled the timing of events to be narrowed down to just a few days.

d. Validation and Performance

Statistical analysis showed that 89.5% of fields that were tilled were correctly identified by the coherence-based approach. Additionally, the timing of tillage operations for corn, soybean, and wheat fields could be narrowed down to a four-day window, highlighting the method's temporal precision.

However, several limitations were noted. First, SAR coherence alone cannot distinguish all types of changes without ancillary information; accurate interpretation often requires additional data such as crop type or management records. Second, the effectiveness of CCD is dependent on the timing of image acquisitions. If multiple operations occur between consecutive SAR images (e.g., harvest followed by tillage), the resulting coherence change may reflect a combined signal, making it difficult to separate individual events. Finally, environmental factors can influence coherence and, consequently, model performance. Changes in soil moisture or heavy rainfall between acquisitions may reduce coherence even in the absence of agricultural activity. Similarly, wet soil conditions or vegetation regrowth—such as the emergence of cover crops—can also affect coherence and must be considered during interpretation.

1.5.6. Summary of Tillage Detection Methods

To conclude the comparison of the algorithms, Table 1.3 presents a summary of the tillage detection algorithms evaluated in this study.

Table 1.3: Summary of benchmarking tillage detection methods

Algorithm	Satellite	Model type	Indicators	Accuracy	Limitations
KappaZeta (2024)	S1, S2, L8, L9.	Learning-based	- Coherence - Crop residue cover	F1-score: - 6-day model= 89.2% - 94.9% - 12-day model = 95.4%	- Misclassification due to precipitation - regional bias stemming from sparse ground truth
Satalino et al. (2018)	S1, S2	Rule-based	- VH backscatter - NDVI	OA = 83%	-
Satalino et al. (2024)	S1, S2	Rule-based	- VH ratio - Coherence - NDVI	- OA = 81% - PA of individual tillage classes = 76%	-
Chome et al. (2016)	S1	Learning-based	Backscatter ratio	OA = 78% to 80%	- Lacks regional adaptability, - Uncertain impact of acquisition timing and geometry
Zhou (2024)	S1, S2, L7, L8.	Learning-based	- NDVI - NBR2 - Backscatter	OA = 66% (10-fold cross-validation)- 76% (external validation)	Detection of short-term tillage activities
Robertson et al. (2023)	S1, RCM.	Rule-based	- Coherence	OA= 89.5%	- Needs ancillary data

			- V/S		- Time sensitivity to image intervals - Environmental effects on coherence

1.6. Copernicus High Resolution Layer Croplands Product

The Copernicus High Resolution Layer (HRL) Croplands product, developed under the European Union's Copernicus Land Monitoring Service, provides comprehensive and consistent annual information on agricultural land use across Europe. The HRL Croplands product includes multiple thematic layers that offer insights into crop types and cropping patterns (CP) at high spatial resolution (10 m). The Minimum Mapping Unit (MMU) of the CP product is 0.25 ha and is available for the period of 2017 to 2021 (CLMS, n.d.).

The CP layer provides detailing critical agricultural characteristics over annual arable lands. These attributes are extracted through the analysis of time series data from Sentinel-1 and Sentinel-2 imagery, enabling the identification of phenological events and temporal land cover dynamics. The HRL Croplands product covers five thematic domains, each accompanied by a confidence layer (CLMS, n.d.):

1. Main Crops: Includes dates of emergence and harvest, as well as the duration of the main growing season.
2. Bare Soil Periods: Captures the length of bare soil presence before and after the main growing season.
3. Secondary Crops: Identifies secondary cropping events—typically occurring during off-season periods—providing details on their emergence and duration.
4. Fallow Land: Maps temporarily uncultivated cropland, with information on spatial extent and the duration of the fallow period for each year.
5. Annual Crop Characteristics: Describes the number of growing seasons per year (up to two) and outlines crop rotation patterns.

1.7. Conclusion on Current State of the Art

This chapter provides an overview of conventional agricultural practices and their alternatives, with a focus on the role of remote sensing, particularly SAR imagery, in monitoring these practices. SAR remote sensing has proven effective in detecting land preparation activities, such as tillage, by capturing changes in surface characteristics. Among the various change detection methods, InSAR coherence has demonstrated promising results in identifying these changes.

Additionally, this chapter compared six tillage detection algorithms, each utilizing distinct indicators and change detection techniques. These algorithms offer valuable insights into the application and effectiveness of remote sensing for tillage detection, highlighting the strengths and challenges associated with each approach.

Finally, this chapter presented an overview of the Copernicus CP product, which offers detailed information on phenological events and temporal dynamics of land cover.

CHAPTER TWO

OBJECTIVES

The main objectives of this master's thesis are threefold. First, to assess the data quality and performance of the Copernicus Cropland product in detecting the bare soil period. Second, to develop a tillage detection algorithm backed up by literature and evaluate its performance. Finally, to integrate the Copernicus-derived bare soil period into the algorithm and validate the results using in-situ observations.

The first and third objectives hold particular relevance for agricultural monitoring, as the bare soil period is a critical indicator for soil management activities, including tillage. By assessing the quality, accuracy, and applicability of this newly available service, the study aims to contribute to more precise soil management practices and reduce misclassification errors. Furthermore, incorporating the Copernicus product into existing methodologies may enhance the overall robustness of tillage detection frameworks.

With respect to the second objective, this study explores the potential of Sentinel-1 SAR data for detecting tillage events, emphasizing the integration of backscatter and coherence metrics. Specifically, the study aims to:

1. Evaluate the performance of backscatter and coherence indicators—both independently and in combination—for detecting tillage events, using a reproduced version of Satalino et al. (2018) and Robertson et al. (2023) methods.
2. Conduct a sensitivity analysis to identify optimal threshold values for change detection.
3. Investigate the influence of external factors, such as precipitation and field orientation, on detection reliability.

Collectively, these objectives are intended to improve the methodology for remote sensing-based tillage monitoring and provide practical insights for the development of scalable, reliable land management tools.

CHAPTER THREE

MATERIALS and METHODS

The subsequent chapter delineates the materials and methods employed to accomplish the stated objectives.

3.1. Data

3.1.1. Ground Truth Data

An intensive field campaign was carried out from March 26th to May 31st, 2021, to collect reference data of 170 agricultural fields, encompassing seven field visits spaced approximately 11 days apart. During each visit, observations were made from adjacent roads, and the surface condition of each field parcel was categorized as *ploughing*, *prepared seedbed*, *crop residuals*, *mounds*, or *covered*. The locations of the surveyed fields are depicted in Figure 3.1.

The Land Parcel Identification System (LPIS) is a digital framework used to record and manage agricultural parcels across European Union Member States (Géoportail de la Wallonie, n.d.). As the field campaign was conducted in the spring of 2021, the LPIS dataset from 2020 was initially used. However, since both parcel geometries and identifiers can change from year to year, a transition from LPIS 2020 to LPIS 2021 was needed to ensure consistency and comparability with other datasets from 2021 employed in this study.

This dataset was used solely as a validation set for the first objective of this study and was subsequently divided into calibration and validation subsets for the second and third objectives.

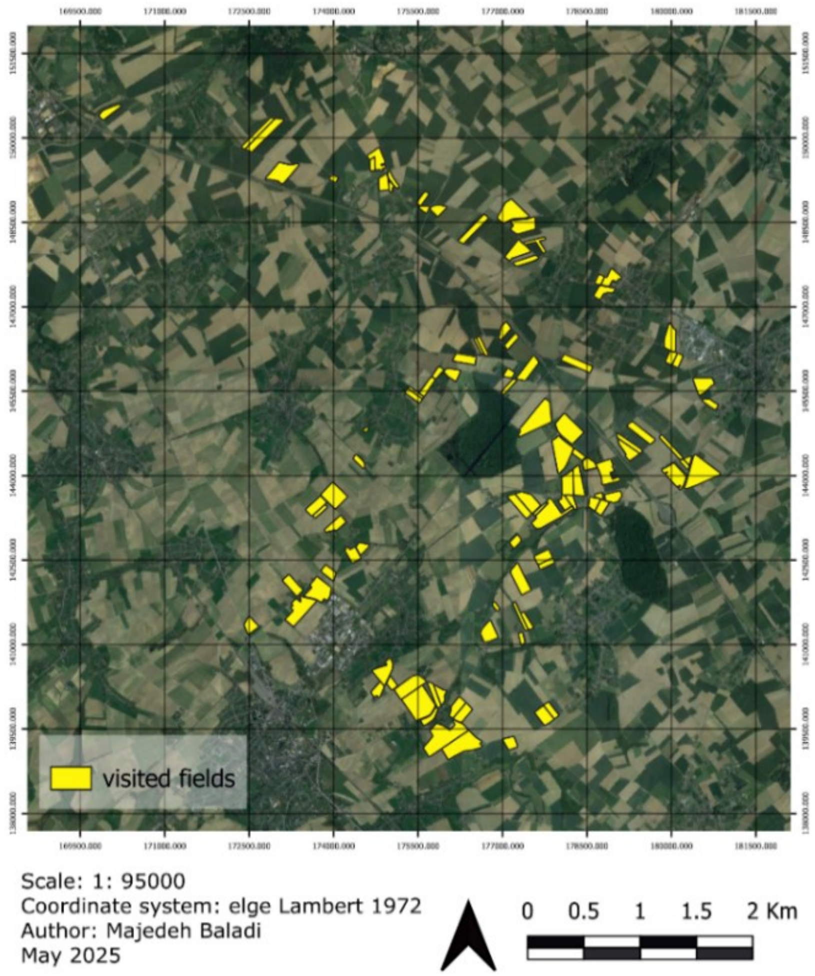

Figure 3.1: Map of the fields visited during the 2021 field campaign, with visited parcels highlighted in yellow. Each field was visited between five to seven times. The figure displays 94 fields due to changes in parcel delineation between the 2020 and 2021 LPIS datasets.

3.1.2. Copernicus CP Product

The CP layer utilized in this study corresponds to the bare soil period, specifically the bare soil before the main crop (BSB). The bare soil layers represent time intervals before and after the primary growing season during which no crop cultivation activities are observed. These periods are delineated based on the detection of crop emergence events within the same year for each individual field.

3.1.3. Satellite Imagery

Sentinel-1 SAR Imagery

Sentinel-1, a key component of the European Union's Copernicus Programme and operated by the European Space Agency (ESA), comprises a constellation of two sun-synchronous, near-polar orbit satellites: Sentinel-1A and Sentinel-1B. Initially, the constellation provided a six-day revisit cycle; however, following the cessation of Sentinel-1B operations on 23 December 2021, the temporal resolution was reduced to a 12-day interval. Operating within the C-band synthetic aperture radar (SAR) frequency range, Sentinel-1 sensors have a central frequency of 5.405 GHz (ESA, n.d.).

The C-SAR instrument onboard Sentinel-1 supports four acquisition modes and is capable of collecting data in multiple polarization configurations, including HH+HV, VV+VH, VV, and HH. In this study, the Interferometric Wide (IW) swath mode and dual-polarization signals (VV and VH) were utilized to derive both SAR backscatter and interferometric coherence products (ESA, n.d.).

Level-1 Single Look Complex (SLC) data were acquired in IW mode during both ascending and descending orbits between January 1st and June 30th. The data acquisitions correspond to relative orbits 37 and 110 for descending pass, and 88 and 161 for ascending pass. In total, 29 images per pass and orbit were acquired. The ascending pass refers to the satellite moving from south to north, typically collecting data in the evening, while the descending pass refers to the satellite moving from north to south, usually during morning hours. These directional differences affect the viewing geometry and surface moisture, which can influence backscatter and coherence measurements. With a ground sampling distance (GSD) of 10 meters, these datasets provide high-resolution measurements of both signal amplitude and phase, essential for the computation of interferometric coherence.

Pre-processing of Sentinel-1 data was carried out using SNAP toolbox. To produce backscatter coefficients (σ^0) for VV and VH polarizations, the following standard processing chain was applied:

1. Splitting of TOPSAR bursts;
2. Application of precise orbit files;
3. Thermal noise removal;
4. Radiometric calibration to σ^0;
5. Debursting of TOPSAR slices;
6. TOPSAR merge.

Sentinel-2 Optical Imagery

The Sentinel-2 mission, developed by ESA as part of the Copernicus Programme, comprises a constellation of twin polar-orbiting satellites equipped with high-resolution multispectral imagers. These instruments capture imagery across 13 spectral bands in the visible, near infrared, and shortwave infrared regions, with spatial resolutions ranging from 10 to 60 meters. The mission provides systematic global coverage of terrestrial surfaces, coastal zones, and inland waters, facilitating applications in land monitoring, agriculture, forestry, and disaster management. A key application of Sentinel-2 data is the derivation of the NDVI, which utilizes reflectance measurements from the red and near-infrared bands to assess vegetation health and density (ESA, n.d.).

3.1.4. Precipitation Data

Given the influence of soil moisture on radar backscatter, precipitation data from AGROMET is incorporated into the analysis. AGROMET is a web-based meteorological platform designed to support agricultural decision-making (CRA-W, n.d.). The platform aggregates data from over 30 meteorological stations within the PAMESEB network, which comprehensively covers the Walloon region. For this study, daily precipitation data, at high spatial resolution (1 km²), were retrieved from the Louvain-la-Neuve station, situated approximately 5 km from the study area. The dataset spans the period from January to June 2021, aligning with the radar data acquisition timeframe.

3.2. Processing

This section, along with Figure 3.2, outlines the processing steps required to prepare the data for algorithm development. These steps include the preparation of field polygons, the extraction of bare soil dates from the Copernicus Cropping Patterns product, and the retrieval of relevant indices from Sentinel-1 and Sentinel-2.

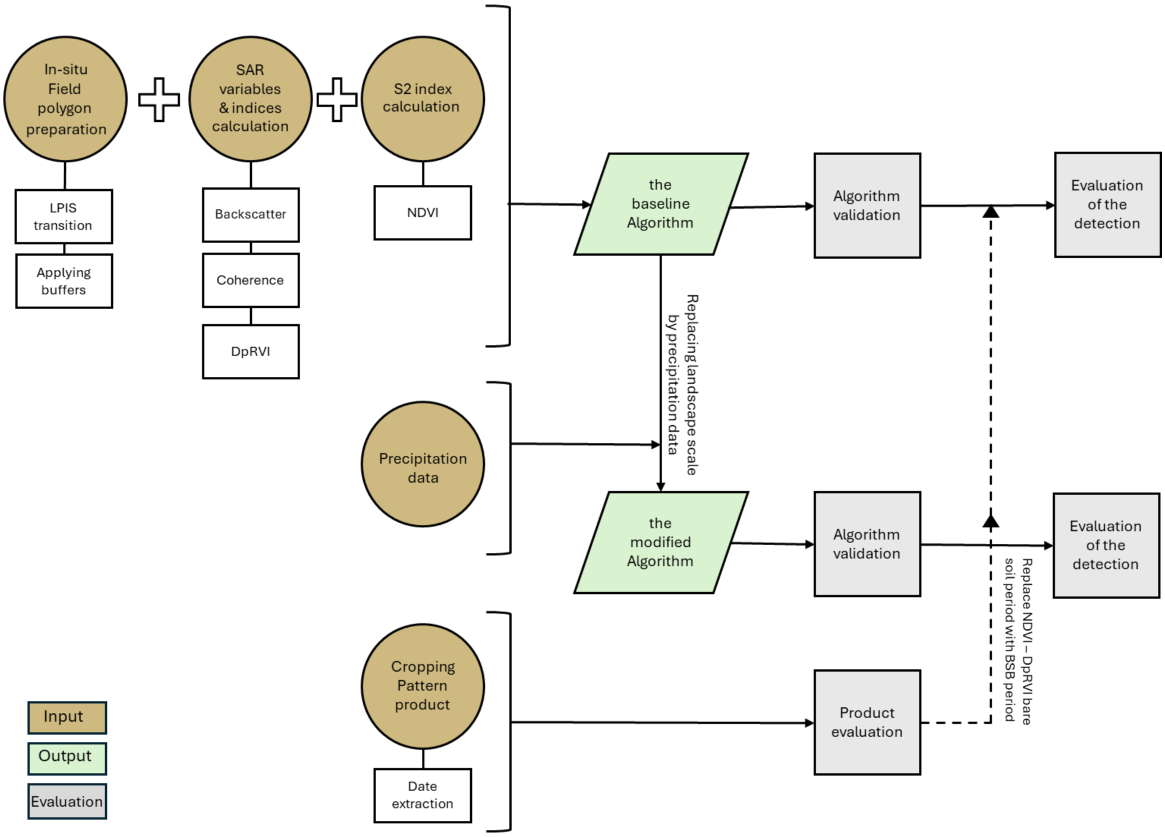

Figure 3.2: Flowchart illustrating the data processing steps and how the resulting inputs were used for developing, modifying, and evaluating the detection algorithms.

3.2.1. Parcel Polygons

As outlined in Section 3.1.1, a transition from the 2020 to the 2021 LPIS dataset was necessary to ensure consistency between field polygon data and the 2021 Copernicus CP data. To define the spatial extent for tillage detection, an outward buffer of 5 kilometres was applied around each field, thereby generating the processing tile. In addition, a 20-meter inward buffer was applied to the field boundaries to enhance the homogeneity of field characteristics and to minimize edge-related noise. This step is particularly important given that subsequent analyses rely on raster data, where field boundaries may influence pixel values. The buffering process helps to reduce the potential impact of mixed pixels along field edges, thereby improving the accuracy of derived statistical measures.

3.2.2. Cropping Patterns Date Extraction

To determine the bare soil period for each agricultural field from the CP dataset, zonal statistics were computed using the Python programming language. This process involved parcel-based averaging to extract a representative value for each field. Since the Copernicus CP express length of bare soil periods in terms of the number of days, while main crop emergence and harvest dates are provided in day-of-year (DOY) format, it was necessary to utilize crop emergence data to define the start and end of the pre-crop bare soil period, and harvest data to delineate the post-crop bare soil period.

In this study, the 25th and 75th percentiles were selected as the primary zonal statistics, instead of commonly used metrics such as mean, median, minimum, or maximum. This choice was made to account for within-field pixel heterogeneity and to mitigate the influence of outlier values. Employing these percentile-based statistics enabled the definition of a time range for both the start and end dates of the bare soil period, thereby providing a measure of temporal consistency. The same methodology was extended to derive a complete crop calendar for each field.

3.2.3. SAR Features and Indices

Backscatter

The computation of backscatter coefficient (σ^0) forms the foundation of the analysis. The formula presented in Section 1.3.2 was employed to derive backscatter coefficient values from the radar backscatter data. To reduce speckle noise and obtain parcel-level insights, zonal statistics were calculated via parcel-based averaging, thereby yielding a single representative value per field. Mean backscatter was computed for both VV and VH polarizations, across ascending and descending passes, covering all four orbital tracks.

Interferometric Coherence

Following a similar approach to that used for deriving backscatter coefficients, mean coherence values for both co-polarized and cross-polarized channels were computed for each agricultural field. These calculations were performed separately for ascending and descending passes using summary statistics, resulting in a single representative coherence value per parcel per acquisition.

DpRVI

The Radar Vegetation Index (RVI) is a widely recognized microwave-based indicator of vegetation cover. It is derived from measured linear scattering intensities of both co-polarized and cross-polarized radar signals and is normalized to ideally range between 0 and 1, with higher values indicating greater vegetation density (Szigarski et al., 2018). Dual-polarization Radar Vegetation Index is calculated using the equation below:

$$DpRVI = \frac{4 \times \sigma_{VH}^0}{\sigma_{VV}^0 + \sigma_{VH}^0}$$

In this context, σ^0 represents the backscatter coefficient in decibels, and VV and VH refer to radar polarization channels.

3.2.4. Sentinel-2 Index

Sentinel-2 images from the same period as the Sentinel-1 data were used to calculate the NDVI. Similar to the calculation of backscatter coefficients and coherence, zonal statistics were applied to obtain a single NDVI value per field. Bands 4 and 8 from the Sentinel-2 imagery were used to compute the vegetation index, following the formula provided below:

$$NDVI = \frac{B8 - B4}{B8 + B4}$$

B4 corresponds to the red band, and B8 corresponds to the near-infrared band.

3.3. Tillage Detection algorithm development (the Baseline Algorithm)

The high-performing and reproducible method employed in this study is based on the approach developed by Satalino et al. (2018; see Section 1.5.2). However, additional steps were incorporated into the analysis, guided by insights from other literature sources such as Robertson et al. (2023; see Section 1.5.5). Figure 3.3 presents the flowchart of the developed tillage detection algorithm.

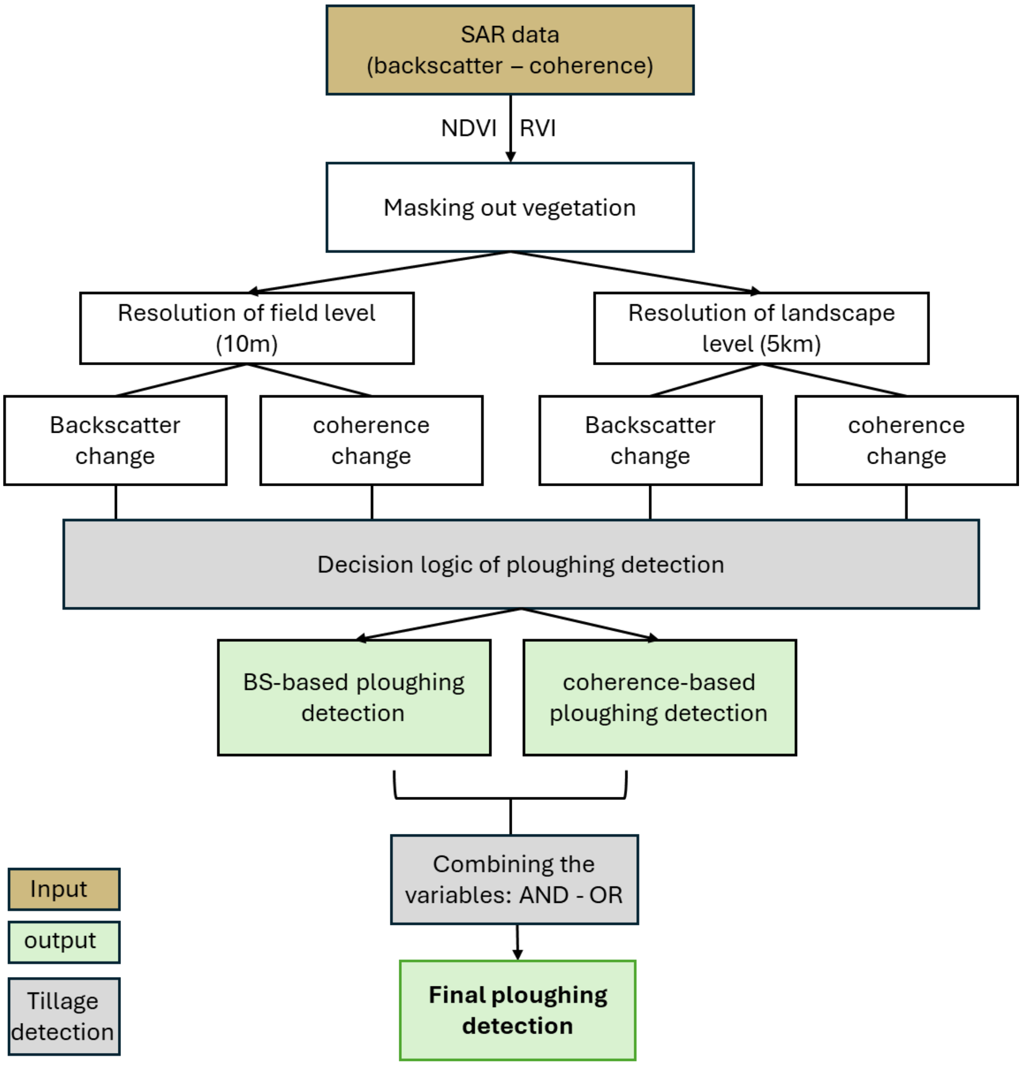

Figure 3.3: Flowchart of the baseline tillage detection algorithm based on methods developed by Satalino et al. (2018) and Robertson et al. (2023).

3.3.1. Backscatter Classification

The first step in developing the algorithm involved identifying the bare soil period for each field. This was accomplished using NDVI and DpRVI values, with thresholds of 0.3 and 0.55, respectively, to delineate bare soil conditions. The NDVI threshold was adopted from Satalino et al. (2018), while the DpRVI threshold was established through a sensitivity analysis aimed at identifying a value that corresponds to the NDVI threshold, given the absence of a widely accepted standard for DpRVI. A six-day rolling window was applied to the time series to reduce potential noise and ensure a more coherent representation of the bare soil period. Following this filtering step, the σ^0 values were computed for each field (referred to as HR – high resolution) using S1 data from VV and VH polarizations and orbits 37 and 110 (descending pass) and 88 and 161 (ascending pass). In parallel, the mean σ^0 within a 5 km buffer surrounding each field was calculated for the same passes and orbits, representing the medium-scale resolution (MR). This additional step was introduced as an alternative approach to account for precipitation effects without relying on external rainfall or soil moisture datasets.

Ploughing activities change surface roughness, which in turn leads to a change in σ^0, typically resulting in an increase. However, similar changes in backscatter can also result from precipitation events or seedbed preparation. To distinguish between tillage and other causes, changes in σ^0 ($\Delta\sigma^0$) were computed between consecutive radar acquisitions at both HR and MR to identify abrupt changes or discontinuities in the soil roughness. Since changes observed in MR are assumed to be primarily driven by precipitation, they were used as a reference to filter out non-field-specific variations from the HR signal. For each time step, $\Delta\sigma^0$ values in HR were compared to those in MR using threshold values established through sensitivity analysis.

Eighty percent of the ground truth data was used to conduct a sensitivity analysis for determining optimal threshold values, while the remaining 20%—comprising 10 tilled and 10 untilled fields—was reserved for algorithm validation. The sensitivity analysis involved incrementally evaluating backscatter change thresholds in 0.01-unit steps, ranging from 0 to the maximum observed backscatter change within the dataset. This systematic approach facilitated the identification of a threshold value capable of more effectively distinguishing tillage-induced changes from other surface variations.

It is important to note that the exact dates of the ploughing events were not recorded in the ground truth data; rather, it was only indicated that ploughing had taken place sometime before the field visit. To address the potential temporal mismatch between field observations and SAR image acquisitions, an event-based approach was employed. Specifically, the analysis focused on identifying field surface transitions – such as from ploughing to seedbed preparation – rather than using every individual field observation. This emphasis on surface change is justified by its direct impact on backscatter intensity. A time window of 0 to +2 days around each identified surface transition was applied for the backscatter-based detection. This choice was informed by the temporal resolution of the SAR imagery: given that the $\Delta\sigma^0$ values were derived from image pairs with a minimum separation of three days, the selected time window effectively accounted for possible discrepancies preceding the transition date. At each threshold increment, the F1-score and overall accuracy were evaluated within this time window to identify the most suitable parameters for reliable classification.

Moreover, the sensitivity analysis contributed to the optimal differentiation between precipitation-induced and tillage-related changes. Once the threshold was established, $\Delta\sigma^0$ values in the high-resolution dataset that coincided with similar changes in the medium-resolution dataset were labelled as *precipitation*, based on the assumption that such overlaps were more likely attributable to rainfall events. The remaining $\Delta\sigma^0$ values in the low-resolution dataset were then categorized into four classes: *ploughing*, *seedbed preparation*, *no change*, and *unclassified*.

Table 3.1 presents the threshold criteria employed for classifying changes at the field level by comparing field-scale and medium-scale backscatter measurements, as established by Satalino et al. (2018).

Table 3.1: Thresholding of the backscatter changes at High and Medium Resolutions (adapted from Satalino et al., 2018)

Thresholding	Reason of Change
$-th_{HR} < \Delta\sigma^0_{HR} < th_{HR}$	No change
$\Delta\sigma^0_{HR} > th_{HR}$ AND $-th_{MR} < \Delta\sigma^0_{MR} < th_{MR}$	Roughness changes likely due to ploughing
$\Delta\sigma^0_{HR} > th_{HR}$ AND $\Delta\sigma^0_{MR} > th_{MR}$	Soil moisture changes likely due to precipitation
$\Delta\sigma^0_{HR} < -th_{HR}$ AND $-th_{MR} < \Delta\sigma^0_{MR} < th_{MR}$	Roughness changes probably due to seedbed preparation after ploughing

Furthermore, the *unclassified* category arose from cases in which the observed change pattern did not meet any of the specific threshold conditions defined by the algorithm, thereby falling outside the scope of the established classification rules.

3.3.2. Coherence Classification

Coherence values were calculated using consecutive radar acquisitions during the bare soil period for each field. These values were computed separately for each polarization, and pass, following the same methodology applied to σ^0. In addition, medium-resolution coherence values were derived to help account for the influence of precipitation. Given that coherence is sensitive to surface changes across both temporal and spatial dimensions—and that ploughing physically disrupts the soil surface—a substantial drop in coherence may serve as a reliable indicator of tillage activity.

To detect such tillage-induced changes, two thresholds were applied. First, a coherence threshold was defined based on the method proposed by Robertson et al. (2023), representing the limit below which ploughing is likely to have occurred. Second, a coherence change threshold was established to capture significant decreases in coherence. Both thresholds were subjected to sensitivity analysis using 0.01-unit increments, applied to the calibration dataset, in order to identify the most appropriate values for the study context. At each increment, the F1-score and overall accuracy were assessed using a time window to determine the most suitable threshold for reliable classification.

For the coherence-based detection, a time window of up to +7 days following the ground observation was applied. This extended window was necessitated by the requirement that coherence values should be derived from SAR image pairs with identical acquisition geometries. In several instances, the available image pairs suitable for coherence computation were acquired more than a few days apart. Consequently, a longer temporal window was required to accommodate these acquisition intervals and ensure that relevant coherence data could still be associated with the corresponding surface transitions.

As with the backscatter-based approach, field level coherence changes that coincided with similar changes in the medium-resolution dataset were labelled as *precipitation*. The remaining field coherence changes were then classified as *ploughing*—if both threshold conditions were met—or *other* if they did not satisfy the criteria. Table *3.2* presents the threshold criteria employed for classifying changes at the field level by comparing field-scale and medium-scale coherence, adapted from Robertson et al. (2023) with modifications tailored to the context of this study.

Table 3.2: Thresholding of coherence at High and Medium Resolutions (adapted from Robertson et al., 2023)

Thresholding	Reason of Change
HR coherence < th_{HR} AND $\Delta\text{coherence}$ < $th_{\Delta\text{coherence}}$ AND MR coherence > th_{HR}	Coherence changes likely due to ploughing
HR coherence < th_{HR} AND MR coherence < th_{HR}	Coherence changes likely due to precipitation
All other combinations	No change

3.3.3. Tillage Detection

For the combined detection approach using both backscatter and coherence data, a unified time window was applied—beginning on the date of the field observation and extending up to seven days afterward—to account for potential temporal discrepancies among backscatter, coherence, and field observation dates. A longer time window was not considered, as the field visits were spaced 11 days apart, and extending the window further would introduce overlap and ambiguity between consecutive observation periods. Within this temporal framework, the F1-score and overall accuracy were computed to evaluate the performance of the event-based detection approach.

The final ploughing detection was conducted using two logical combination strategies—AND and OR—based on the methodology proposed by Satalino et al. (2024). The AND approach identifies a ploughing event only when both the backscatter- and coherence-based classifications independently detect ploughing for a given field and time step. Conversely, the OR approach classifies a ploughing event when either the backscatter or coherence signal alone indicates ploughing.

3.4. Modifying Tillage Detection Algorithm

To enhance the tillage detection methodology, a modified version of the algorithm proposed by Satalino et al. (2018) was implemented. This adaptation introduced direct precipitation filtering in place of the original medium-scale filtering approach, with the aim of increasing the confidence in identifying ploughing events. Figure 3.4 presents the flowchart of the modified tillage detection algorithm.

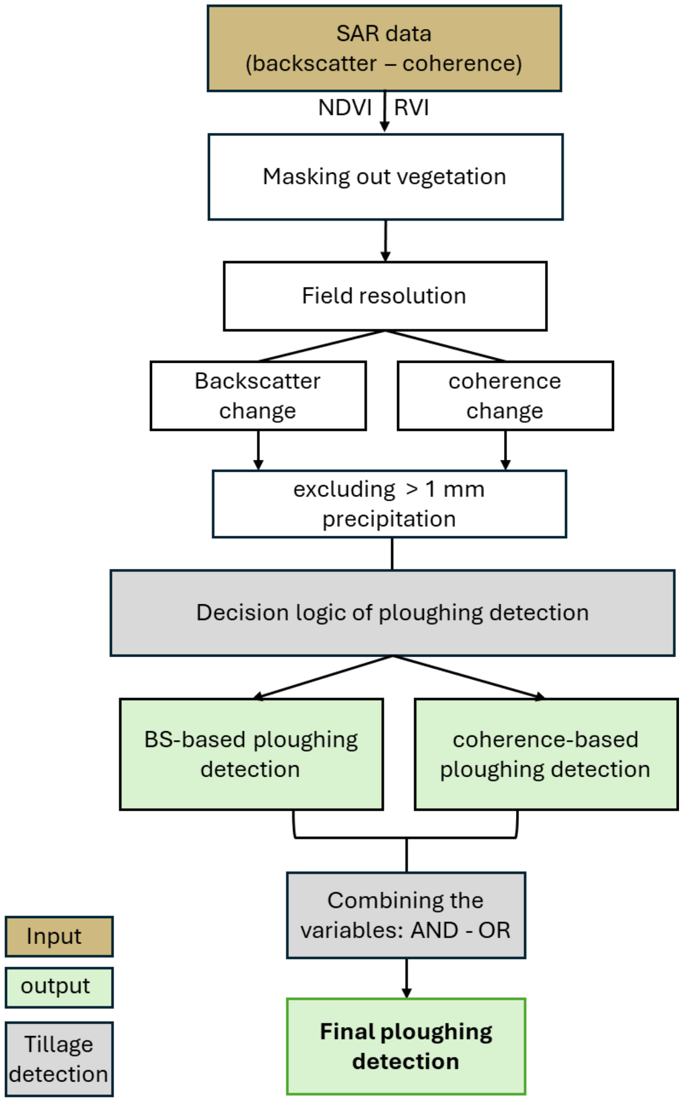

Figure 3.4: Flowchart of the modified tillage detection algorithm. The algorithm uses precipitation data instead of landscape resolution to account for the moisture effect.

In this modified method, backscatter values (σ^0) and their temporal changes ($\Delta\sigma^0$) were first calculated for each agricultural field using consecutive radar acquisitions. To reduce the confounding influence of precipitation on radar backscatter, time steps associated with daily precipitation totals exceeding 1 mm were excluded from further analysis. While some studies adopt a less restrictive approach—removing data only when precipitation occurs within a few hours prior to image acquisition—this study employed a more conservative filtering criterion. Given the use of both ascending and descending S1 passes and the objective of ensuring comparability with previous medium-scale analyses, full exclusion of high-precipitation days was preferred. This stricter approach minimized potential residual effects of rainfall on the radar signal and supported more robust identification of surface changes. The remaining σ^0 and $\Delta\sigma^0$ values were then used for classification. Based on thresholds established through sensitivity analysis and the threshold criteria employed for classifying changes at the field level, presented in Table 3.3, change in σ^0 were classified as either ploughing or other, using a time window of up to +7 days. This extended time window, compared to that used in the baseline algorithm, was implemented to compensate for the reduced temporal density of observations resulting from the removal of precipitation-affected data. The longer interval between the remaining acquisitions necessitated a broader window to ensure that relevant backscatter changes associated with ploughing events could still be effectively captured.

Table 3.3: Thresholding of the backscatter changes at field resolution for the modified algorithm

Thresholding	Reason of Change
$\Delta\sigma^0_{HR} > th_{HR}$	Roughness changes likely due to ploughing
$\Delta\sigma^0_{HR} < th_{HR}$	Other reasons

The same procedure was applied to the coherence data. Coherence values and their changes were first computed for each field across consecutive image pairs. Subsequently, all dates with recorded precipitation exceeding 1 mm were excluded to minimize the influence of weather-related noise. Classification was then performed using two thresholds: one corresponding to the maximum coherence value typically observed during ploughing events, and another capturing significant drops in coherence. These threshold criteria, as outlined in Table 3.4, were used to classify the filtered coherence data as either *ploughing* or *other*, within a +7-day time window following each event.

Table 3.4: Thresholding of the coherence at field resolution for the modified algorithm

Thresholding	Reason of Change
HR coherence < th_{HR} AND $\Delta\text{coherence} < th_{\Delta\text{coherence}}$	Coherence changes likely due to ploughing
All other combinations	Other reasons

Final tillage detection was conducted using two logical operators using time window of +7 days. Similar to the baseline algorithm, the AND method classified a ploughing event only when both backscatter and coherence data indicated *ploughing*. The OR method classified an event as ploughing when either variable independently detected a ploughing signal for the same time step.

3.5. Evaluation of the Algorithms

Based on the field campaign data (Section 3.1.1), a total of 94 agricultural fields were selected. Each field had a minimum area of 1 hectare to ensure valid geometry after applying a 20-meter inward buffer. The fields were categorized according to surface condition, including ploughing, prepared seedbed, crop residues, mounds, or covered soil. Among these categories, fields identified as having undergone ploughing were of particular interest, as the objective of this study is to detect tillage events occurring near the time of field visits. However, since not all fields showed evidence of ploughing, the dataset also enabled evaluation of algorithm performance with respect to false positive detections.

To assess detection performance, 20% of the ground truth data—corresponding to 20 fields—was reserved for validation. The evaluation was done on all the eight configurations of the two main algorithms developed in this study:

- The baseline algorithm (Section 3.3), which uses landscape resolution to filter out moisture effects and NDVI – DpRVI to mask vegetation.
- The modified algorithm (Section 3.4), which replaces landscape resolution with precipitation data for moisture filtering, while retaining NDVI – DpRVI for vegetation masking.

These configurations varied across satellite acquisition parameters, including:

- **Pass direction:** Ascending vs. Descending
- **Relative orbit number:** 37 and 110 (Descending), 88 and 161 (Ascending)
- **Polarization mode:** VV and VH

For consistency, the same time window used during algorithm development and calibration was applied to all evaluations, including the backscatter-based, coherence-based, and combined detection approaches. Performance was quantified using the F1-score and overall accuracy, assessing each configuration ability to detect tillage events.

In addition, to explore whether vegetation masking using bare soil information could enhance detection performance, the best-performing configuration of each algorithm was re-evaluated by replacing NDVI – DpRVI with bare soil data derived from the Copernicus CP product.

3.6. Field Orientation and Area Evaluation

The arrangement of tillage rows can influence radar backscatter observed in SAR imagery. When these rows are oriented perpendicular to the radar's line of sight, a larger portion of the surface reflects energy back to the sensor, resulting in stronger backscatter. Conversely, parallel row orientations tend to yield weaker returns due to reduced surface interaction. This directional sensitivity is notably less pronounced in cross-polarized SAR data (Michelson, 1994; McNairn and Brisco, 2004). The radar line of sight in S1 ascending passes is approximately 78°, while in descending passes it is around -80° (equal to 280°) (Dai et al., 2022).

To further assess the influence of viewing geometry on ploughing detection performance, the confusion matrix was analysed in relation to both field size and row orientation. Agricultural fields were categorized into three orientation classes based on their alignment relative to the radar beam direction: parallel, perpendicular, and other. Table 3.5 summarizes this classification scheme, illustrating how ploughing row directions were conditioned with respect to the radar beam angle. Each class in the confusion matrix—true positives, true negatives, false positives, and false negatives—was then examined by analysing their distribution across field area and orientation categories. This analysis was conducted to identify potential biases or systematic trends in detection accuracy linked to field geometry and tillage direction.

Table 3.5: Classification of ploughing row orientation relative to radar beam direction.

Angle Difference (°)	Orientation Category
difference ≤ 20	Parallel
70 ≤ difference ≤ 110	Perpendicular
20 < difference < 70 110 < difference < 180	Other

3.7. Copernicus Croplands Product Evaluation

Among the various layers of the Copernicus Cropland product, the *bare soil* layer was of particular interest. Its accuracy in identifying bare soil periods was evaluated using the F1-score and overall accuracy, with ground-truth in-situ observations serving as the reference. Each field observation point was treated as an individual data instance, resulting in a total of 578 observations. This approach was selected to allow for a more detailed analysis, enabling the identification of specific temporal misalignments and potential underlying causes of misclassification.

CHAPTER FOUR

RESULTS

This chapter presents the results of the study and is organized into three main sections: Copernicus product date extraction and evaluation, detection of tillage, and incorporating the bare soil period derived from Copernicus CP product into the best-performing configuration of each tillage detection algorithm.

4.1. Copernicus CP Product

This section provides an in-depth exploration and evaluation of the Copernicus Cropland product, with an emphasis on its accuracy in capturing bare soil conditions across agricultural fields.

4.1.1. CP Date Extraction

Figure 4.1 illustrates the annual crop cycle of a field. The coloured segments represent key phenological stages: bare soil period before the main crop (BSB) in khaki, main crop duration in green that is driven from main crop emergence (MCE) and main crop harvest (MCH), and bare soil period after the main crop (BSA) in yellow. In most cases, the periods did not overlap, indicating high consistency in the satellite-derived indicators. However, in some cases—such as illustrated in Figure 4.2, which shows the overlap between the BSB and the Main Crop periods—uncertainty in the MCE date, resulting from the temporal gap between the dates when 25% and 75% of the pixels were classified as MCE, affects the detection of the bare soil period by introducing ambiguity in determining its start. This uncertainty can also propagate to the estimation of MCH and BSA dates. Moreover, in both figures, the field cover status points align well with the bare soil period derived from CP layer.

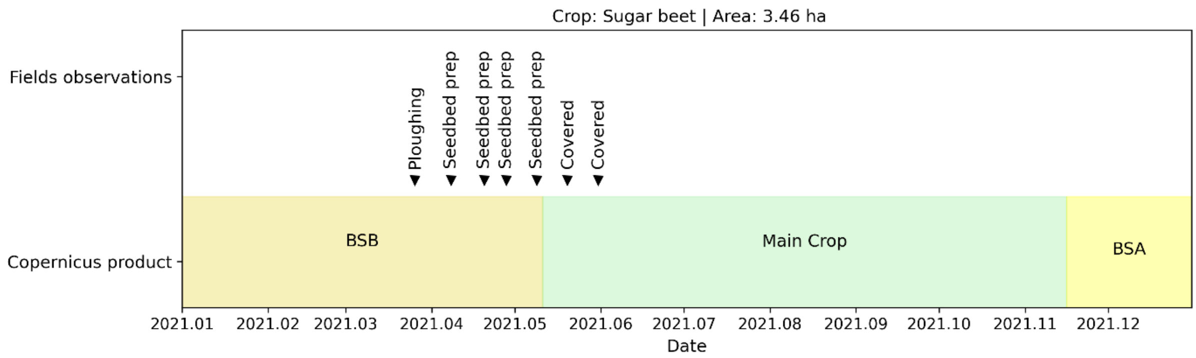

Figure 4.1: Cropping patterns throughout 2021 and field cover status for field 14758. BSB denotes the bare soil period preceding main crop emergence, while BSA represents the bare soil period following main crop harvest.

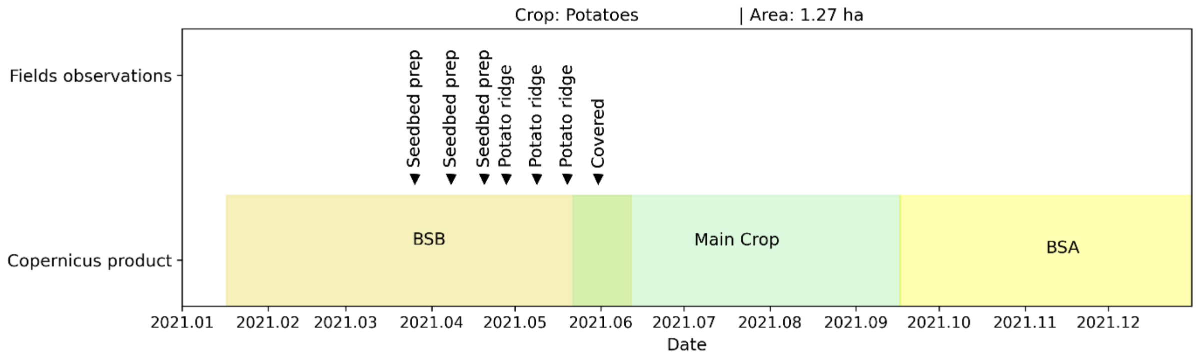

Figure 4.2: Cropping patterns throughout 2021 and field cover status for field 15959. BSB denotes the bare soil period preceding main crop emergence, while BSA represents the bare soil period following main crop harvest.

The discrepancy in the MCE observed in Figure 4.2 is further illustrated in Figure 4.3, where the field exhibits two distinct DOY values for the emergence date. This inconsistency subsequently affects the estimation of the bare soil period preceding the main crop, as demonstrated in Figure 4.4.

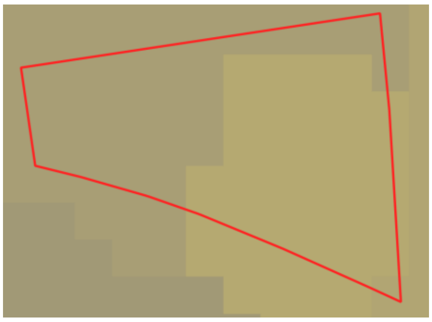

Figure 4.3: Main Crop Emergence differences for a field, based on Copernicus Cropping Patterns layer at 10 m spatial resolution.

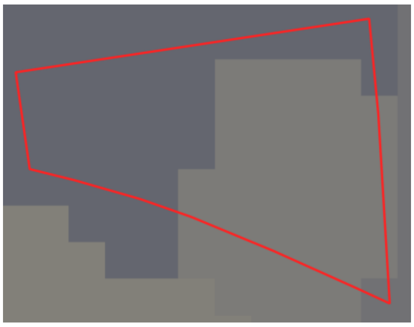

Figure 4.4: Bare Soil Before differences for a field, based on Copernicus Cropping Patterns layer at 10 m spatial resolution.

The period of bare soil was not always consistent with the in-situ observations. As demonstrated in Figure 4.5, the product has been shown to indicate crop emergence earlier than field observations. Despite the continued presence of in-situ data indicating seedbed preparation, the CP layer has been identified as the point at which the bare soil period concludes, and the main crop emerges.

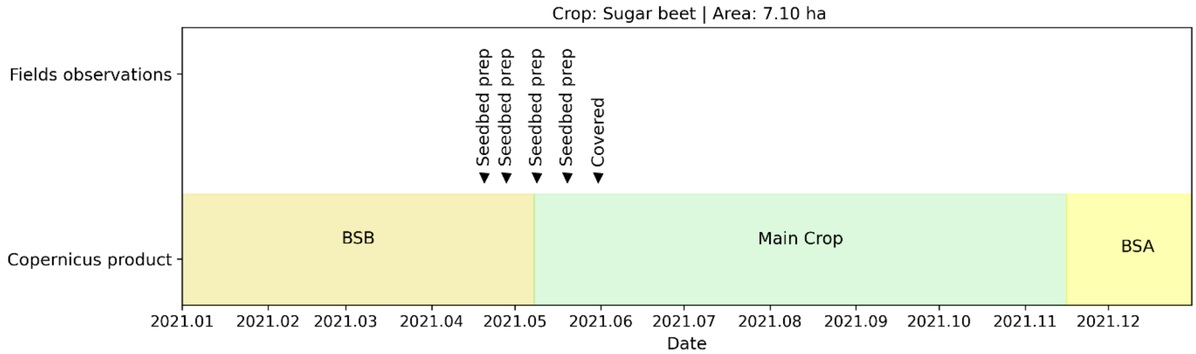

Figure 4.5: Cropping patterns throughout 2021 and field cover status for field 16530. BSB denotes the bare soil period preceding main crop emergence, while BSA represents the bare soil period following main crop harvest.

4.1.2. Evaluation of CP layers BSB detection

Figure 4.6 presents the accuracy assessment of bare soil period detection based on the CP layer detections. When evaluated across all observation dates collectively, the CP layer product achieved an overall accuracy of 84% and an F1-score of 85%, indicating a high level of agreement between the detected and reference labels for bare soil conditions. Despite these promising aggregate metrics, the performance of the product varies across individual observation dates. The temporal accuracy matrices, presented in Figure 4.7, reveal fluctuations in detection performance. Notably, the highest number of misclassifications occurs in May, during which the product tends to misclassify bare soil as vegetated cover, leading to a decline in precision at those specific time points. The detailed confusion matrices are provided in Appendix, Figure 8.1.

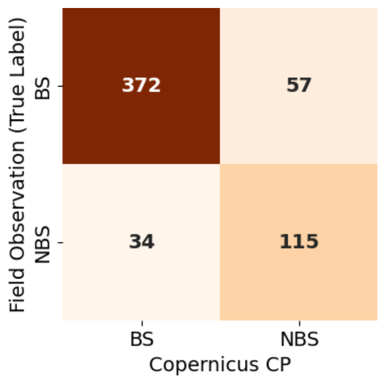

Figure 4.6: Confusion matrices derived from the comparison between in-situ observations and Cropping Patterns product detections. The matrix represents the aggregated results across all observation dates. BS refers to the bare soil class, and NBS indicates the non-bare soil class.

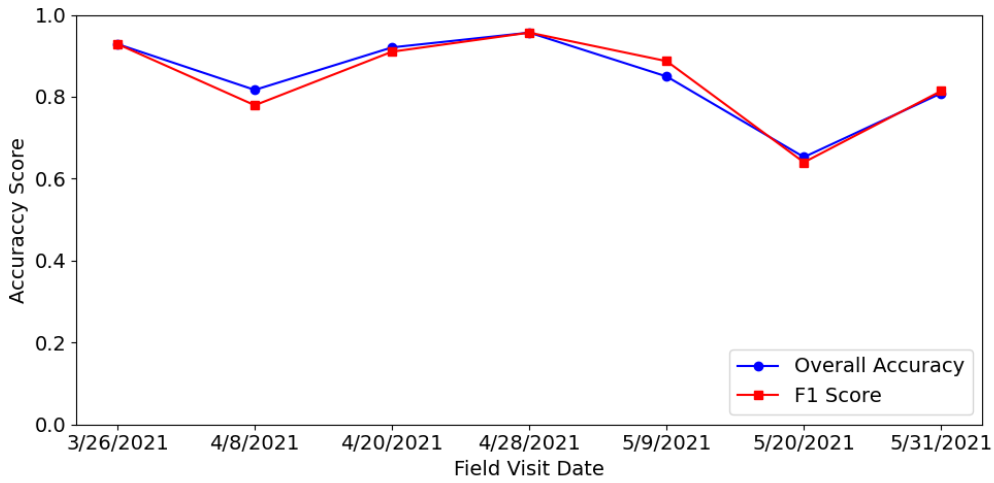

Figure 4.7: Accuracy score fluctuations derived from the comparison between in-situ observations and Cropping Pattern product detections, presenting detection performance for each individual field visit date.

4.2. The Baseline Algorithm (based on Satalino et al. (2018) and Robertson et al. (2023))

This section encompasses both the calibration and validation results for backscatter-based detection, coherence-based detection, and a combined approach that integrates the outputs of both methods (see Figure 3.3). Furthermore, the effects of field angle and field area on the performance of the algorithm is analysed.

4.2.1. Calibration

The algorithm calibration was carried out using a holdout subset comprising 80% of the dataset, which was utilized for sensitivity analysis of the thresholds. This section presents the results derived from the sensitivity analysis, showcasing the highest achieved accuracy of ploughing detection.

Tillage Detection Based on Backscatter

The backscatter change at both field and medium resolutions was initially computed following the original method, which involved using the increase in backscatter values. However, a sensitivity analysis revealed that this approach failed to identify suitable thresholds for reliable tillage detection. Across all algorithm configurations tested, the F1-score remained at 0, indicating no discernible pattern of backscatter increase associated with tillage activities, even when a broader temporal window of ±7 days around field observations was applied (see Table 8.1 and Figure 8.2 in the Appendix). Upon visual inspection of the time series data and under the assumption that tillage events occurred in close proximity to the recorded field observation dates, a slight decrease in backscatter was observed following ploughing events in most cases. The observed consistency supported interpreting declining backscatter values as a signature of ploughing.

Table 4.1 presents the field and medium-resolution thresholds used for classifying backscatter changes at the field level, as determined through sensitivity analysis. The VV polarization on the ascending pass, orbit 88 was selected for further analysis and presentation in this section.

Table 4.1: HR and MR thresholds resulted from sensitivity analysis. The algorithm configurations refer to the polarization, pass, and orbit number of the pass used for the backscatter change calculations.

Algorithm configuration (polarization – pass – orbit)	**HR $\Delta\sigma^0$ threshold (dB)**	**MR $\Delta\sigma^0$ threshold (dB)**
VH – Descending – 110	-1.8	-1.55
VH – Descending – 37	-2.5	-2
VH – Ascending – 161	-2.6	-2.05
VH – Ascending – 88	-3.5	-2.7
VV – Descending – 110	-3	-2.7
VV – Descending – 37	-2.5	-1.4
VV – Ascending – 161	-2.34	-2.1
VV – Ascending – 88	-1.68	-1.61

Figure 4.8 presents the σ^0 and $\Delta\sigma^0$ timeseries for a field at both field (HR) and medium (MR) resolutions, as well as the corresponding classification results for backscatter change during the identified bare soil period (See Figure 8.3 in the Appendix for NDVI and DpRVI plot). Figure 4.9 compares these classifications with precipitation records and in situ observations. The comparison with precipitation data indicates that the algorithm did not consistently differentiate backscatter changes induced by rainfall. Nevertheless, it was capable of detecting rainfall events following extended dry periods, as well as identifying sharp spikes in precipitation. Furthermore, when assessed against in-situ observations, the algorithm successfully detected one ploughing event during a bare soil period, which corresponded with the recorded ground truth.

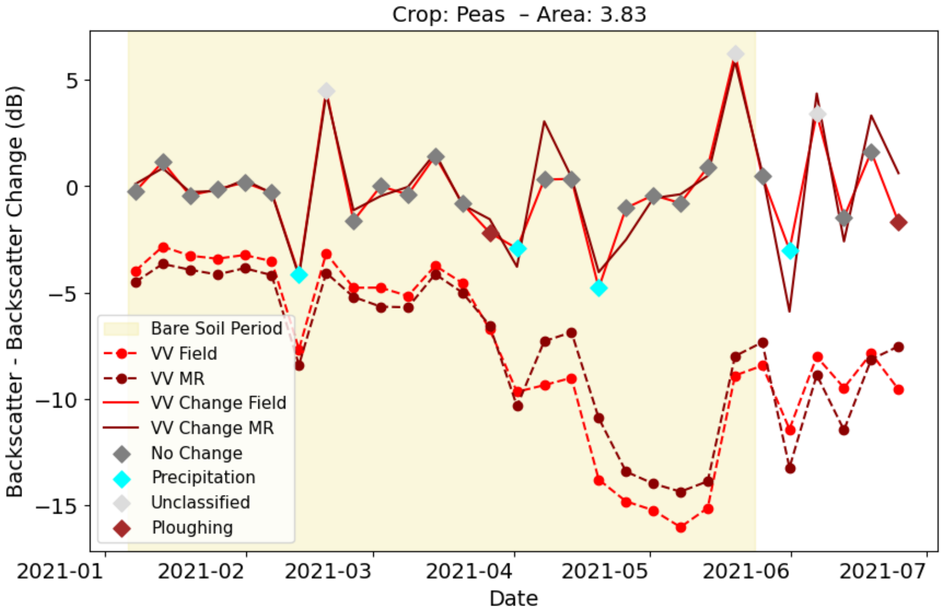

Figure 4.8: VV backscatter timeseries and change classification from orbit 88 of ascending pass for field 15949.

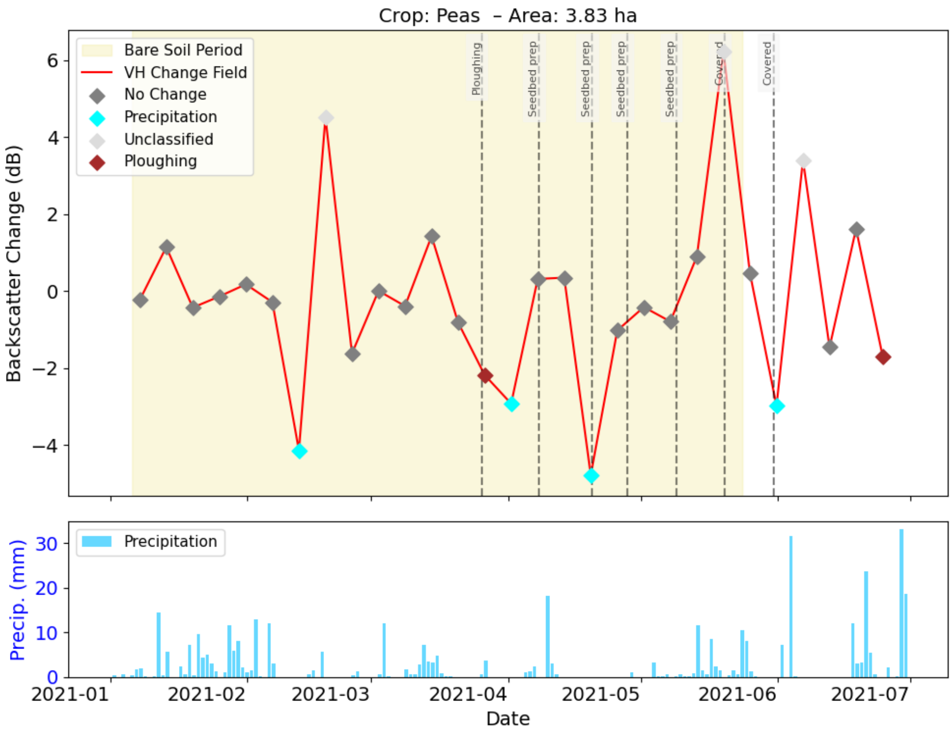

Figure 4.9: Backscatter change classification (VV-ascending-88), precipitation, and in situ observation of the field for field 15949.

Figure 4.10 illustrates an example of tillage detection based on backscatter data. In this case, the change induced by seedbed preparation was misclassified as ploughing. Moreover, as shown in Figure 4.11, the algorithm was able to correctly detect seedbed preparation in certain instances. Both Figures 4.10 and 4.11 exhibit a degree of misalignment with the precipitation data, indicating that rainfall-related changes were not always accurately distinguished.

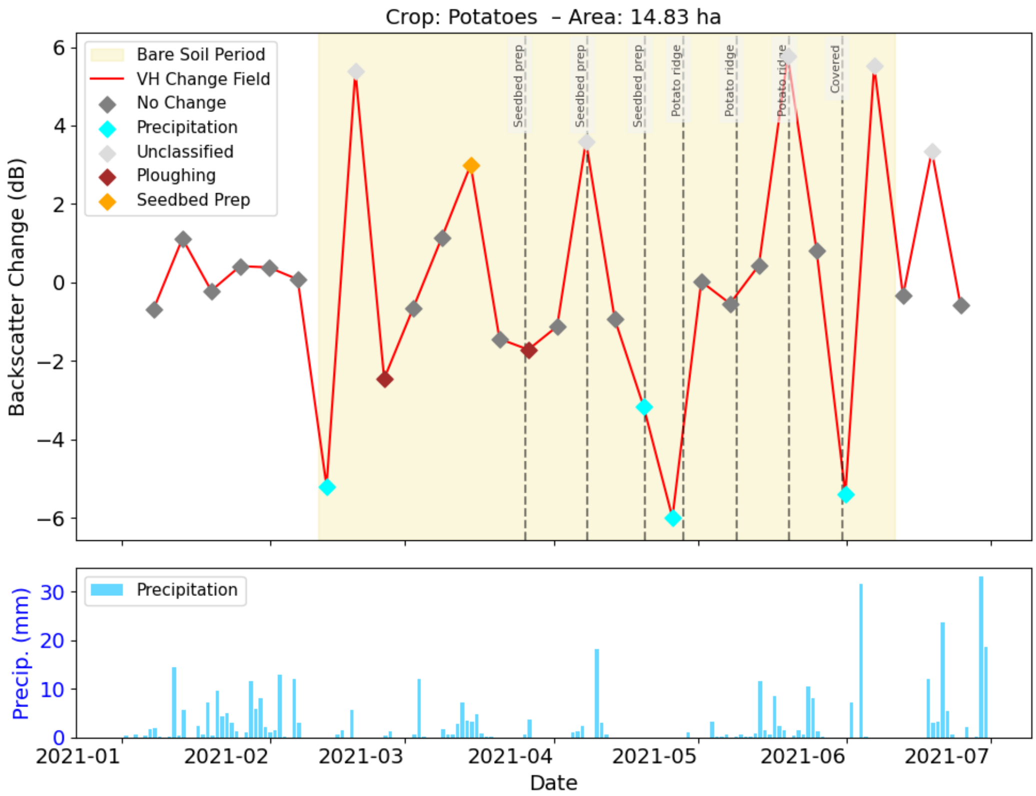

Figure 4.10: Misclassification of seedbed preparation as ploughing using backscatter change classification (VV-ascending-88). The plot is for field 16344, showing precipitation, and in situ observation.

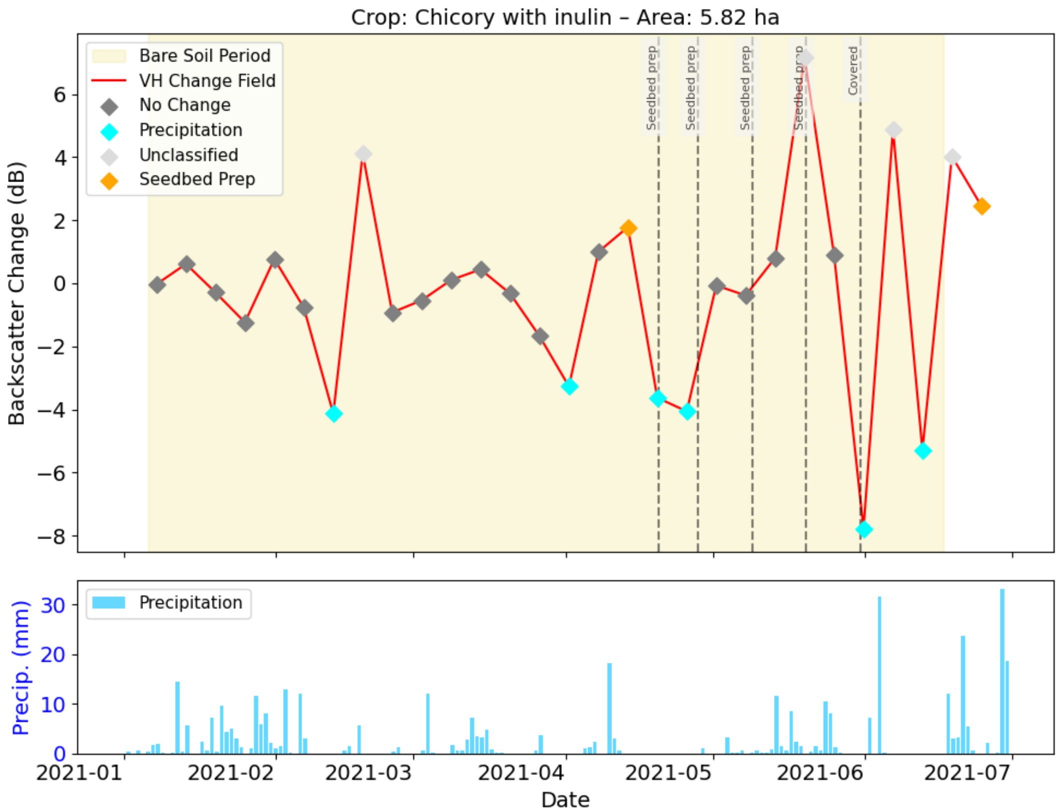

Figure 4.11: Classification of seedbed preparation based on backscatter change detection (VV-ascending-88). The plot corresponds to field 15711 and includes precipitation data and in-situ observations.

In addition to the misclassification of seedbed preparation as ploughing, the algorithm also misclassified potato ridging as ploughing in some cases, as illustrated in Figure 4.12, as it has the similar effect on the soil surface.

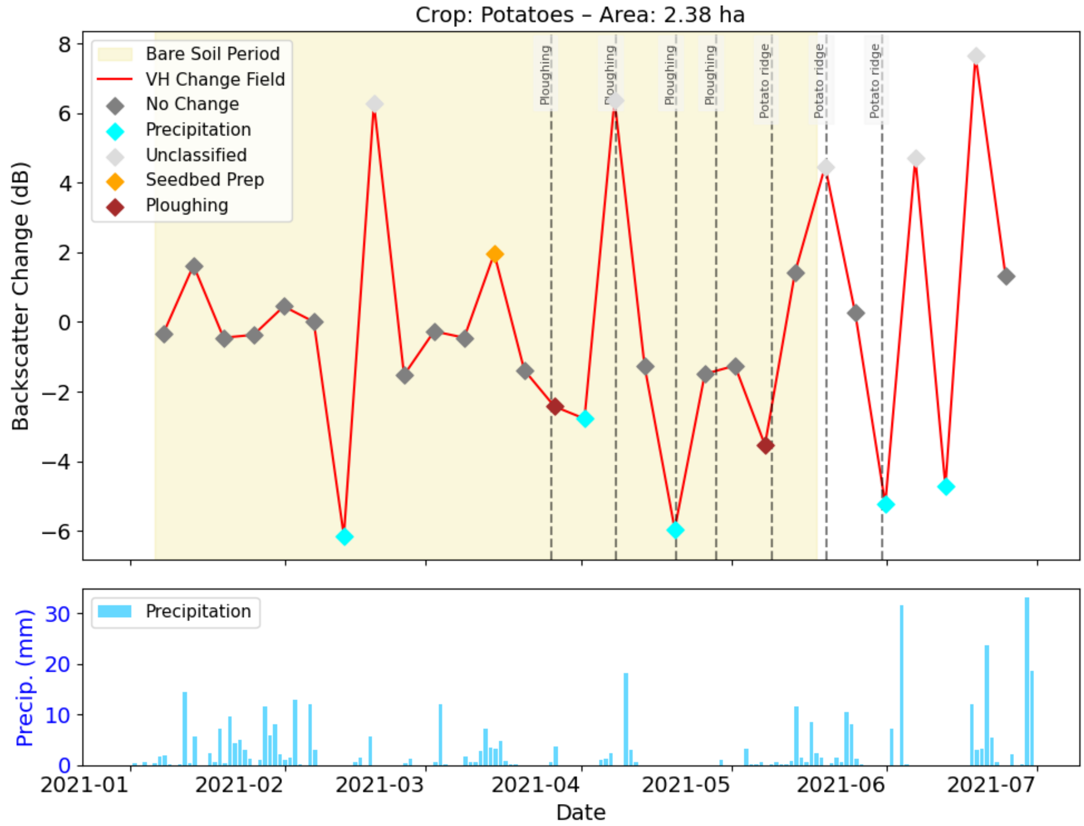

Figure 4.12: Misclassification of potato ridging as ploughing based on backscatter change detection (VV-ascending-88). The plot corresponds to field 15961 and includes precipitation data and in-situ observations.

Finally, Figure 4.13 presents an example where the algorithm successfully detected ploughing prior to seedbed preparation. However, due to the absence of corresponding in-situ observations for this period, the accuracy of the detection could not be verified.

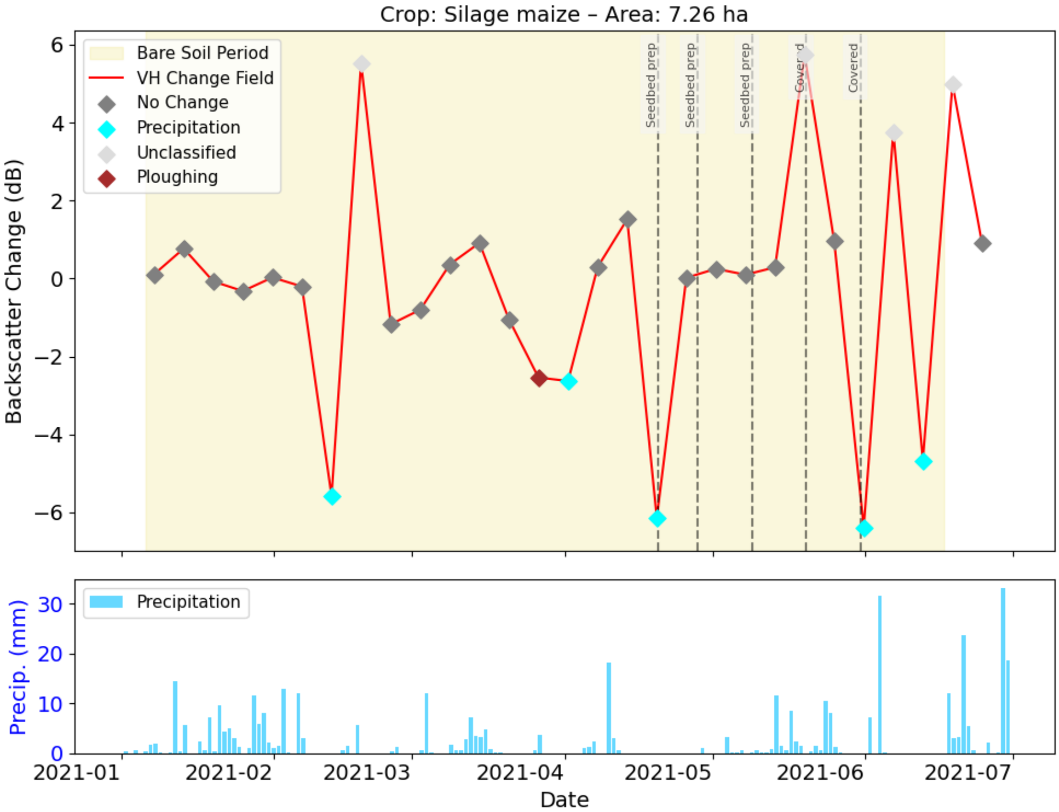

Figure 4.13: Example of unvalidated ploughing detection based on backscatter change (VV-ascending-88) for field 15912. The plot includes available in-situ observations.

Figure 4.14 presents an instance of ploughing detection and misdetection by the algorithm, compared to the field observation, to further investigate tillage detection based on backscatter change. The confusion matrix reveals that, despite the thresholds being derived through sensitivity analysis on the calibration dataset, the algorithm frequently failed to correctly detect ploughing events. The highest accuracy achieved for ploughing detection using backscatter yielded an overall accuracy of 87% and an F1-score of 60%.

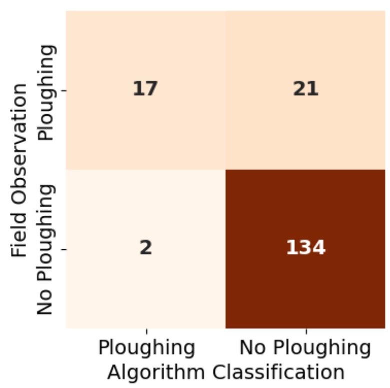

Figure 4.14: Confusion matrix derived from the comparison between in-situ observations and algorithm's backscatter change classification for VV ascending orbit 88 configuration.

Table 4.2 presents the accuracy of ploughing detection using various algorithm configurations backscatter during the calibration process. The results indicate that the backscatter and its temporal change, at their best configuration, achieved an F1-score of 60%. Furthermore, configurations using ascending pass data demonstrated higher accuracy compared to those using descending pass data.

Table 4.2: Accuracy analysis of various algorithm configurations derived from the calibration process.

Algorithm configuration (polarization – pass – orbit)	**OA (%)**	**F1-score (%)**
VH – Descending – 110	72	0
VH – Descending – 37	72	0
VH – Ascending – 161	78	0
VH – Ascending – 88	83	41
VV – Descending – 110	75	12
VV – Descending – 37	75	0
VV – Ascending – 161	78	0
VV – Ascending – 88	87	60

Tillage Detection Based on Coherence

Table 4.3 presents the thresholds used for classifying coherence changes at the field level, as determined through sensitivity analysis. The VV polarization on the ascending pass was selected for further analysis and presentation in this section.

Table 4.3: Coherence threshold and change to distinguish ploughing-induced coherence change, resulted from sensitivity analysis. The Coherence configurations refer to the polarization and pass of the images used for the coherence calculations

Algorithm configurations (polarization – pass)	**HR coherence threshold**	**HR coherence threshold**
VV – Descending	0.4	- 0.45
VV – Ascending	0.4	- 0.5
VH – Descending	0.3	- 0.5
VH – Ascending	0.4	- 0.3

Figure 4.15 presents an example of coherence at both field and medium resolutions during the bare soil period, along with the corresponding ploughing detection based on field-level changes. In this case, the detected ploughing events corresponds to the in-situ observation. However, the detection occurred later than the field observation, highlighting a temporal discrepancy between ground-based observations and satellite image acquisition.

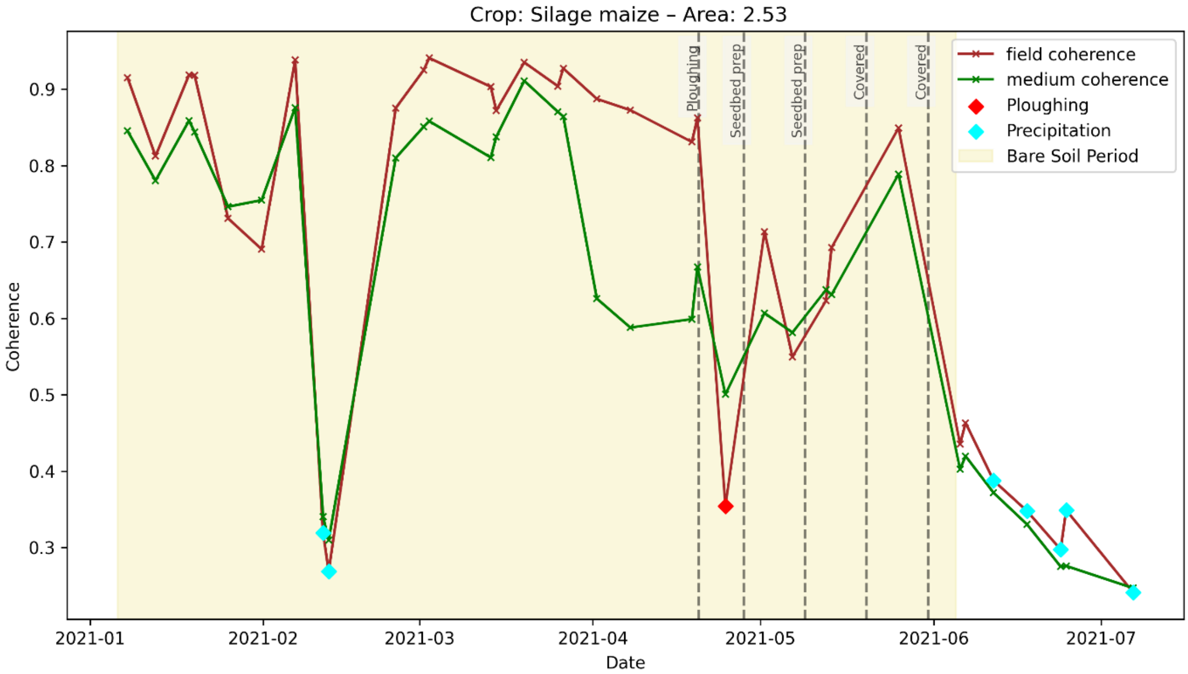

Figure 4.15: VV coherence of ascending pass and its associated standard deviation in field 16352 and its medium resolutions, along with the corresponding ploughing detection result.

Figure 4.16 presents an example where potato ridging was misclassified as ploughing, while the actual ploughing event was not detected and no significant drop in coherence was observed at the expected time. Moreover, a few instances of seedbed preparation were misclassified as ploughing in the algorithm’s detection. This result highlights the possibility that the visible ploughing marks in the field may have originated from an earlier ploughing event at the beginning of the year, during which a substantial drop in coherence was recorded. However, the absence of in-situ observations during that period prevents validation of this hypothesis.

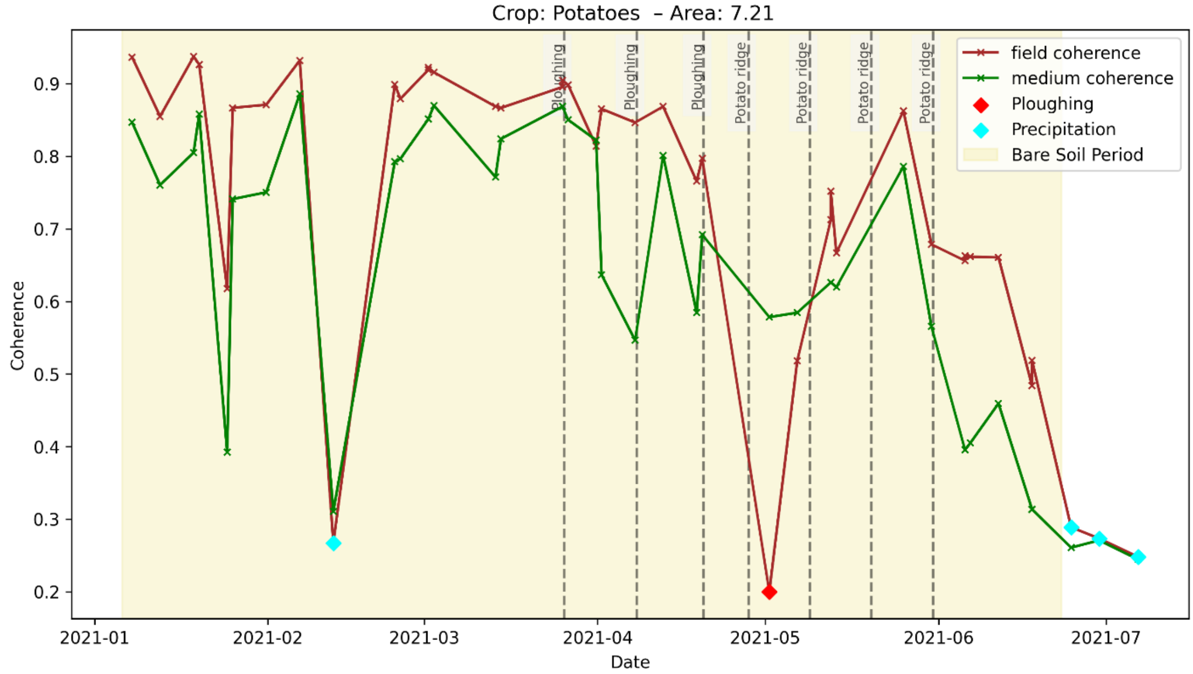

Figure 4.16: Misclassification of potato ridging as ploughing using VV coherence from the ascending pass and its associated standard deviation for field 17173, along with medium-resolution coherence and in-situ observations

Furthermore, certain ploughing detections—such as the one presented in Figure 4.17—could not be validated due to the lack of corresponding in-situ observations. The decline in field coherence following the ploughing detection is likely attributed to surface modifications associated with seedbed preparation.

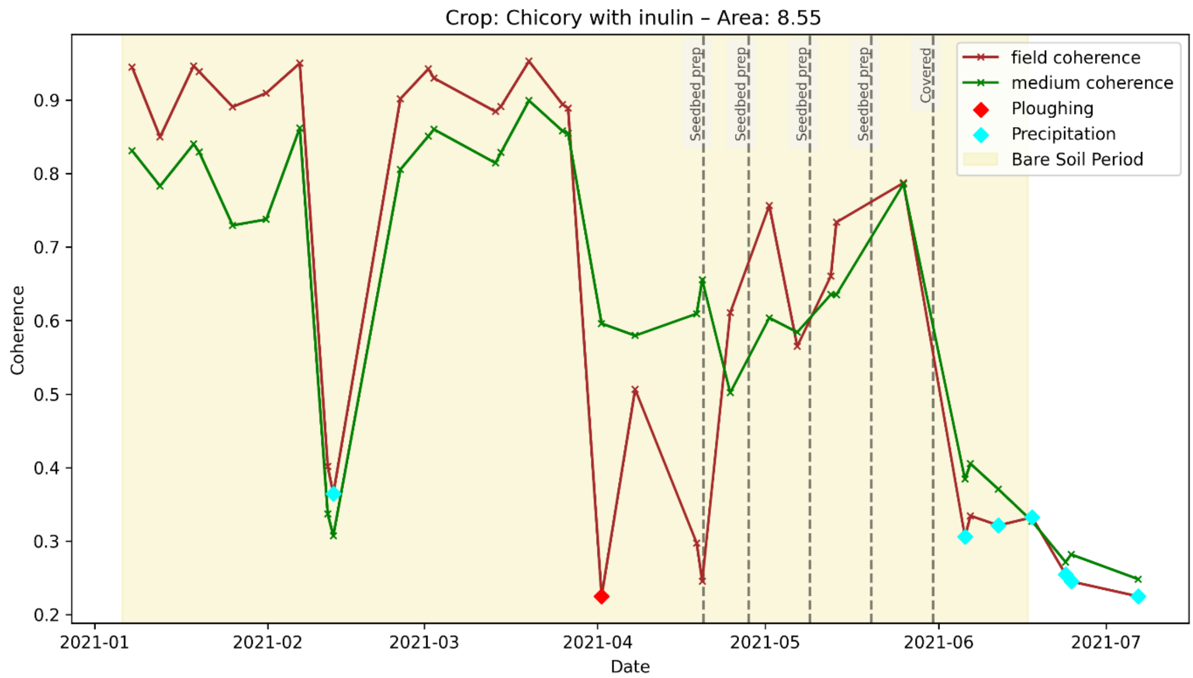

Figure 4.17: Example of unvalidated ploughing detection based on coherence change for field 14755. The plot includes available in-situ observations.

Figure 4.18 presents cases of ploughing misdetection and misclassification by the algorithm. While half of the ploughing events were successfully detected, misclassifications of other field activities—such as seedbed preparation or potato ridging—remained infrequent. This suggests that both the sensitivity analysis and the defined temporal detection window were appropriately calibrated. The highest accuracy achieved for ploughing detection using coherence resulted in an overall accuracy of 86% and an F1-score of 61%.

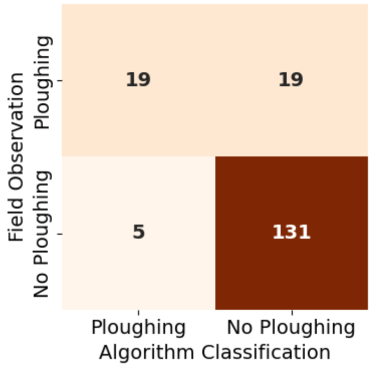

Figure 4.18: Confusion matrix derived from the comparison between in-situ observations and algorithm's VV Ascending coherence classification.

Table 4.4 summarizes the accuracy of ploughing detection achieved using various algorithm configurations based on coherence during the calibration process. The configurations employing data from the ascending pass for both polarizations outperformed those utilizing descending pass data.

Table 4.4: Accuracy analysis of various algorithm configurations derived from the calibration process.

Algorithm configurations (polarization – pass)	**OA (%)**	**F1 (%)**
VV – Descending	72	5
VV – Ascending	86	61
VH – Descending	78	0
VH – Ascending	87	58

Tillage Detection Based on Coherence and Backscatter

The final determination of ploughing detection was done using two approaches: AND and OR. The OR operator enhances the detection of tilled areas by identifying a larger number of events, whereas the AND operator narrows the scope of detected events, offering greater confidence and identifying robust tillage changes.

Table 4.5 presents all algorithm configurations alongside their corresponding accuracy assessment results. The highest overall accuracy during the calibration phase was achieved using the ascending pass and orbit 88, exceeding 80% for both the AND and OR decision rules in both VV and VH polarizations. Moreover, the ascending pass consistently outperformed the descending pass across all configurations, regardless of the approach applied.

Table 4.5: Accuracy analysis of various algorithm configurations derived from the calibration process for both AND and OR approaches used in combining backscatter and coherence for ploughing detection.

Algorithm configuration		**Accuracy Results**			
Backscatter (polarization – pass –orbit)	**Coherence** (polarization – pass)	**AND**		**OR**	
		OA (%)	**F1 (%)**	**OA (%)**	**F1 (%)**
VH – Descending – 110	VH – Descending	78	0	69	0
VH – Descending – 37	VH – Descending	78	0	70	27
VH – Ascending – 161	VH – Ascending	78	0	84	53
VH – Ascending – 88	VH – Ascending	84	44	88	67
VV – Descending – 110	VV – Descending	76	5	69	10
VV – Descending – 37	VV – Descending	77	0	70	7
VV – Ascending – 161	VV – Ascending	78	5	83	58
VV – Ascending – 88	VV – Ascending	82	39	87	70

Figure 4.19 depicts the confusion matrix generated for the AND approach of VV Ascending, orbit 88. It indicates that the algorithm's best performance was the detection of 10 ploughing events out of 38, with a high level of confidence. Furthermore, the misclassification of other changes as ploughing was minimal. The OR approach, on the other hand, achieved an overall accuracy of 87% and an F1-score of 70%. Figure 4.20 presents the confusion matrix for OR ploughing detection. While the OR approach leads to a higher number of false positives—where other field changes are occasionally misclassified as ploughing—it also substantially improves the detection of actual ploughing events, as reflected in the increased number of true positives.

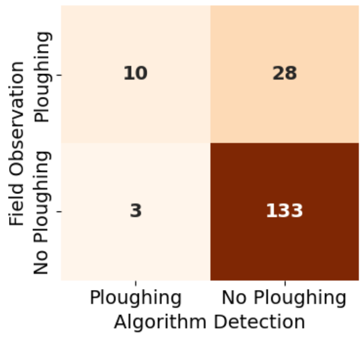

Figure 4.19: Confusion matrix derived from the comparison between in-situ observations and algorithm AND operator classification.

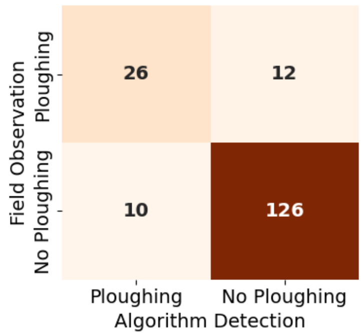

Figure 4.20: Confusion matrix derived from the comparison between in-situ observations and algorithm OR operator classification.

4.2.2. Validation

The following section presents the outcomes of algorithm validation conducted on a holdout subset comprising 20% of the dataset, corresponding to 20 fields. It is worth mentioning that given the exact ploughing date is not known, and detecting tillage events as close as possible to the actual field observation date is critical, an event-based accuracy assessment provides informative and contextually relevant evaluation in this case.

Backscatter-based Detection

The validation of backscatter-based ploughing detection demonstrated a high F1-score when utilizing orbit 88 of ascending-pass backscatter data. The results, presented in Table 4.6, highlight that the configuration employing VV polarization on ascending orbit 88 yielded the highest accuracy. This finding underscores the effectiveness of this particular configuration when relying solely on backscatter data for ploughing detection.

Table 4.6: Accuracy assessment of backscatter-based ploughing detection during the validation process, highlighting the performance of various configurations.

Algorithm configuration (polarization – pass – orbit)	OA (%)	F1 (%)
VH – Descending – 110	78	0
VH – Descending – 37	78	0
VH – Ascending – 161	80	0
VH – Ascending – 88	88	57
VV – Descending – 110	78	0

VV – Descending – 37	78	0
VV – Ascending – 161	80	0
VV – Ascending – 88	88	67

To further investigate the best configuration in terms of accuracy, Figure 4.21 presents cases of ploughing misdetection and misclassification by the VV polarization on ascending orbit 88 configuration. While more than half of the ploughing events were successfully detected, misclassifications of other field activities—such as seedbed preparation or potato ridging—remained infrequent.

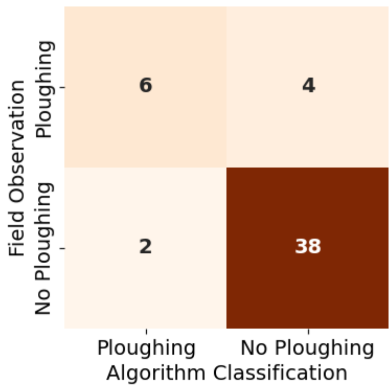

Figure 4.21: Event-based confusion matrix derived from the backscatter-based algorithm validation VV polarization in the ascending orbit 88 pass.

Coherence-based Detection

Table 4.7 presents the results of the validation process for coherence-based ploughing detection. The analysis reveals that coherence data from the ascending pass yields a higher F1-score. These findings align with the outcomes of the calibration process.

Table 4.7: Accuracy assessment of coherence-based ploughing detection during the validation process, highlighting the performance of various configurations.

Algorithm configurations (polarization – pass)	**OA (%)**	**F1 (%)**
VV – Descending	77	14
VV – Ascending	88	57
VH – Descending	80	0
VH – Ascending	86	46

To further evaluate the most accurate configuration, Figure 4.22 illustrates representative cases of ploughing misdetection and misclassification using coherence data from the VV polarization in the ascending pass. Although only approximately half of the actual ploughing events were successfully detected, the rate of misclassification for non-ploughing events remained minimal.

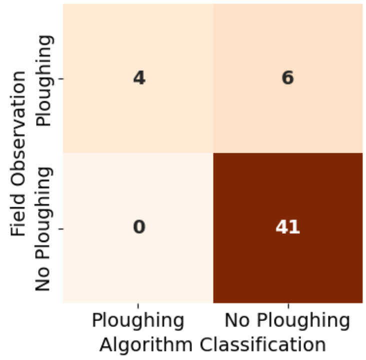

Figure 4.22: Event-based confusion matrix derived from the coherence-based algorithm validation for VV polarization in the ascending pass.

These results are consistent with the outcomes of the calibration phase, confirming the reliability of both approaches in terms of accuracy and overall performance.

Tillage Detection Based on Coherence and Backscatter

The validation results of the final tillage classification algorithm, which integrates both coherence and backscatter information, are presented in Table 4.8. This assessment reinforces the effectiveness of the ascending pass configurations, which consistently outperformed descending ones. The highest performing configuration was observed for the VH polarization on the ascending orbit 88. Analysis of detection and misdetection patterns in this configuration, as presented in Figures 4.23 and 4.24, indicates that when ploughing was confirmed by both backscatter and coherence data, the algorithm achieved high precision despite a relatively low number of detections. In contrast, the use of the OR operator led to a higher overall detection rate. These findings are consistent with the trends observed during the calibration phase, highlighting the trade-off between detection sensitivity and precision.

Table 4.8: Accuracy analysis of various algorithm configurations derived from the validation process for both AND and OR approaches used in combining backscatter and coherence for ploughing detection.

Algorithm configuration		Accuracy Results			
Backscatter (polarization – pass – orbit)	**Coherence** (polarization – pass)	**AND**		**OR**	
		OA (%)	**F1 (%)**	**OA (%)**	**F1 (%)**
VH – Descending – 110	VH – Descending	80	0	75	24
VH – Descending – 37	VH – Descending	80	0	77	0
VH – Ascending – 161	VH – Ascending	80	0	86	46
VH – Ascending – 88	VH – Ascending	86	46	94	82
VV – Descending – 110	VV – Descending	80	0	75	13
VV – Descending – 37	VV – Descending	80	0	75	13
VV – Ascending – 161	VV – Ascending	80	0	82	47
VV – Ascending – 88	VV – Ascending	86	46	84	64

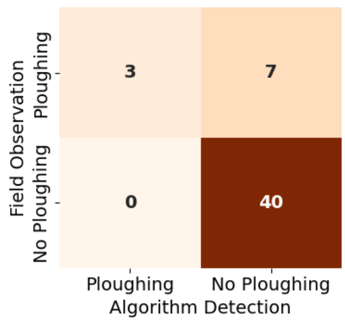

Figure 4.23: Confusion matrix resulting from the validation of the algorithm combining backscatter and coherence detection using the AND operator, evaluated against in-situ observations.

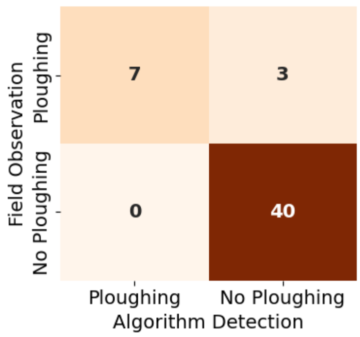

Figure 4.24: Confusion matrix resulting from the validation of the algorithm combining backscatter and coherence detection using the OR operator, evaluated against in-situ observations.

4.2.3. Angle and Area Effects on Detection

Figure 4.25 presents the analysis of the full dataset, encompassing both calibration and validation subsets, in relation to the angle between ploughing row orientation and the satellite radar beam. The results indicate that most fields are oriented at angles that are neither parallel nor perpendicular to the radar beam, based on the classification scheme defined in Table 3.5. Furthermore, the orientation distributions of the calibration and validation subsets closely mirror that of the full dataset.

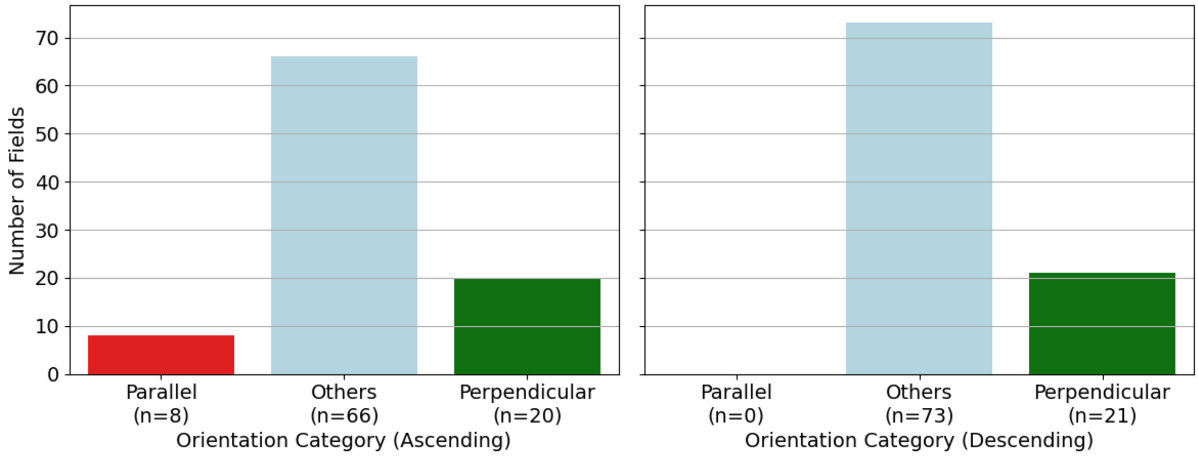

Figure 4.25: Angle between ploughing rows and the satellite radar beam of ascending and descending pass for the entire dataset. Each plot shows the orientation category and the number of fields in each category.

To further investigate the influence of ploughing angle on detection performance, Figures 4.26 to 4.29 illustrate the algorithm's results for both the calibration and validation datasets using the best-performing configuration (VH – ascending – orbit 88), alongside the corresponding field areas. No clear pattern emerged regarding the correct or incorrect detection of ploughing events in relation to field orientation. This lack of observable trend is primarily attributed to the unbalanced distribution of fields across the orientation categories. Similarly, no consistent relationship was found between field area and the accuracy of ploughing detection.

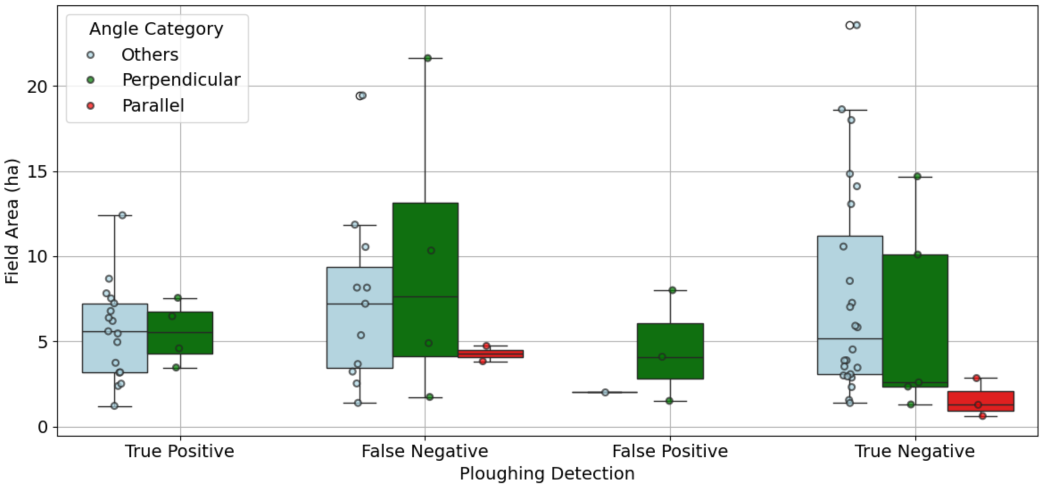

Figure 4.26: Effects of ploughing angle and field area on detection performance using the OR operator, based on the calibration dataset and the VH–ascending–orbit 88 configuration.

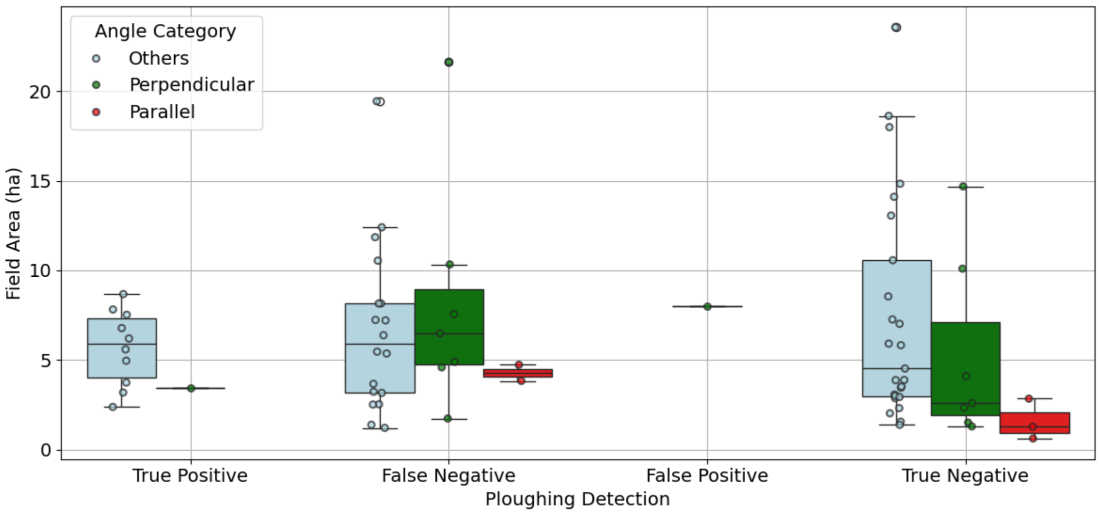

Figure 4.27: Effects of ploughing angle and field area on detection performance using the AND operator, based on the calibration dataset and the VH–ascending–orbit 88 configuration.

Similar results were observed in the validation dataset with respect to both ploughing angle and field area. The dataset included very few fields that were oriented parallel to the radar beam, all of which were correctly detected. It also demonstrated accurate detection of most perpendicular fields. However, as previously noted, the limited number of field samples—particularly in certain orientation categories—restricts the ability to draw definitive conclusions or generalize the results.

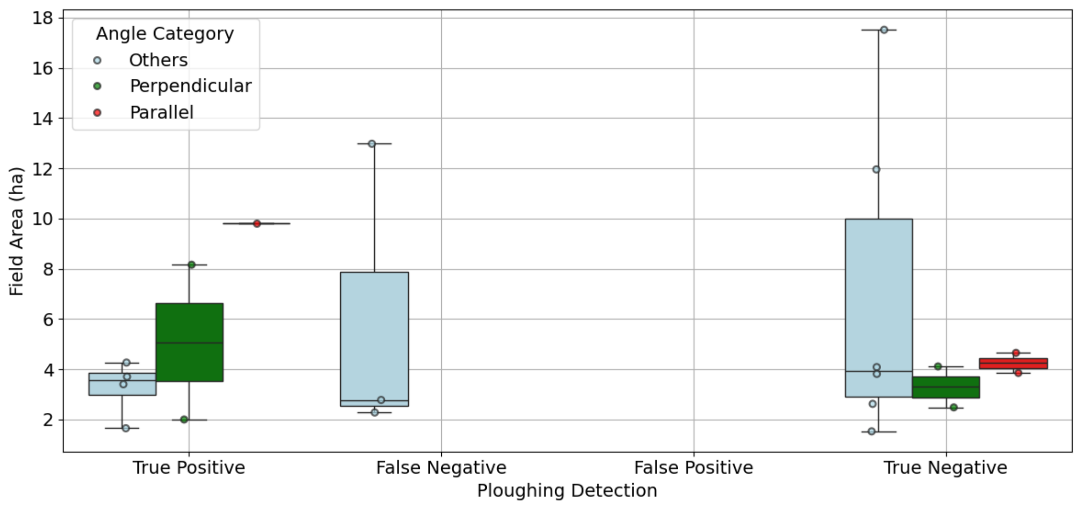

Figure 4.28: Effects of ploughing angle and field area on detection performance using the OR operator, based on the validation dataset and the VH–ascending–orbit 88 configuration.

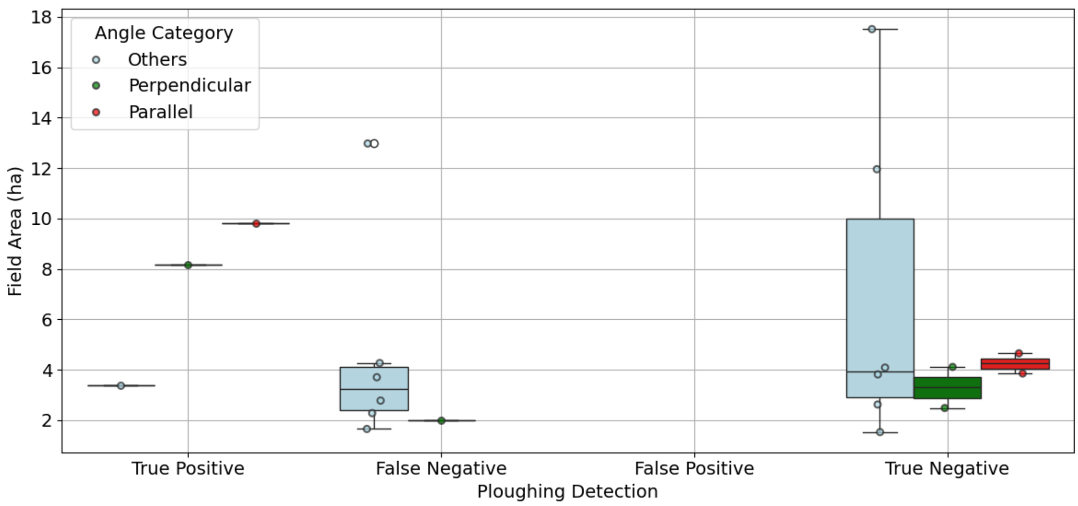

Figure 4.29: Effects of ploughing angle and field area on detection performance using the AND operator, based on the validation dataset and the VH–ascending–orbit 88 configuration.

4.3. Algorithm Modification: Precipitation Data Filtered

4.3.1. Calibration

The same dataset used to calibrate the original algorithm was also employed in this modified version; however, a key difference is that all data corresponding to days with precipitation exceeding 1 mm were filtered out. This section presents the highest accuracy achieved among the configurations evaluated in the sensitivity analysis. Comprehensive results, including configuration-specific tables and corresponding confusion matrices, are provided in the Appendix, Table 8.2.

Tillage Detection Based on Backscatter

Figure 4.30 illustrates the ploughing detection results based exclusively on backscatter data. The detection algorithm was calibrated to optimize the identification of ploughing events, achieving an overall accuracy of 87% and an F1-score of 73% (see Appendix, Table 8.2). While the presence of false positives reduced the precision of the backscatter-based method—particularly when applying a logical OR operator—it significantly increased the overall detection rate of ploughing events.

The accuracy assessment across all configurations indicates a general improvement; however, the highest accuracy was again achieved using the ascending pass, consistent with the results obtained from the previous algorithm.

Tillage Detection Based on Coherence

Figure 4.31 presents the ploughing detection results based on coherence data. With an overall accuracy of 88% and an F1-score of 67%, the coherence-based method outperformed the baseline algorithm (section 4.2.1). in both metrics. Moreover, the rate of false ploughing detections was lower in this approach, indicating improved reliability in distinguishing true ploughing events from other surface disturbances. However, the VH polarization, descending pass resulted in the approximately same accuracy, but the confusion matrix showed a lower TP detection (see Appendix, Table 8.3). The same accuracy was due to the less misclassifications of non-ploughing events achieved by descending pass.

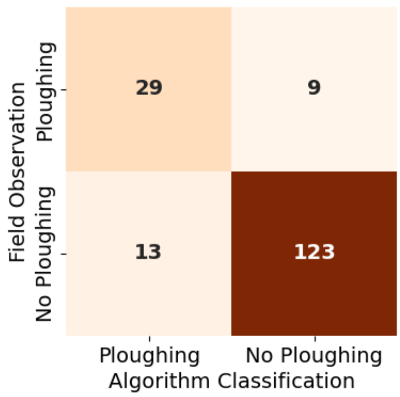

Figure 4.30: Confusion matrix derived from the comparison between in-situ observations and modified algorithm's backscatter change classification.

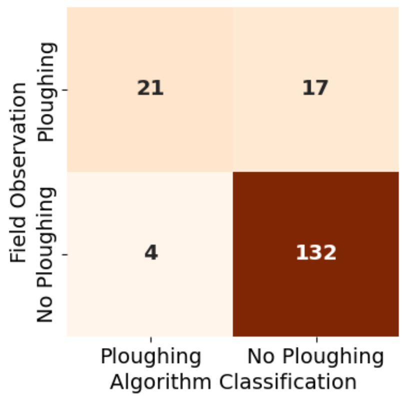

Figure 4.31: Confusion matrix derived from the comparison between in-situ observations and modified algorithm's coherence classification.

Tillage Detection Based on Coherence and Backscatter

Figures 4.32 and 4.33 illustrate the final ploughing detection results obtained by combining backscatter- and coherence-based outputs using logical AND and OR approaches. The AND approach yielded an overall accuracy of 89% and an F1-score of 66%. In contrast, the OR operator resulted in an overall accuracy of 87% and an F1-score of 74%. Both high-performing configurations were derived from VV ascending data; however, the AND approach yielded the best results using orbit 88, while the OR approach performed best with orbit 161. A possible explanation for this difference lies in the sensitivity of the logical operators to observation geometry. The AND approach, which requires both coherence and backscatter to detect ploughing simultaneously, benefits more from orbits with lower incidence angles—such as orbit 88—which tend to capture surface changes more robustly due to stronger signal returns and reduced geometric distortion. In contrast, the OR approach only requires one of the variables to indicate ploughing, making it less dependent on optimal viewing conditions. As a result, the influence of incidence angle is less pronounced, and higher-angle orbits like orbit 161 can still yield competitive results under the more relaxed detection criteria. A detailed analysis of all configurations is presented in Appendix, Table 8.4.

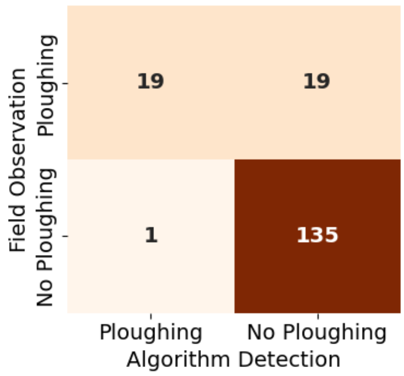

Figure 4.32: Confusion matrix derived from the comparison between in-situ observations and modified algorithm AND operator classification.

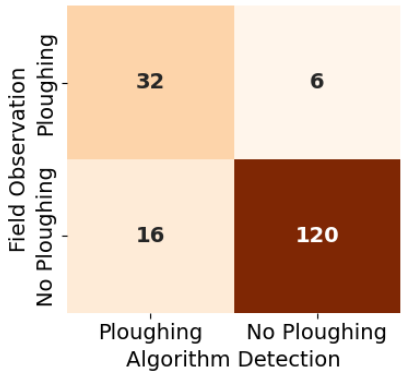

Figure 4.33: Confusion matrix derived from the comparison between in-situ observations and modified algorithm OR operator classification.

4.3.2. Validation

The algorithm was validated using the same 20% validation dataset, corresponding to 20 fields. The coherence-based method achieved an overall accuracy of 88% and an F1-score of 63% (see Table 8.6 in the Appendix). In contrast, the backscatter-based method produced a lower overall accuracy of 66% and an F1-score of 37% (see Table 8.5 in the Appendix).

The highest accuracy among the combined configurations, shown in Table 4.9, was obtained using the ascending pass. Specifically, the VV–ascending–161 configuration yielded the highest AND accuracy across all configurations of both the original and modified algorithms. Additionally, the VH–ascending–161 configuration achieved the highest OR F1-score of 80%, outperforming all other combinations.

A noticeable difference was observed in the performance of ploughing detection between ascending and descending passes (see Appendix, Table 8.7 for detailed confusion matrices).

Under the AND logic, VV polarization outperformed VH, while for the OR logic, the difference between VV and VH was less pronounced. Figures 4.34 and 4.35 illustrate the confusion matrices of highest final ploughing detection accuracies obtained by combining backscatter- and coherence-based outputs using logical AND and OR approaches.

Table 4.9: Accuracy analysis of various modified algorithm configurations derived from the validation process for both AND and OR approaches used in combining backscatter and coherence for ploughing detection.

Algorithm configuration		**Accuracy Results**			
Backscatter (polarization – pass – orbit)	**Coherence (polarization – pass)**	**AND**		**OR**	
		OA (%)	**F1 (%)**	**OA (%)**	**F1 (%)**
VH – Descending – 110	VH – Descending	80	0	86	53
VH – Descending – 37	VH – Descending	82	18	82	57
VH – Ascending – 161	VH – Ascending	84	33	92	80
VH – Ascending – 88	VH – Ascending	84	33	84	64
VV – Descending – 110	VV – Descending	80	0	67	0
VV – Descending – 37	VV – Descending	80	0	78	27
VV – Ascending – 161	VV – Ascending	90	67	86	72
VV – Ascending – 88	VV – Ascending	88	57	72	50

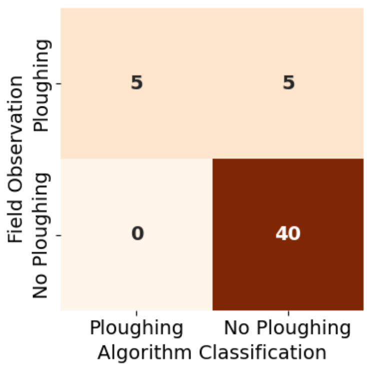

Figure 4.34: Confusion matrix derived from the comparison between in-situ observations and modified algorithm AND operator classification (VV ascending, orbit number 161).

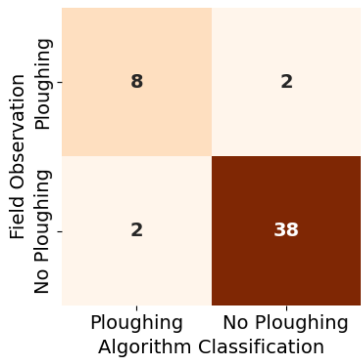

Figure 4.35: Confusion matrix derived from the comparison between in-situ observations and modified algorithm OR operator classification (VH ascending, orbit number 161).

4.3.3. Angle and Area Effects on Detection

Figures 4.36 to 4.39 presents the angle and area of the ploughing detection classes. The validation dataset tended to classify the parallel and perpendicular angled fields more correctly than the other angled fields, however this trend was not observed in calibration dataset. This result showed the ungeneralizable pattern since both the datasets were unbalanced.

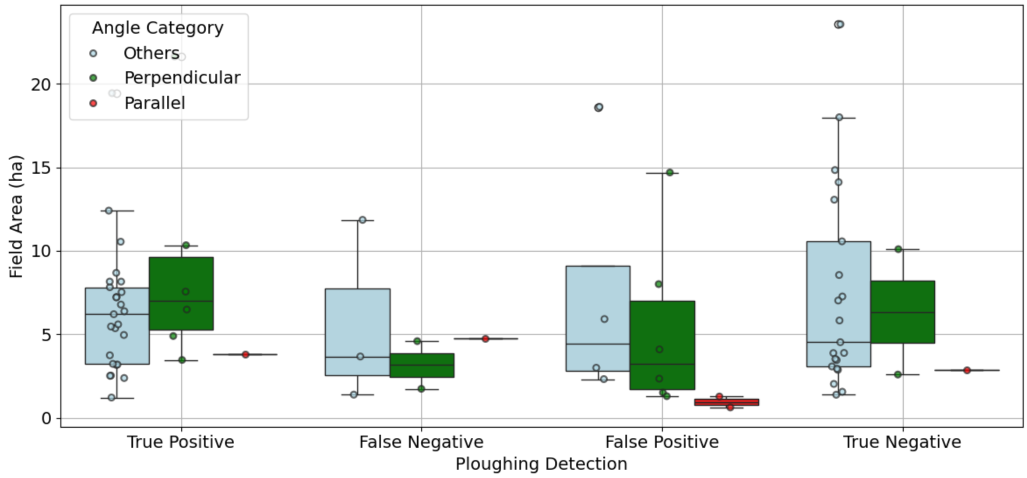

Figure 4.36: Effects of ploughing angle and field area on detection performance using the OR operator, based on the calibration dataset and the VV–ascending–orbit 161 configuration of the modified algorithm.

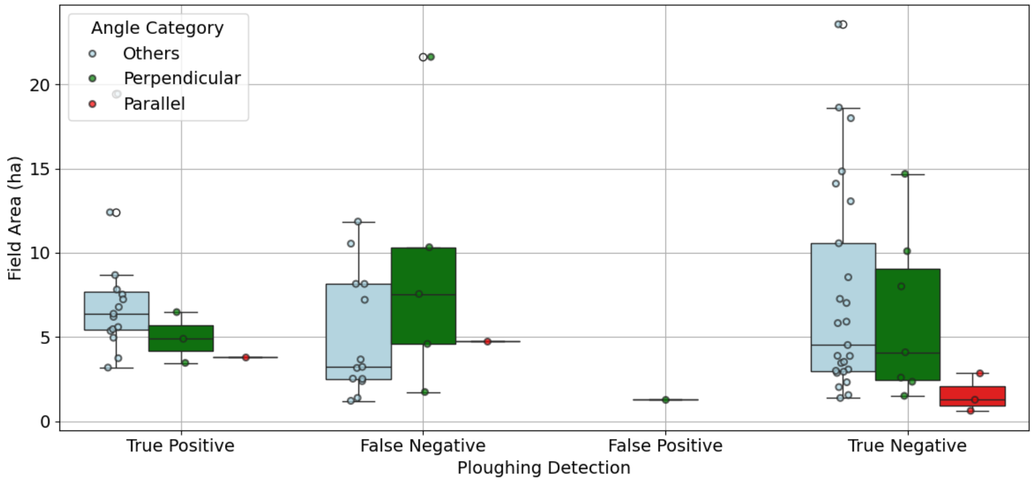

Figure 4.37: Effects of ploughing angle and field area on detection performance using the AND operator, based on the calibration dataset and the VV–ascending–orbit 88 configuration of the modified algorithm.

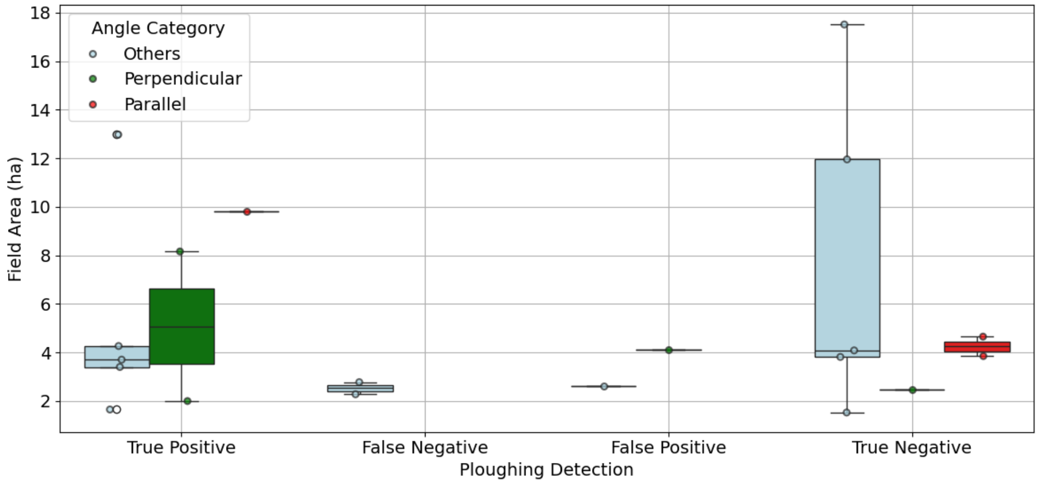

Figure 4.38: Effects of ploughing angle and field area on detection performance using the OR operator, based on the validation dataset and the VH–ascending–orbit 161 configuration of the modified algorithm.

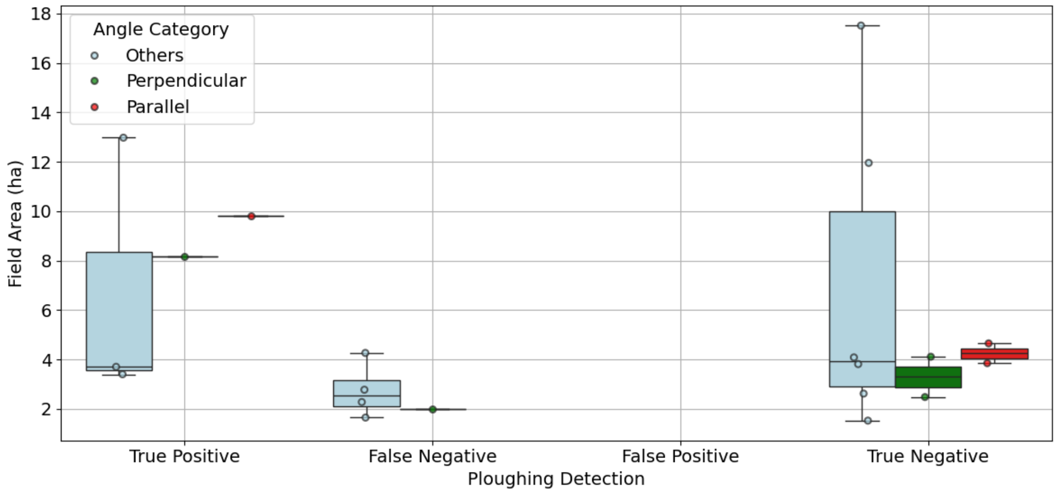

Figure 4.39: Effects of ploughing angle and field area on detection performance using the AND operator, based on the validation dataset and the VV–ascending–orbit 161 configuration of the modified algorithm.

4.4. Integrating the Copernicus Bare Soil Period into the top-performing configurations of the algorithms

To further refine the detection of ploughing events, the Copernicus Bare Soil Period was integrated into the best-performing configurations during the validation of both the original and modified algorithms. This integration, illustrated in Figures 4.40 to 4.43, aimed to address the limitations of using vegetation indices such as NDVI and DpRVI to identify bare soil conditions.

In the original algorithm, incorporating the Copernicus bare soil product into the best-performing OR configuration—VH polarization, ascending orbit, orbit number 88—resulted in a slight decrease in overall accuracy (from 94% to 92%), while the F1-score remained unchanged. Similarly, in the AND configuration for the same setup, overall accuracy declined from 86% to 82%, again with no change in the F1-score.

In contrast, when the Copernicus bare soil product was used in place of NDVI and DpRVI in the modified algorithm, a slight improvement in the F1-score was observed for the OR configuration. This improvement, illustrated by the confusion matrices in Figures 4.42 and 4.43, was primarily attributed to a reduction in false positives.

A closer examination of the confusion matrices reveals a reduction in the total number of non-ploughing events compared to the version using the NDVI- and DpRVI-derived bare soil period. This difference arises from the varying representations of surface cover transition periods between the NDVI-DpRVI and the Copernicus CP product. In particular, transitions from bare soil to vegetation cover—classified as non-ploughing—were more effectively masked by the CP product.

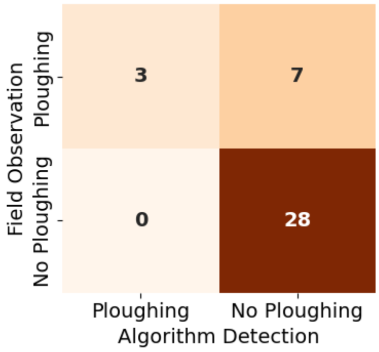

Figure 4.40: Confusion matrix for ploughing event detection using the Copernicus bare soil period within the AND VH-ascending-88 operator configuration of the algorithm.

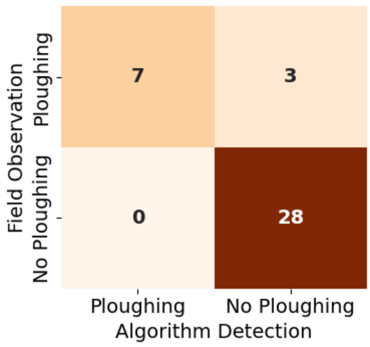

Figure 4.41: Confusion matrix for ploughing event detection using the Copernicus bare soil period within the OR operator VV-ascending-88 configuration of the algorithm.

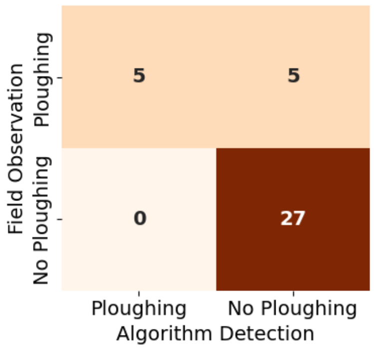

Figure 4.42: Confusion matrix for ploughing event detection using the Copernicus bare soil period within the AND operator VV-ascending-161 configuration of the modified algorithm.

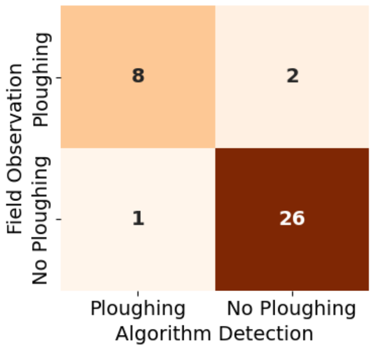

Figure 4.43: Confusion matrix for ploughing event detection using the Copernicus bare soil period within the OR operator VH-ascending-161 configuration of the modified algorithm.

CHAPTER FIVE

DISCUSSION

This chapter discusses the results presented in Chapter 4, with a particular emphasis on addressing the research objectives. It is structured into four main sections: (1) a discussion on the evaluation of the Copernicus Bare Soil Period; (2) a discussion on the results of the two algorithms used for tillage detection; (3) an analysis of the impact of incorporating the Copernicus bare soil period into the detection algorithm; and (4) a reflection on the limitations of the current approach and potential directions for future research.

5.1. CP Product Bare Soil Detection

The CP is a product with European coverage, encompassing a wide range of agronomic conditions. Notably, no overall accuracy assessment is provided in the product's user manual. In this study, a relatively precise accuracy assessment has been conducted for the specific context of the silty region of Wallonia, an area characterized by intensive agricultural practices.

The findings indicate that the Copernicus CP layer achieves a high overall accuracy of 84%. However, its performance fluctuates across different time steps, particularly during periods of phenological transition. The highest number of misclassifications occurs during the transition from bare soil to vegetated cover. At these times, bare soil is more frequently misclassified as non-bare soil, resulting in a reduction in precision.

This discrepancy may stem from differences between field observations and satellite-based assessments of vegetation cover. Small patches of newly emerged vegetation may be recorded as vegetated in field observations, while satellite imagery may not detect them until they expand. Additionally, the product's tendency to classify bare soil as vegetated cover—suggesting earlier crop emergence than observed in the field—may result from two factors. First, it may reflect a misclassification of seedbed preparation as non-bare soil, which can be considered a relatively minor issue since seedbed preparation generally occurs close to the actual crop emergence date. Second, it may be attributed to the model's definition of crop emergence, which is based on the appearance of the first unfolded leaves. This phenological stage may precede the threshold typically used in field assessments to identify vegetated cover.

5.2. Tillage Detection Algorithms

5.2.1. Algorithm development and Polarization Considerations

The decision to evaluate both VV and VH polarizations in this study was informed by contrasting findings in the existing literature. For instance, Satalino et al. (2018) highlighted the high sensitivity of VH backscatter to surface roughness and developed their tillage detection algorithm exclusively using VH data. Conversely, Chome et al. (2016) reported that VV polarization exhibited greater sensitivity to tillage activities than VH. These divergent perspectives justified the comprehensive assessment of both polarizations and acquisition geometries in this study to understand their influence on tillage detection accuracy.

However, the use of backscatter data alone for tillage detection proved to be less effective than anticipated, despite the precedents set by earlier studies. While previous research suggested that deep ploughing typically leads to an increase in backscatter due to enhanced surface roughness, such patterns were not consistently observed in the operational context of this study. The backscatter time series did not demonstrate a clear increase coinciding with tillage events. Consequently, the baseline algorithm based on the change detection approach using field-resolution backscatter yielded an F1-score of 0 across all configurations, indicating its inability to accurately detect tillage events.

A plausible explanation for this variability lies in the complexity of the underlying surface dynamics. As McNairn and Brisco (2004) noted, the type of tillage implements and the number of passes significantly influence surface roughness characteristics, thereby affecting both the intensity and behaviour of backscatter signals. Additionally, the surface conditions before and after the tillage event can markedly influence backscatter changes. For example, the presence of crop residue prior to tillage may initially contribute to volume scattering. If tillage then smoothens the surface and incorporates crop residue into the soil, the anticipated increase in surface roughness—and consequently in backscatter—may not be observed. Instead, the backscatter may stabilize or even decrease following the tillage event, likely due to a reduction in volume scattering.

In light of the variability and ambiguity associated with backscatter changes, this study adopted an approach based on observed reductions following tillage events, aiming to improve robustness in event detection. This methodological decision followed a detailed comparative analysis of field- and medium-resolution backscatter time series, with particular attention to periods surrounding field visits. A consistent pattern of decreased backscatter following tillage was identified, which was further validated by an F1-score of 67% and an overall accuracy of 88%. These results demonstrate not only the algorithm’s ability to accurately detect tillage events proximate to field observations, but also its robustness in avoiding false detections of unrelated surface changes.

However, it should be noted that the detected backscatter reductions may not be uniquely indicative of ploughing or harrowing alone, as similar signal responses could also result from other surface-disturbing practices such as rolling. This introduces a potential source of classification ambiguity, particularly in the absence of more detailed and temporally resolved in-situ observations.

5.2.2. Performance of Backscatter- and Coherence-Based Approaches

The backscatter-based detection algorithm demonstrated limited effectiveness, even after the application of sensitivity analyses. Notably, the exclusion of precipitation-affected data—expected to reduce noise—did not yield significant improvements in detection accuracy. These results suggest that backscatter alone may not serve as a reliable indicator of tillage activities. This outcome contrasts with the findings of Satalino et al. (2018), which may be explained by differences in dataset size, quality, or site-specific conditions. Expanding the calibration and validation dataset could help refine threshold definitions and improve classification reliability.

Coherence-based detection yielded similar results to the backscatter, further reinforcing that using each variable alone might not be as promising as the combination of the two. Therefore, integrating coherence with backscatter further improved detection performance by reducing the incidence of false positives. This outcome is consistent with the approach proposed by Satalino et al. (2024) who demonstrated that combining both variables enhances the robustness and reliability of tillage detection.

Overall, the adapted version of Satalino’s algorithm (the baseline algorithm developed in this study) performed well. Despite variations in performance across configurations—none of which were fully specified in the original study—the results here remained consistent and coherent. The algorithm successfully distinguished between tilled and non-tilled fields, achieving a relatively high overall accuracy.

5.2.3. Best Algorithm Configuration and Its Implications

The highest F1-score achieved by a configuration was 82%, obtained using the OR logical operation. This performance was associated with VH polarization, aligning with the original algorithm proposed by Satalino et al., who also favoured VH polarization. In contrast, results from the AND operator showed comparable accuracy for both VV and VH polarizations, when derived from the same pass (ascending) and orbit. This outcome suggests that the influence of polarization on detection performance may be limited when stricter logical conditions are applied. This finding is further supported by the literature. Benninga et al. (2020) noted that VV polarization is more sensitive to surface moisture than VH. Consequently, in a more inclusive detection strategy such as the OR approach, VH polarization performs better, likely due to its relative insensitivity to moisture-related noise. However, under the more restrictive AND condition, where both backscatter and coherence must jointly indicate ploughing, the impact of soil moisture is minimized, allowing both polarizations to yield similarly high performance.

Nonetheless, the subtle variations observed across configurations may be attributed to differences in radar incidence angle, which influence backscatter intensity, as well as the orientation of tillage patterns relative to the radar beam. Among all configurations, the highest detection accuracies were consistently achieved using the ascending pass, regardless of polarization or orbit. This result highlights the critical role of acquisition geometry and incidence angle in the accurate detection of tillage events. Notably, this finding contrasts with the results reported by Chome et al. (2016), who observed superior accuracy with descending pass data. The difference in performance between ascending and descending passes may be partially explained by their respective acquisition times: approximately 5:58 a.m. for descending and 5:30 p.m. for ascending passes. Chome et al. (2016) suggested that morning dew could increase surface moisture, thereby enhancing radar signal and improving classification performance. However, the findings of the present study suggest that this early morning moisture may, in fact, obscure tillage-induced backscatter changes, leading to reduced classification accuracy. Consequently, the ascending pass consistently yielded superior detection performance, underscoring its reliability for tillage monitoring.

Finally, the modest variations in algorithm performance across configurations raise concerns regarding the robustness of the thresholds established through sensitivity analysis. Two main factors likely contributed to this limitation: (1) the relatively small number of fields used for calibration and validation, which limits the generalizability of backscatter and coherence change signatures; and (2) the reliance on a temporal window for performance and accuracy assessment, necessitated by the lack of precise tillage dates. As tillage could have occurred at any point prior to the field visit, this window-based approach introduced an inherent degree of uncertainty into the detection and evaluation process. Although, the misalignment between Sentinel-1 acquisition dates and field visit dates further justified the use of temporal windows, despite their associated limitations.

5.2.4. Impact of Precipitation Removal: Baseline vs Modified Algorithm

To mitigate the influence of precipitation on detection accuracy, a modified version of the algorithm was implemented by excluding dates with recorded precipitation exceeding 1 mm. This adjustment aimed to refine threshold calibration and evaluate potential improvements in detection performance. A comparison between the backscatter-based detection results of the modified and baseline algorithms indicates an increase in accuracy across all configurations. This improvement can be attributed to two primary factors. First, the removal of precipitation-affected dates reduced signal noise, thereby enhancing the detection of ploughing-induced backscatter changes. Second, the exclusion of certain dates extended the temporal intervals between consecutive observations, thereby requiring a longer time window for backscatter-based detection. This extended window enhanced the accuracy of tillage detection using backscatter alone.

The F1-scores achieved by both the original and modified algorithms using the OR approach were similar, each exceeding 80%. However, a notable improvement was observed in the F1-score for the AND approach when the modified algorithm was applied. These results suggest that while the removal of precipitation-affected data had limited impact on the more permissive OR approach, it enhanced the performance of the stricter AND method. In terms of polarization, both VV and VH yielded comparably high accuracies. This can be attributed to the removal of moisture-related noise, which improved the performance of VV polarization due to its known sensitivity to soil moisture.

Overall, these findings indicate that the modified algorithm offers a more robust framework for reliable ploughing detection, aligning well with the study's objectives. Furthermore, the consistently better performance of the ascending pass compared to the descending pass underscores the importance of acquisition timing in tillage detection.

5.2.5. Influence of Tillage Orientation (Angle Effect)

Existing literature indicates that tillage rows oriented perpendicular to the radar beam produce stronger backscatter signals than those aligned parallel to it. This angular dependency is generally less pronounced in cross-polarized channels, such as VH. In this study, the observed discrepancies in algorithm's response could be partly explained by the limited number of fields with tillage orientations that were strictly parallel or perpendicular to the radar beam. In contrast, the majority of fields exhibited intermediate angles, which has reduced the ability to fully capture and generalize the angular effects observed in previous studies.

Moreover, the angular effect appeared more prominent in the results obtained using the OR logical operator. This is likely because the OR configuration places greater emphasis on backscatter, which is more sensitive to tillage orientation. In contrast, the AND operator—requiring both coherence and backscatter criteria to be met—has diminished the influence of backscatter alone.

5.2.6. Accuracy Assessment: why Event-based Evaluation?

This study employed an event-based assessment approach. The rationale for adopting this method is rooted in the limitations of parcel-based evaluations. While parcel-based assessments offer a general overview of algorithm performance—by verifying whether fields labelled as tilled were detected as such—they can be misleading. Detections may occur well before the actual field visit, introducing logical inconsistencies. Furthermore, the use of a temporal window can obscure false positives by attributing unrelated detections to tillage events.

In contrast, the event-based approach enabled a more detailed evaluation of the algorithm's behaviour across different surface cover transitions. It is important to recognize that ploughing and precipitation are not the only factors influencing backscatter variations. Other agricultural activities—such as seedbed preparation, potato ridging, and similar surface-disturbing practices—also alter soil structure and can generate backscatter signatures that closely resemble those of ploughing. This was particularly evident in the algorithm's misclassifications. The event-based method made it possible to identify such misclassifications, including transitions from bare soil to sowing and from sowing to potato ridge, which were erroneously detected as tillage events. Although this approach increased the number of true negatives, it offered a broader perspective on the algorithm's performance by highlighting its sensitivity to surface changes beyond ploughing.

Despite its advantages, the event-based method is constrained by the absence of precise tillage dates, which introduces temporal uncertainty and limits both the accuracy of ploughing detection and the robustness of performance evaluation. In certain cases, the algorithm identified potential ploughing events for which no corresponding ground truth data were available to validate their correctness. These undetermined instances were excluded from the accuracy assessment, as they often fell outside the defined evaluation window. However, such exclusions may lead to an underestimation of the algorithm's actual performance. Additionally, the event-based framework influences the threshold selection for ploughing detection, potentially complicating the distinction between primary and secondary tillage. To refine the evaluation and resolve these ambiguities, a more detailed reference dataset is required.

5.3. Effect of Bare Soil Period Implementation

NDVI- and DpRVI-derived bare soil indicators are susceptible to misclassification, particularly during transitional periods or in areas with sparse vegetation. To address this limitation, the Copernicus-derived bare soil mask—based on consistent and validated land cover observations—was incorporated with the expectation that it would provide a more robust temporal constraint for ploughing detection. This was intended to enhance reliability and reduce false detections driven by vegetative changes.

However, the integration of the Copernicus product did not lead to a meaningful improvement in tillage detection accuracy. The observed slight increase in overall accuracy is likely due to the omission of transitional surface states (e.g., from bare soil to vegetative cover) in the Copernicus dataset—states that are more readily captured using NDVI and DpRVI time series.

The primary difference between the Copernicus-derived bare soil mask and the NDVI-/DpRVI-based estimates lies in the delineation of the start and end dates of the bare soil periods. While this temporal misalignment had limited impact on the detection of spring ploughing—where tillage events typically occur outside the predefined bare soil windows—the Copernicus product may prove more effective in post-harvest tillage detection. In such cases, ploughing often occurs shortly after harvest, making accurate identification of bare soil conditions more critical for reliable detection.

5.4. Limitations and Future Directions

Despite the promising outcomes of this study, several limitations must be acknowledged, and multiple avenues for future work remain open. Addressing these issues will be essential for improving the robustness, generalizability, and operational applicability of the proposed tillage detection framework.

One of the most significant limitations is the relatively small size and limited heterogeneity of the ground truth dataset. A larger and more diverse calibration set would facilitate the development of more representative and reliable thresholds for both backscatter and coherence metrics. In particular, increasing the variety of field management practices would help capture a broader range of tillage signatures. Similarly, a more comprehensive validation dataset would allow for a more rigorous and statistically meaningful performance assessment, reducing the risk of overfitting and enhancing model transferability.

Another key constraint was the absence of precise tillage dates. In many cases, tillage was inferred based on field visit records and temporal windows, introducing uncertainty into the accuracy assessment. Applying a time window for accuracy assessment and threshold sensitivity analysis—set to one week in this study—can be considered a double-edged sword. Due to the absence of precise tillage timing in the ground truth data, a time window was necessary to align with the temporal resolution of the satellite acquisitions used for calculating coherence and backscatter change. While this approach helps accommodate uncertainties in observation timing, the results demonstrated a high sensitivity of the detection algorithm to the chosen window length. This underscores both the necessity and the potential limitations of using fixed time windows in the presence of temporally imprecise ground observations. Moreover, as noted by Robertson et al. (2023), fields may undergo secondary or even tertiary tillage. Without knowledge of the exact timing of these events, correctly identifying and counting each tillage instance becomes difficult. This limitation reduces the precision that an event-based method could otherwise offer in capturing the number and timing of tillage operations per field. Therefore, recording the exact date of tillage operations—ideally through closer collaboration with farmers or the use of automated logging tools—would significantly improve the reliability of evaluation and model calibration.

A further limitation lies in the inability of this study to differentiate between specific types of tillage operations, such as ploughing, harrowing, or rolling. While Satalino et al. (2024) methodology enables such distinctions, this work was constrained by a lack of detailed field-level tillage records. Future research should prioritize the collection of activity-specific ground observations, including the type, intensity, and depth of tillage. This additional metadata would not only improve the interpretability of observed backscatter and coherence responses but also enable the development of more refined classification schemes and thresholds.

Finally, while preliminary findings suggested a potential influence of tillage row orientation on detection performance, a comprehensive analysis of this angular effect was not possible due to the limited availability of clearly categorized orientation data. Future datasets should include explicit documentation of tillage row directions, allowing fields to be grouped into angular classes (e.g., parallel, perpendicular, oblique) relative to the radar line of sight. Such categorization would enable a more systematic investigation into the interaction between radar geometry and surface disturbance, ultimately leading to more reliable, orientation-aware detection strategies.

In summary, while this study demonstrates the feasibility of detecting tillage using Sentinel-1 backscatter and coherence, its findings underscore the importance of improving ground truth data quality, precision, and diversity. Future work should aim to expand the dataset, incorporate more detailed metadata, and explore orientation-dependent and activity-specific detection approaches to fully exploit the capabilities of radar remote sensing for agricultural practices monitoring.

CHAPTER SIX

CONCLUSION

The primary objective of this master's thesis was to develop a tillage detection algorithm grounded in existing literature and to investigate the potential of Sentinel-1-derived metrics for detecting tillage activities. To address this objective, both backscatter and coherence data derived from Sentinel-1 imagery were analysed for their ability to detect tillage events. The analysis was further supported by a field campaign conducted in 2021 in the region of Gembloux, Belgium, which provided valuable in-situ observations to complement the satellite data.

The proposed tillage detection algorithm, which utilized both cross-polarized (VH) and co-polarized (VV) signals, yielded a two-level classification scheme distinguishing between high-confidence and low-confidence detections. Although the lack of precise tillage dates within the ground truth dataset posed a significant limitation for the accuracy assessment, the findings demonstrated that, beyond polarization, the satellite pass had a notable influence on algorithm performance.

A more detailed ground truth dataset, including exact tillage dates, would enable a more comprehensive and reliable evaluation of the algorithm's effectiveness. Such temporal precision would also facilitate finer assessments of confidence levels and support improvements in threshold calibration and detection robustness. In addition, incorporating high-resolution imagery from sources such as Google Earth or orthophotos could help increase the effective temporal resolution of the monitoring framework, enabling the detection of short-term tillage-induced surface changes.

More broadly, despite the limitations imposed by the ground truth data and the inherent difficulty in capturing the short-lived remote sensing signature of tillage events, the initial results obtained from the developed method offered valuable insights into the feasibility and challenges of tillage detection using radar data. Furthermore, the algorithm showed a reasonable capacity to distinguish between tillage and seedbed preparation activities—two practices that often produce similar effects on the surface—suggesting that the method is sensitive to subtle differences in soil disturbance.

Additionally, the findings of this study indicated that, for the detection of transient events such as tillage, the use of alternative strategies—such as employing medium-scale analysis rather than filtering out data affected by noise or potential errors (e.g., precipitation)—can also yield effective results. This approach allows for the retention and utilization of a larger portion of the available dataset, which is particularly important when targeting events that occur within short temporal windows. By focusing on broader temporal patterns rather than discarding potentially informative observations, medium-scale analysis offers a practical balance between noise tolerance and detection sensitivity. Nevertheless, further research is needed to systematically evaluate the trade-offs associated with this approach, particularly in diverse agro-ecological contexts and under varying environmental conditions.

Although there remains considerable scope for enhancing the detection method—particularly in refining its sensitivity to tillage-induced surface changes and enabling it to identify secondary or tertiary tillage events where applicable—the results of this study contribute meaningfully to the field of agricultural monitoring. The proposed approach aligns with the objectives of the Common Agricultural Policy, which advocates for improved monitoring of conventional agricultural practices in order to mitigate their environmental impacts and promote the transition toward more sustainable farming systems.

BIBLIOGRAPHY

Ahmed, F., Fernandez, M., Baker, L., Brock, S., & Jekums, A. (2021). The politics of knowledge: understanding the evidence for agroecology, regenerative approaches, and indigenous foodways. *Global Alliance for the Future of Food*.

ASF. (n.d.). Introduction to SAR [Figure]. https://tinyurl.com/yhyujt4a.

Baghdadi, N., Cresson, R., Pottier, E., Aubert, M., Zribi, M., Jacome, A., & Benabdallah, S. (2012). A potential use for the C-band polarimetric SAR parameters to characterize the soil surface over bare agriculture fields. *IEEE Transactions on Geoscience and Remote Sensing, 50(*10 PART1), 3844–3858. https://doi.org/10.1109/TGRS.2012.2185934.

Balenzano, A., Mattia, F., Satalino, G., & Davidson, M. W. J. (2011). Dense Temporal Series of C- and L-band SAR Data for Soil Moisture Retrieval Over Agricultural Crops. *IEEE Journal of Selected Topics in Applied Earth Observations and Remote Sensing*, *4*(2), 439–450. https://doi.org/10.1109/JSTARS.2010.2052916.

Benninga, H. J. F., van der Velde, R., & Su, Z. (2020). Sentinel-1 soil moisture content and its uncertainty over sparsely vegetated fields. *Journal of Hydrology X*, *9*, 100066.

Busari, M. A., Kukal, S. S., Kaur, A., Bhatt, R., & Dulazi, A. A. (2015). Conservation tillage impacts on soil, crop and the environment. International Soil Water Const Result, 3, 119e129.

Cho, S., Xiu, H., & Matsuoka, M. (2023). Backscattering Characteristics of SAR Images in Damaged Buildings Due to the 2016 Kumamoto Earthquake. *Remote Sensing*, *15*(8). https://doi.org/10.3390/rs15082181.

Chomé, G., Baret, P., & Defourny, P. (2016). Mapping farming practices in Belgian intensive cropping systems from Sentinel-1 SAR time-series. *Living Planet Symposium 2016* (Prague, Czech Republic, May 9–13, 2016). In *Proceedings of Living Planet Symposium 2016*.

Copernicus Land Monitoring Service. (n.d.). https://land.copernicus.eu/en/products/high-resolution-layer-croplands.

CRA-W. (n.d.). *AGROMET: A web-based weather platform for agricultural decision support systems*. https://www.cra.wallonie.be/en/agromet. Visited on 01-05-2025.

Dai, K., Feng, Y., Zhuo, G., Tie, Y., Deng, J., Balz, T., & Li, Z. (2022). Applicability analysis of potential landslide identification by InSAR in Alpine-Canyon terrain—Case study on Yalong River. *IEEE Journal of Selected Topics in Applied Earth Observations and Remote Sensing*, *15*, 2110-2118.

Derpsch, R., Friedrich, T., Kassam, A., & Li, H. (2010). Current status of adoption of no-till farming in the world and some of its main benefits. *International journal of agricultural and biological engineering*, *3*(1), 1-25.

ESA. (n.d.) SentiWiki: Sentinel-1 & Sentinel-2. https://sentiwiki.copernicus.eu/web. Visited on 01-05-2025.

FAO. (n.d.). definition of conservative agriculture. https://www.fao.org/conservation-agriculture/en/. Visited on 10-10-2024.

FAO. (2001). *Guidelines and reference materials for promoting integrated soil and nutrient management in Farmer Field Schools: Reference material for the module on tillage*. Food and Agriculture Organization of the United Nations, Land and Plant Nutrition Management Service, Land and Water Development Division.

Geoportail Wallonie. (n.d.). *Géoportail de la Wallonie*. https://geoportail.wallonie.be/home.html. visited on 2024-11-20.

Gupta Choudhury, S., Srivastava, S., Singh, R., Chaudhari, S., Sharma, D., Joshi, P., Tripathi, R., Kumar, S., Singh, S., & Sarkar, D. (2014). Tillage and residue management effects on soil aggregation, organic carbon dynamics and yield attribute in rice–wheat cropping system under reclaimed sodic soil. *Soil and Tillage Research*, 76–83.

Harikrishnan. (2019). *Confusion matrix, accuracy, precision, recall, F1 score*. Medium. https://medium.com/analytics-vidhya/confusion-matrix-accuracy-precision-recall-f1-score-ade299cf63cd. Visited on 10-01-2025.

Hassan, W., Li, Y., Saba, T., Jabbi, F., Wang, B., Cai, A., Wu, J., (2022). Improved and Sustainable Agroecosystem, Food Security and Environmental Resilience Through Zero Tillage with Emphasis on Soils of Temperate and Subtropical Climate Regions: A Review. International Soil and Water Conservation Research. 10, 530–545.

Hobbs, P. R., Sayre, K., & Gupta, R. (2008). The role of conservation agriculture in sustainable agriculture. *Philosophical Transactions of the Royal Society B: Biological Sciences*, *363*(1491), 543-555.

Hou, P., Liu, Y., Liu, W., Yang, H., Xie, R., Wang, K., ... & Li, S. (2021). Quantifying maize grain yield losses caused by climate change based on extensive field data across China. *Resources, Conservation and Recycling*, *174*, 105811.

Jasrotia, P., Kumari, P., Malik, K., Kashyap, P. L., Kumar, S., Bhardwaj, A. K., & Singh, G. P. (2023). Conservation agriculture based crop management practices impact diversity and population dynamics of the insect-pests and their natural enemies in agroecosystems. In *Frontiers in Sustainable Food Systems* (Vol. 7). Frontiers Media S.A. https://doi.org/10.3389/fsufs.2023.1173048.

JCBL. (2024). *Disc plough* [Photograph]. https://tinyurl.com/bdd6yfj5.

Joerg, H., Pardini, M., Hajnsek, I., & Papathanassiou, K. P. (2017). On the Separation of Ground and Volume Scattering Using Multibaseline SAR Data. *IEEE Geoscience and Remote Sensing Letters*, *14*(9), 1570–1574. https://doi.org/10.1109/LGRS.2017.2723980.

Joshi, N., Baumann, M., Ehammer, A., Fensholt, R., Grogan, K., Hostert, P., Jepsen, M. R., Kuemmerle, T., Meyfroidt, P., Mitchard, E. T. A., Reiche, J., Ryan, C. M., & Waske, B. (2016). A review of the application of optical and radar remote sensing data fusion to land use mapping and monitoring. In *Remote Sensing* (Vol. 8, Issue 1). MDPI AG. https://doi.org/10.3390/rs8010070.

KappaZeta. (2024, August). *KappaZeta webinar: AI-based tillage detection for improved agricultural and climate policies* [Video]. YouTube. https://www.youtube.com/watch?v=ERODp6pcnhQ.

Kristensen, E. F., Sørensen, C., & Asabe. (2006). *Ridge tillage of organic row crops*. https://doi.org/10.13031/2013.21016.

KUHN. (n.d.). *Strip till*. https://tinyurl.com/nhhwakza.

Lal, R. (1993) Tillage effects on soil degradation, soil resilience, soil quality, and sustainability. Soil and Tillage Research, 27, 1-8. http://dx.doi.org/10.1016/0167-1987(93)90059-X

McNairn, H., & Brisco, B. (2004). The application of C-band polarimetric SAR for agriculture: A review. *Canadian journal of remote sensing*, *30*(3), 525-542.

McNairn, H., Jiao, X., Gaweesh, O., Schultz, S., Davidson, A., & Joosse, P. (2024, July). SAR Coherent Change Detection To Monitor Beneficial Agricultural Practices. In *IGARSS 2024-2024 IEEE International Geoscience and Remote Sensing Symposium* (pp. 1253-1255). IEEE.

Michelson, D. B. (1994). ERS-I SAR backscattering coefficients from bare fields with different tillage row directions. *International Journal of Remote Sensing*, *15*(13), 2679–2685. https://doi.org/10.1080/01431169408954275

NASA. (n.d.). *Synthetic Aperture Radar*. https://www.earthdata.nasa.gov/learn/earth-observation-data-basics/sar.

O'donoghue, T., Minasny, B., & McBratney, A. (2022). Regenerative Agriculture and Its Potential to Improve Farmscape Function. In *Sustainability (Switzerland)* (Vol. 14, Issue 10). MDPI. https://doi.org/10.3390/su14105815.

Okorie, B. O., & Niraj, Y. (2022). Effects of different tillage practices on soil fertility properties: A review. *International Journal of Agriculture and Environmental Research*, *8*(1), 176-193. https://doi.org/10.51193/ijaer.2022.8112.

QUIVOGNE. (n.d.). *Disc ploughing* [Photograph]. https://tinyurl.com/nhhev2sy.

Riechmann Bros. (n.d.). *Moldboard ploughing* [Photograph]. https://tinyurl.com/4zfnty49.

Robertson, L. D., McNairn, H., van der Kooij, M., Jiao, X., Ihuoma, S., & Joosse, P. (2023). Monitoring autumn agriculture activities using Synthetic Aperture Radar (SAR) and coherence change detection. *Heliyon*, *9*(6).

Sabery, S. M., Bystrov, A., Navarro-Cía, M., Gardner, P., & Gashinova, M. (2021). Study of low terahertz radar signal backscattering for surface identification. *Sensors, 21*(9). https://doi.org/10.3390/s21092954.

Satalino, G., Mattia, F., Balenzano, A., Lovergine, F. P., Rinaldi, M., De Santis, A. P., ... & Moreno, J. F. (2018, July). Sentinel-1 & Sentinel-2 data for soil tillage change detection. In *IGARSS 2018-2018 IEEE International Geoscience and Remote Sensing Symposium* (pp. 6627-6630). IEEE.

Satalino, G., Palmisano, D., Balenzano, A., Lovergine, F., Mattia, F., Nutini, F., Boschetti, M., Verza, G., Rinaldi, M., Ruggieri, S., Ciavarella, F., Manganiello, C., Gómez, V. P., & García, D. A. N. (2024). *Copernicus Sentinels For Tillage Change Detection*. 1249–1252. https://doi.org/10.1109/igarss53475.2024.10641126.

Sharma, C., Pathak, P., Kumar, A., & Gautam, S. (2024). Sustainable regenerative agriculture allied with digital agri-technologies and future perspectives for transforming Indian agriculture. In *Environment, Development and Sustainability*. Springer Science and Business Media B.V. https://doi.org/10.1007/s10668-024-05231-y1.

Shutterstock. (2024). *[Tractor in the field with subsoiler used for deep tillage, loosening and breaking up soil at depths*] [Stock photo]. https://www.shutterstock.com/.

Sivasankar, T., Kumar, D., Srivastava, H. S., & Patel, P. (2018). *Advances in Radar Remote Sensing of Agricultural Crops: A Review*. *8*(4).

Srivastava, H. S., Patel, P., & Navalgund, R. R. (2006). How far SAR has fulfilled its expectation for soil moisture retrieval. *Microwave Remote Sensing of the Atmosphere and Environment V*, *6410*, 641001. https://doi.org/10.1117/12.693946.

Sumberg, J., & Giller, K. E. (2022). What is 'conventional'agriculture?. *Global Food Security*, *32*, 100617.

Syahali, S., & Ewe, H. T. (2016). *Backscattering Analysis for Snow Remote Sensing Model with Higher Order of Surface-Volume Scattering* (Vol. 48).

Szigarski, C., Jagdhuber, T., Baur, M., Thiel, C., Parrens, M., Wigneron, J. P., ... & Entekhabi, D. (2018). Analysis of the radar vegetation index and potential improvements. *Remote sensing*, *10*(11), 1776.

Thenkabail, P. S. (2010). Global croplands and their importance for water and food security in the twenty-first century: Towards an ever green revolution that combines a second green revolution with a blue revolution. In *Remote Sensing* (Vol. 2, Issue 9, pp. 2305–2312). https://doi.org/10.3390/rs2092305.

Tian, X., Engel, B. A., Qian, H., Hua, E., Sun, S., & Wang, Y. (2021). Will reaching the maximum achievable yield potential meet future global food demand?. *Journal of Cleaner Production*, *294*, 126285.

Van Tricht, K., Gobin, A., Gilliams, S., & Piccard, I. (2018). Synergistic use of radar sentinel-1 and optical sentinel-2 imagery for crop mapping: A case study for Belgium. *Remote Sensing*, *10* (10). https://doi.org/10.3390/rs10101642.

Voormansik, K., Zalite, K., Sünter, I., Tamm, T., Koppel, K., Verro, T., Brauns, A., Jakovels, D., & Praks, J. (2020). Separability of mowing and ploughing events on short temporal baseline sentinel-1 coherence time series. In *Remote Sensing* (Vol. 12, Issue 22, pp. 1–17). MDPI AG. https://doi.org/10.3390/rs12223784.

Wang, Y., Yu, A., Wang, P., Shang, Y., Wang, F., Lyu, H., ... & Chai, Q. (2025). No-tillage with total green manure mulching can improve soil moisture and temperature environment, promote maize root structure and photosynthetic capacity to increase maize yield. *Journal of Integrative Agriculture*.

Zhang, W., Yu, Q., Tang, H., Liu, J., & Wu, W. (2024). Conservation tillage mapping and monitoring using remote sensing. *Computers and Electronics in Agriculture*, *218*. https://doi.org/10.1016/j.compag.2024.108705.

Zhou, Y. (2024). *Modelling the Space-Time Dynamics of Soil Organic Carbon Stock: From Point to Landscape Scale* (Doctoral dissertation, UCL-Université Catholique de Louvain). http://hdl.handle.net/2078.1/294795.

APPENDIX

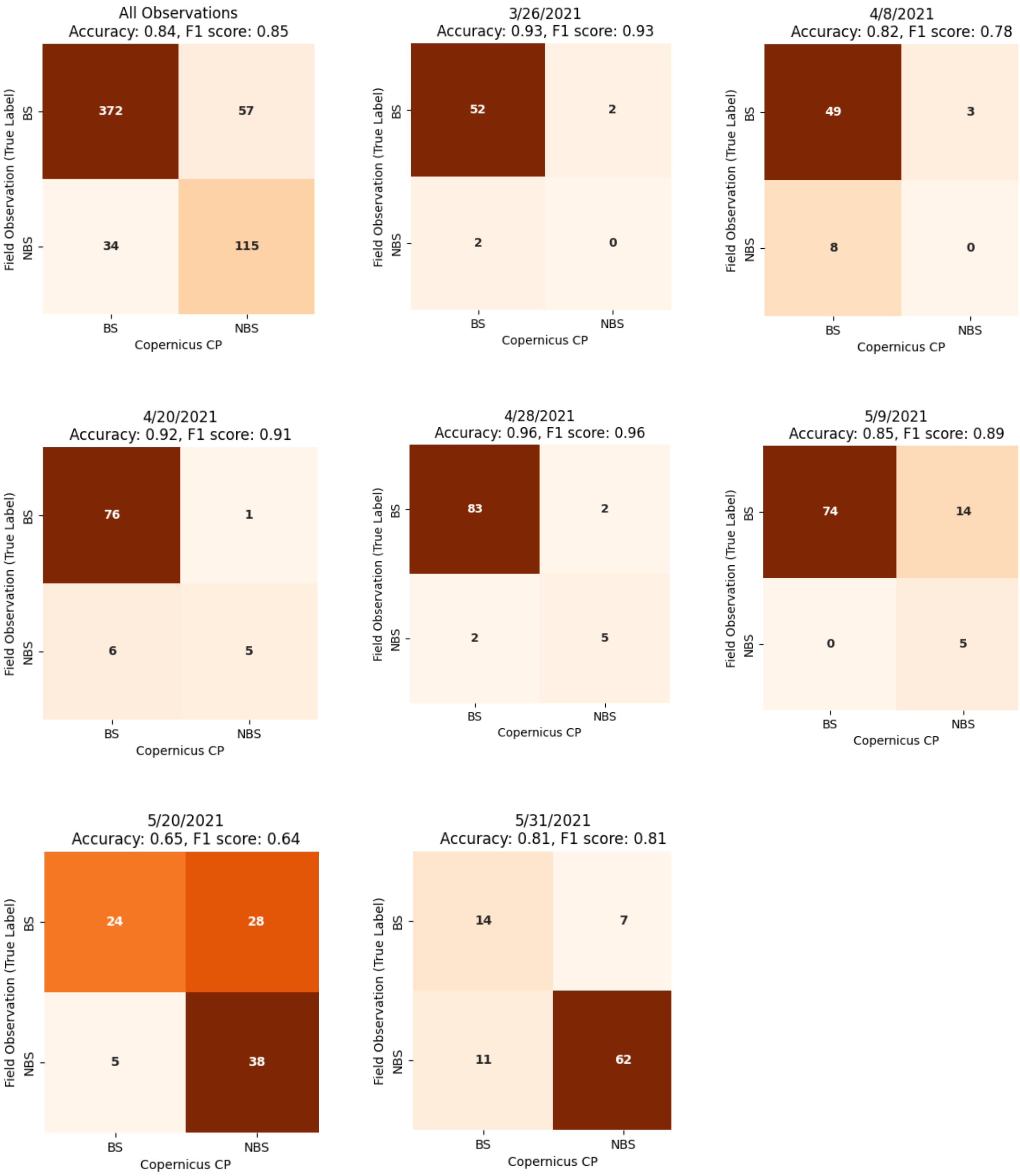

Figure 8.1: Confusion matrices derived from the comparison between in-situ observations and Cropping Patterns product detections, presenting classification performance for each individual field visit date.

Table 8.1: HR and MR thresholds resulted from sensitivity analysis of raw backscatter and its changes in the calibration process, and the result of the accuracy assessment.

Algorithm configuration (polarization – pass – orbit)	HR $\Delta\sigma^0$ threshold (dB)	MR $\Delta\sigma^0$ threshold (dB)	OA (%)	F1 (%)
VH – Descending – 110	1.5	0.5	77	0
VH – Descending – 37	2	1	77	0
VH – Ascending – 161	1.5	0.5	78	0
VH – Ascending – 88	3.5	2.5	77	0
VV – Descending – 110	1.5	0.5	77	0
VV – Descending – 37	2.5	1.5	77	0
VV – Ascending – 161	2.5	1	78	0
VV – Ascending – 88	2.5	1.6	76	0

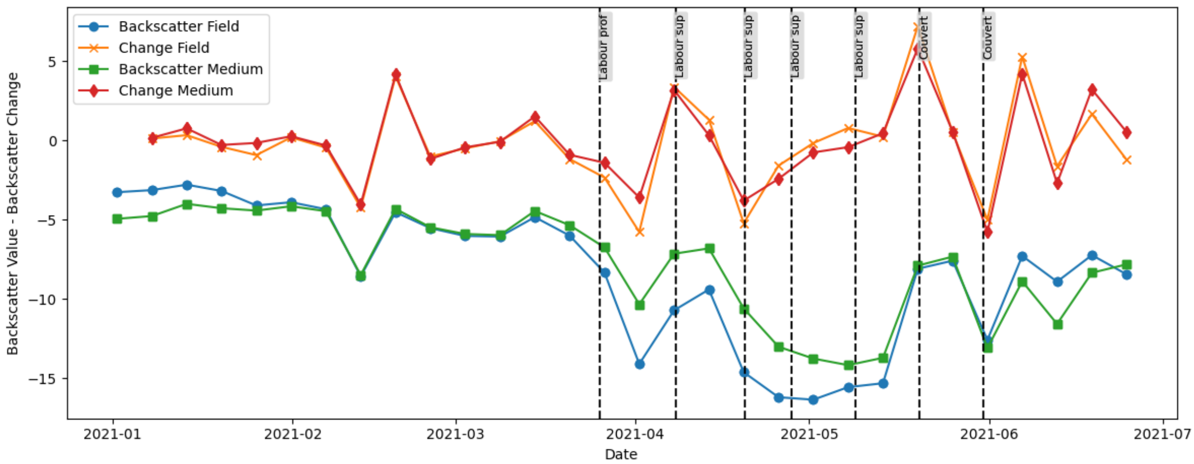

Figure 8.2: VV backscatter time series and change classification for orbit 88 of the ascending pass. This example is representative from a broader perspective, as it illustrates the absence of significant backscatter spikes near the date of the field observation or prior to it—indicating no evident ploughing activity detected in this period.

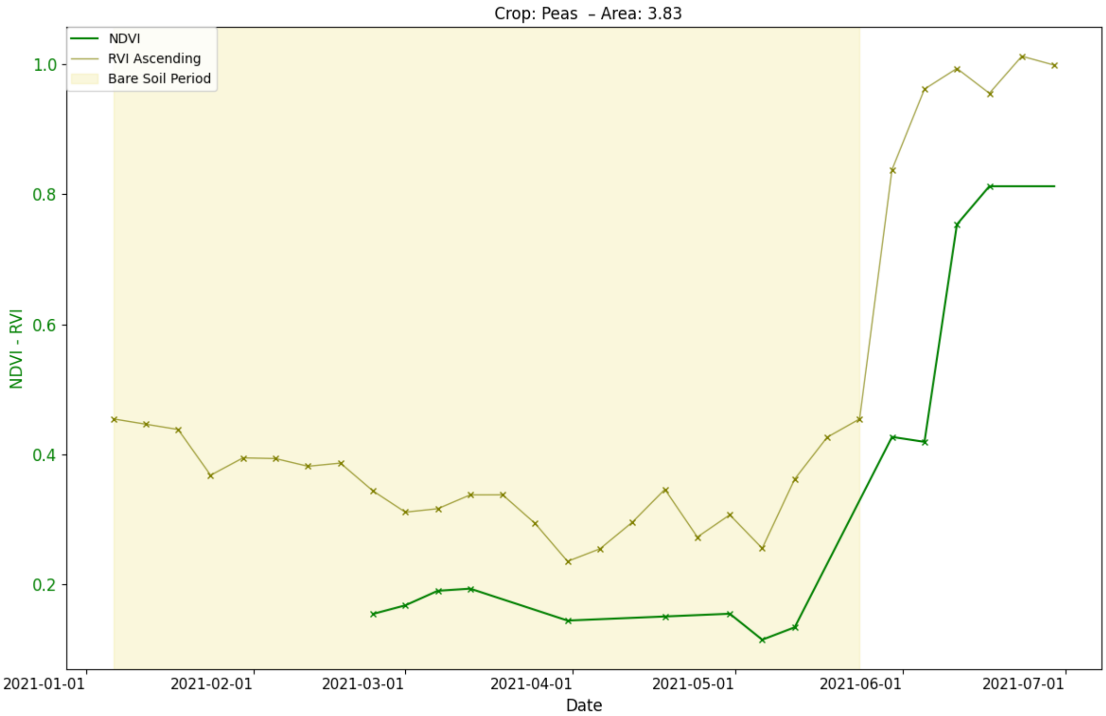

Figure 8.3: Bare soil period extracted from the NDVI and DpRVI indices shown in khaki.

Table 8.2: Accuracy assessment of backscatter-based ploughing detection during the calibration process of modified algorithm, highlighting the performance of various configurations.

Algorithm configuration (polarization – pass – orbit)	**HR $\Delta\sigma^0$ threshold (dB)**	**OA**	**F1**	**Confusion Matrix**
VH – Descending – 110	-3.5	71	19	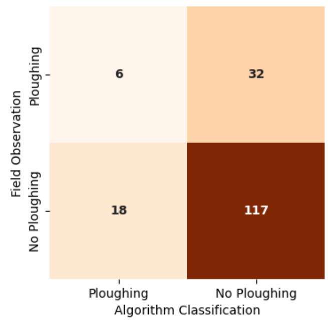
VH – Descending – 37	-2.5	73	42	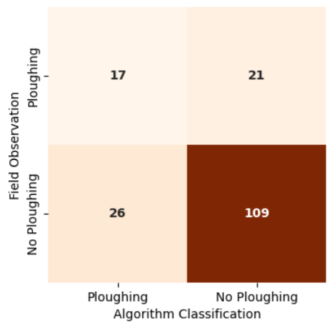

VH – Ascending – 161	-2.6	85	60	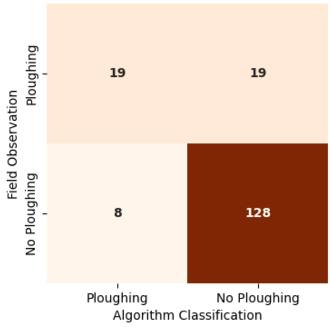
VH – Ascending – 88	-3.5	76	44	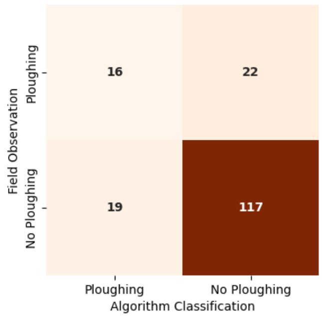
VV – Descending – 110	-3	69	23	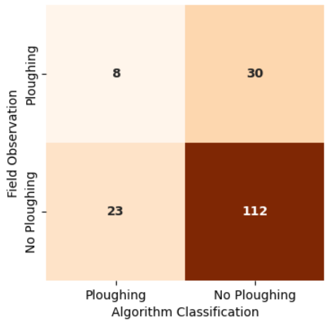
VV – Descending – 37	-2.5	67	4	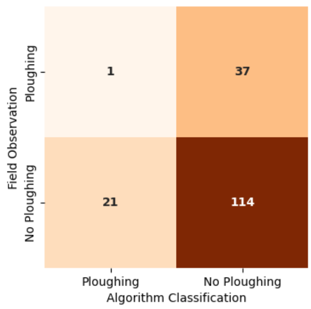
VV – Ascending – 161	-2.34	87	73	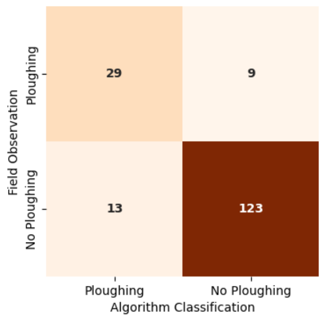

VV – Ascending – 88	-3.5	74	57	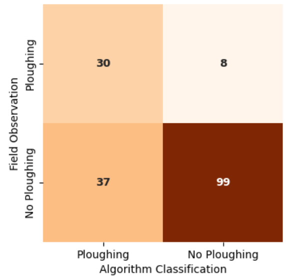

Table 8.3: Accuracy assessment of coherence-based ploughing detection during the calibration process of modified algorithm, highlighting the performance of various configurations.

Algorithm configurations (polarization – pass)	**HR coherence threshold**	**HR coherence threshold**	**OA**	**F1**	**Confusion Matrix**
VV – Descending	0.4	- 0.45	80	19	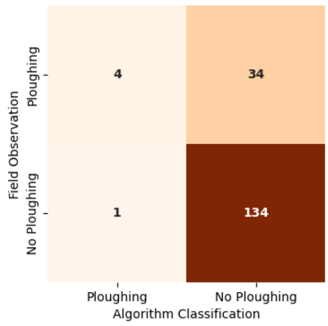
VV – Ascending	0.4	- 0.5	88	67	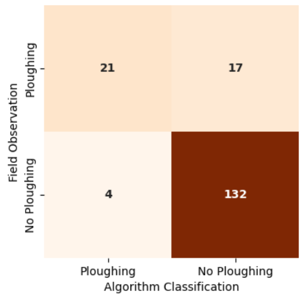
VH – Descending	0.3	- 0.4	88	66	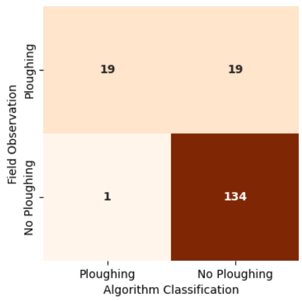

<table>
<tr><td>VH – Ascending</td><td>0.4</td><td>- 0.3</td><td>86</td><td>59</td><td>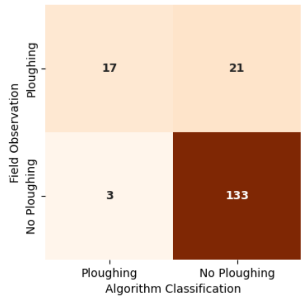</td></tr>
</table>

Table 8.4: Accuracy assessment of final ploughing detection during the calibration process of modified algorithm, highlighting the performance of various configurations.

<table>
<tr><th>Algorithm configuration</th><th colspan="2">AND</th><th rowspan="2">CM</th><th colspan="2">OR</th><th rowspan="2">CM</th></tr>
<tr><th>(polarization – pass – orbit)</th><th>OA</th><th>F1</th><th>OA</th><th>F1</th></tr>
<tr><td>VH – Descending – 110</td><td>78</td><td>0</td><td>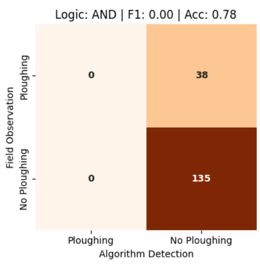</td><td>82</td><td>61</td><td>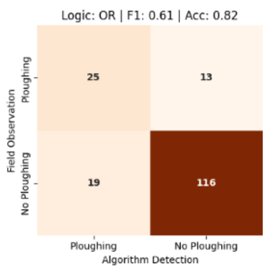</td></tr>
<tr><td>VH – Descending – 37</td><td>84</td><td>45</td><td>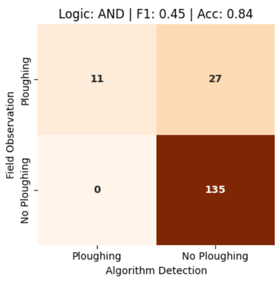</td><td>77</td><td>56</td><td>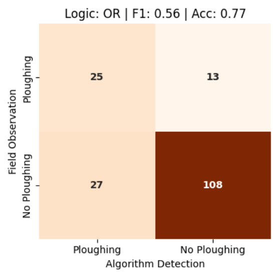</td></tr>
<tr><td>VH – Ascending – 161</td><td>78</td><td>0</td><td>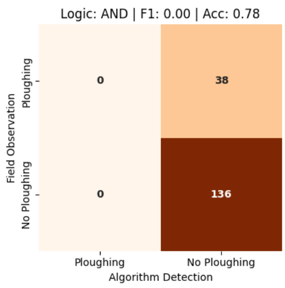</td><td>85</td><td>60</td><td>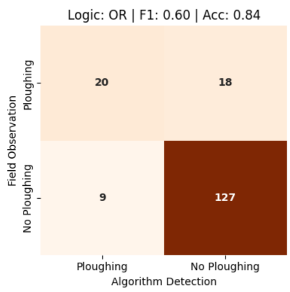</td></tr>
</table>

<table>
<tr><th></th><th></th><th></th><th></th><th></th><th></th><th></th></tr>
<tr><td>VH – Ascending – 88</td><td>78</td><td>0</td><td>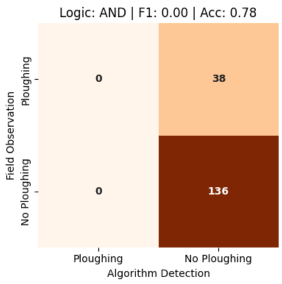</td><td>76</td><td>45</td><td>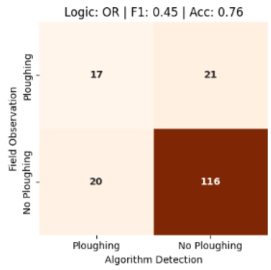</td></tr>
<tr><td>VV – Descending – 110</td><td>80</td><td>19</td><td>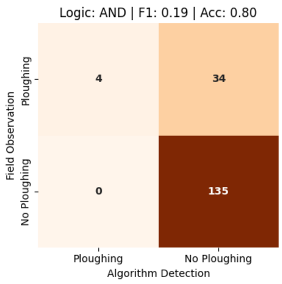</td><td>69</td><td>23</td><td>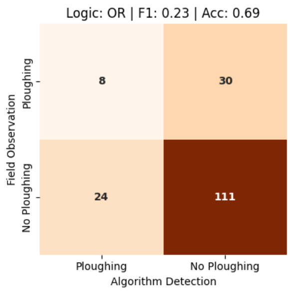</td></tr>
<tr><td>VV – Descending – 37</td><td>78</td><td>0</td><td>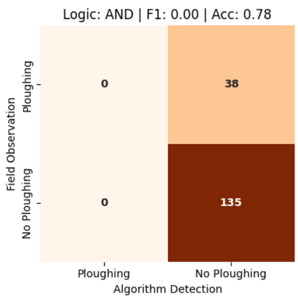</td><td>68</td><td>15</td><td>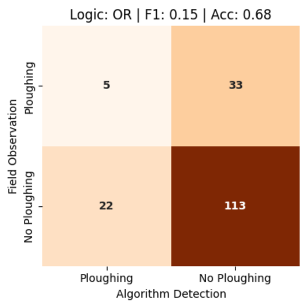</td></tr>
<tr><td>VV – Ascending – 161</td><td>88</td><td>63</td><td>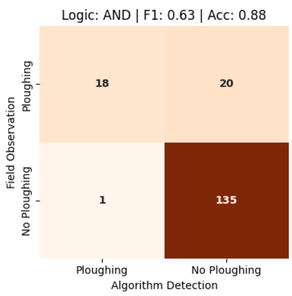</td><td>87</td><td>74</td><td>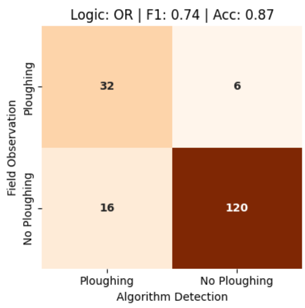</td></tr>
<tr><td>VV – Ascending – 88</td><td>89</td><td>66</td><td>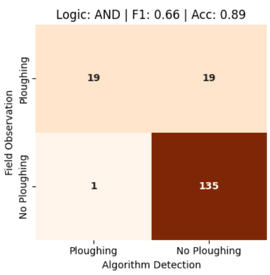</td><td>74</td><td>58</td><td>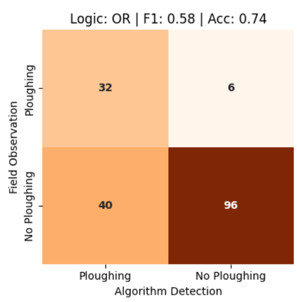</td></tr>
</table>

Table 8.5: Accuracy assessment of backscatter-based ploughing detection during the validation process of modified algorithm, highlighting the performance of various configurations.

Algorithm configuration (polarization – pass – orbit)	**HR $\Delta\sigma^0$ threshold (dB)**	**OA (%)**	**F1(%)**	**CM**
VH – Descending – 110	-3.5	74	0	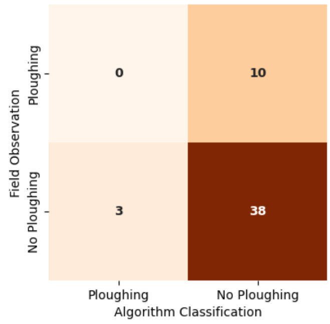
VH – Descending – 37	-2.5	61	29	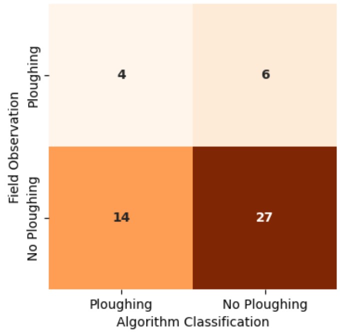
VH – Ascending – 161	-2.6	66	37	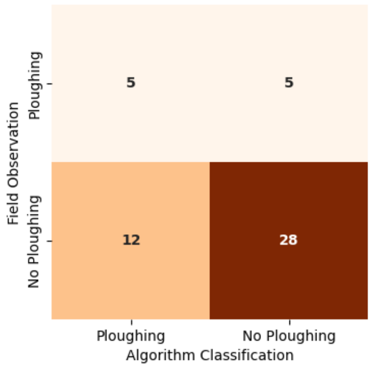
VH – Ascending – 88	-3.5	70	35	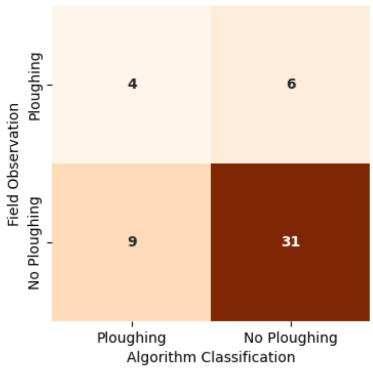

VV – Descending – 110	-3	71	0	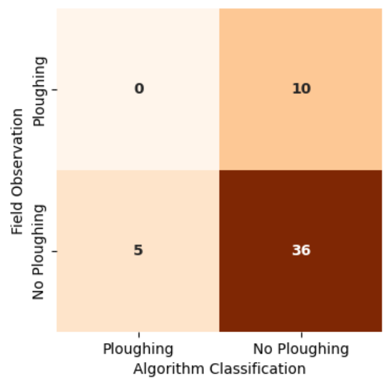
VV – Descending – 37	-2.5	67	19	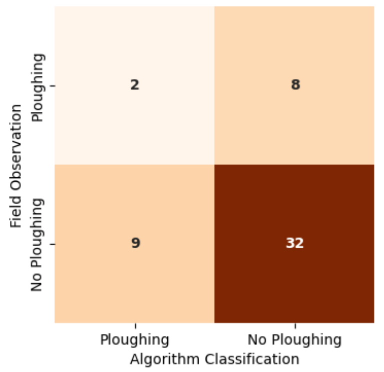
VV – Ascending – 161	-2.34	60	38	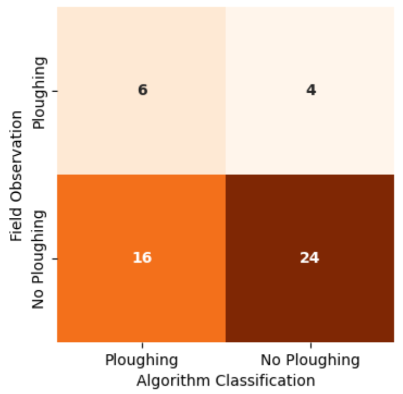
VV – Ascending – 88	-3.5	54	0	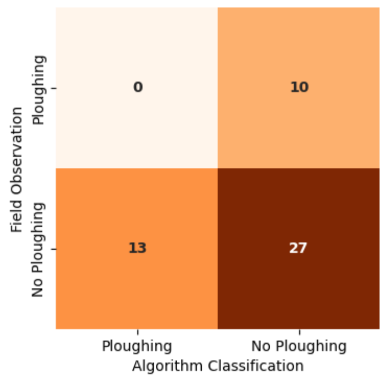

Table 8.6: Accuracy assessment of coherence-based ploughing detection during the validation process of modified algorithm, highlighting the performance of various configurations.

Algorithm configurations (polarization – pass)	HR coherence threshold	HR coherence threshold	OA (%)	F1 (%)	CM
VV – Descending	0.4	- 0.45	80	0	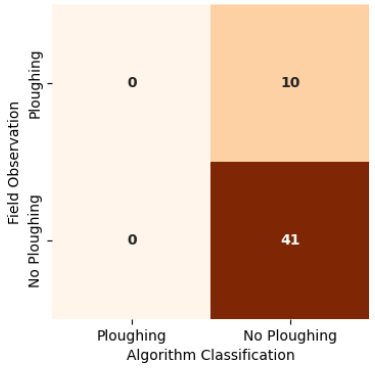
VV – Ascending	0.4	- 0.5	88	63	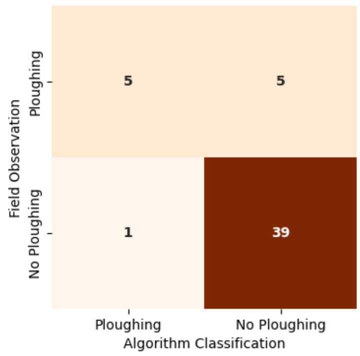
VH – Descending	0.3	- 0.4	88	57	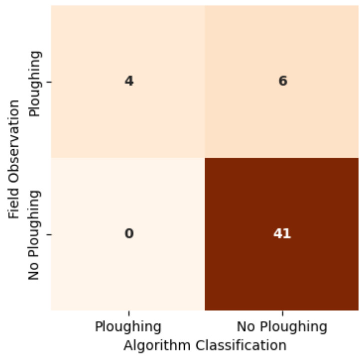
VH – Ascending	0.4	- 0.3	82	31	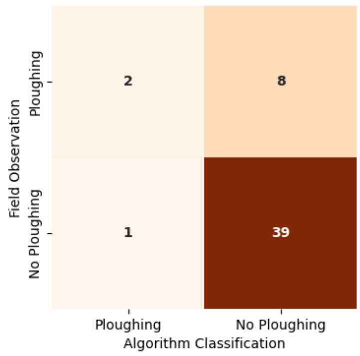

Table 8.7: Accuracy assessment of final ploughing detection during the validation process of modified algorithm, highlighting the performance of various configurations.

<table>
<tr><th>Algorithm configuration</th><th colspan="2">AND</th><th rowspan="2">CM</th><th colspan="2">OR</th><th rowspan="2">CM</th></tr>
<tr><th>(polarization – pass – orbit)</th><th>OA</th><th>F1</th><th>OA</th><th>F1</th></tr>
<tr><td>VH – Descending – 110</td><td>80</td><td>0</td><td>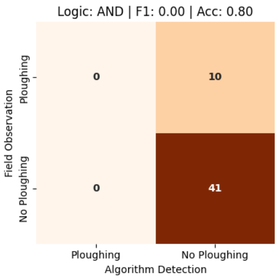</td><td>86</td><td>53</td><td>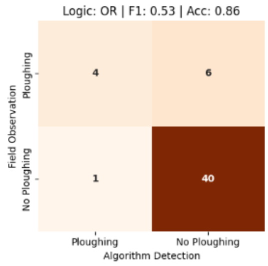</td></tr>
<tr><td>VH – Descending – 37</td><td>82</td><td>18</td><td>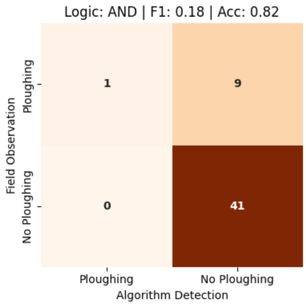</td><td>82</td><td>57</td><td>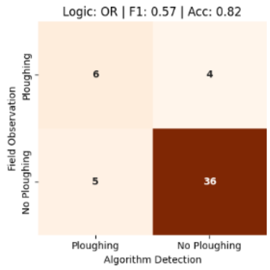</td></tr>
<tr><td>VH – Ascending – 161</td><td>84</td><td>33</td><td>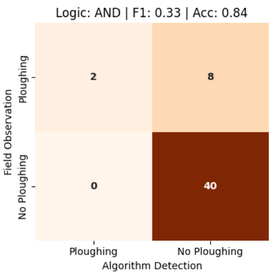</td><td>92</td><td>80</td><td>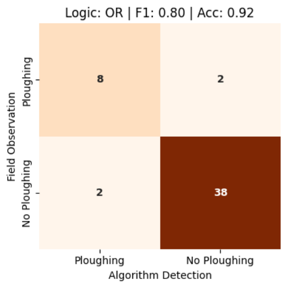</td></tr>
<tr><td>VH – Ascending – 88</td><td>84</td><td>33</td><td>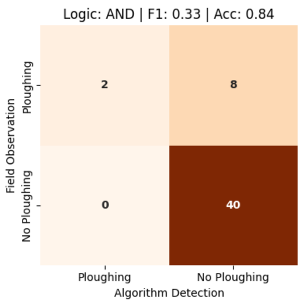</td><td>84</td><td>64</td><td>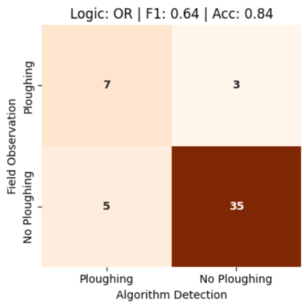</td></tr>
</table>

VV – Descending – 110	80	0	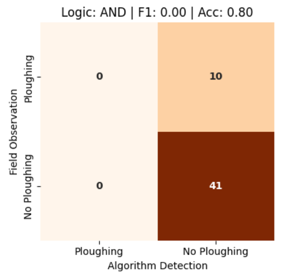	67	0	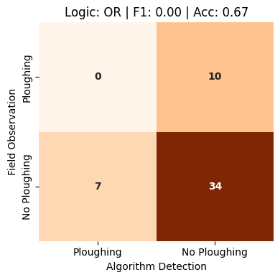
VV – Descending – 37	80	0	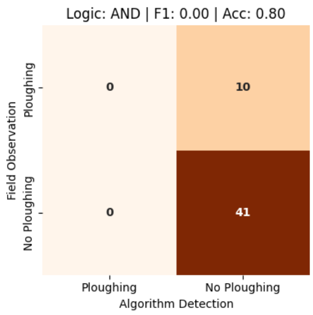	78	27	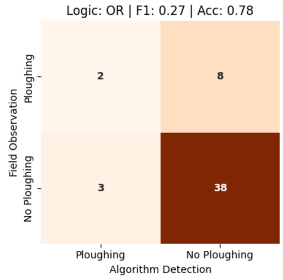
VV – Ascending – 161	90	67	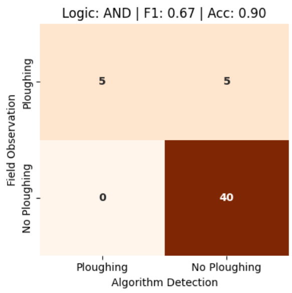	86	72	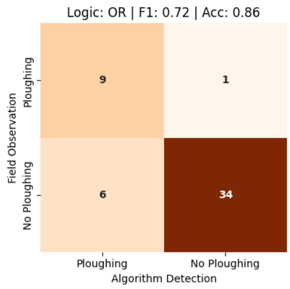
VV – Ascending – 88	88	57	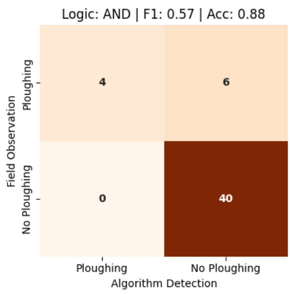	72	50	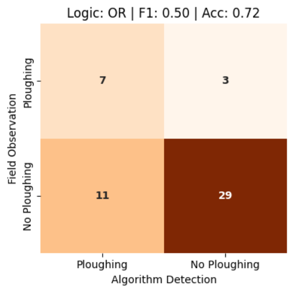

Soil tillage detection performances using Sentinel time series and Copernicus product in Wallonia

Majedeh Baladi

Monitoring soil disturbance activities such as tillage is essential for promoting sustainable agricultural practices and supporting soil health. However, detecting these short-lived events through remote sensing presents significant challenges due to their subtle surface signatures and the influence of external factors like precipitation and vegetation cover. This study investigates the potential of Sentinel-1 C-band synthetic aperture radar (SAR) data—specifically backscatter and interferometric coherence metrics—for tillage detection in Wallonia, Belgium. Two rule-based algorithms are developed: a baseline version that filters out soil moisture using a landscape-based approach, and a modified version that replaces this with precipitation data. Both algorithms use VV and VH polarized backscatter and coherence signals and apply a two-level detection framework to distinguish high- and low-confidence tillage events, based on the joint behaviour of radar metrics. The modified version achieves higher overall accuracy, suggesting that integrating precipitation data can enhance detection performance. The results demonstrate that the combined use of backscatter and coherence improves the sensitivity of detection. The analysis further indicates that satellite pass direction (ascending vs. descending) significantly influences detection performance, with ascending passes yielding more convincing results—likely due to the reduced impact of morning dew. Importantly, the absence of precise tillage dates and pre-tillage field conditions in the ground truth dataset limit both detection accuracy and the ability to validate results with high temporal confidence. Despite these limitations, the study confirms the viability of SAR time series for tillage monitoring and contribute to ongoing efforts in agricultural monitoring under the Common Agricultural Policy and support the development of more sustainable, accountable land management practices.

UNIVERSITÉ CATHOLIQUE DE LOUVAIN
Faculté des bioingénieurs
Croix du Sud, 2 bte L7.05.01, 1348 Louvain-la-Neuve, Belgique | **www.uclouvain.be/agro**